Fall 2015

The role of anion chemistry in the development of tetraphenylethylene-based molecular sensors and crystal engineering of N-haloarylpyridinium salts

Christopher James Kassl
University of Iowa

THE ROLE OF ANION CHEMISTRY IN THE DEVELOPMENT OF TETRAPHENYLETHYLENE-BASED MOLECULAR SENSORS AND CRYSTAL ENGINEERING OF N-HALOARYLPYRIDINIUM SALTS

by

Christopher James Kassl

A thesis submitted in partial fulfillment
of the requirements for the Doctor of Philosophy
degree in Chemistry in the
Graduate College of
The University of Iowa

December 2015

Thesis Supervisor: Associate Professor F. Christopher Pigge

Graduate College
The University of Iowa
Iowa City, Iowa

CERTIFICATE OF APPROVAL

_____

PH.D. THESIS

_____

This is to certify that the Ph.D. thesis of

Christopher James Kassl

has been approved by the Examining Committee for
the thesis requirement for the Doctor of Philosophy degree
in Chemistry at the December 2015 graduation.

Thesis Committee: _____
F. Chris Pigge, Thesis Supervisor

_____
Edward Gillan

_____
Leonard MacGillivray

_____
Daniel Quinn

_____
Michael Schultz

This thesis is dedicated to Mom and Dad. With love and respect, always.

In the clearing stands a boxer, and a fighter by his trade and he carries the reminders of every glove that laid him down and cut him till he cried out in his anger and his shame, "I am leaving, I am leaving." But the fighter still remains.

- Paul Simon, Art Garfunkel
Excerpt from "The Boxer" (1969)

For every complex problem, there is an answer that is clear, simple, and wrong.

- H. L. Mencken

Contradictions do not exist. Whenever you think you are facing a contradiction, check your premises. You will find that one of them is wrong.

- Ayn Rand

ACKNOWLEDGEMENTS

If I listed all the people that helped me to achieve what I have up to this point, this would probably be the longest section of my thesis. I will therefore limit this section to the key players; those who had a significant, dynamic and continuous impact on my education, development and establishment as a scientist proud of his work and eagerly awaiting what lies ahead.

I would like to thank my advisor and mentor, Dr. Christopher Pigge for his guidance, his patience and above all his belief in me. His charisma knew no bounds and he always communicated a dedication for his role and his field that few could hope to match. Through failure and success, trial and error, ennui and exuberance, he was there for all of it. I'm glad to have had him as a boss.

I would also like to thank my former colleague, roommate and close friend Dr. Paul Mueller for his continuous encouragement, advice and support. We motivated and helped each other throughout our time in Iowa City and his discipline, kindness, strength of character and unique brand of humor were an inspiration and invaluable to me. But his cooking is still terrible.

The Pigge research group has been home to some great scientists and people. I would like to thank my current fellow graduate student inmates Ashabha, Madhur, Moustafa, as well as undergraduates Lucas, Dan, Emberose, Brianna, Mckayla and past graduate Dr. Lokesh Pawar for their professional candor and personal charm. Thank you all for making it fun.

I would also like to thank Dr. Dale Swenson for his guidance and expertise in the area of X-ray crystallography, Dr. Lynn Teesch and Vic Parcell for their service and help

in the mass spectrometry facility, Dr. Santhana Velupillai and Dr. Fu Chen for their maintenance of the NMR facilities, Tim Koon in Chem Stores inventory, Janet Kugley in graduate student admissions, Sharon Robertson in the front office, Benjamin Revis in the glassblowing shop, Frank Turner in the machine shop and Peter Franke in the IT department.

Lastly I would like to thank my parents, friends and family who were a witness to every step of the way. Thank you all so much for your love and unwavering support.

ABSTRACT

Anions play a variety of roles in biology, bioinorganic chemistry, organic chemistry and mineralogy. As such, the directed coordination of anions in molecular complexation and the development of synthetic receptor molecules represent a burgeoning field for supramolecular chemistry in solution phase recognition and solid-state crystal engineering.

The desire to develop solution phase anion sensors utilizing the optoelectronic properties of tetraphenylethylene (TPE), in particular its capacity to participate in aggregation-induced emission (AIE) enhancement has resulted in the synthesis of two new classes of TPE-based anion sensors. The first class features a series of ureas off of a tetrasubstituted TPE framework capable of detecting a range of anions with its sensitivity toward these anions directly influenced by the basicity of the anion. The second class of TPE-based sensors displays a unique sensitivity toward the presence of pyrophosphate anion and is the first known example of a neutral TPE-based pyrophosphate sensor that does not require a zinc cofactor as a requisite of detection.

Our interest in utilizing anions in the self-assembly of organic materials resulted in the synthesis of twelve N-halophenyl pyridinium salts that are capable of assembling the solid state as a direct consequence of a combination of hydrogen- and halogen-bonding intermolecular forces and their interaction with a halide counterion. In four examples, the abundance of iodine halogen-bond donors relative to counterion acceptors resulted in the formation of extended halogen-bonded networks in the crystal structures that proved to be sufficiently strong to avoid disruption by an abundance of competing hydrogen bond donors.

Five additional examples of TPE-based halopyridinium salts were analyzed via crystallographic methods to examine what role the counterion will play, if any, in the directed assembly of these materials with the aid of potentially strong halogen bond donors. Three examples feature the presence of a traditionally coordinating anion and two examples study the types of assembly motifs that may be encountered when the anion is noncoordinating. Conclusions from this study prompted the synthesis of TPE-based pyridinium- and imidazolium salts potentially capable of participating in anion recognition through solution phase halogen bonding.

PUBLIC ABSTRACT

Anions play a variety of roles in biology, bioinorganic chemistry, organic chemistry and mineralogy. As such, the directed coordination of anions in molecular complexation and the development of synthetic receptor molecules represent a burgeoning field for supramolecular chemistry in solution phase recognition and solid-state crystal engineering.

The desire to develop solution phase anion sensors utilizing the optoelectronic properties of tetraphenylethylene (TPE), in particular its capacity to participate in aggregation-induced emission (AIE) enhancement has resulted in the synthesis of two new classes of TPE-based anion sensors. The first class features a series of ureas off of a tetrasubstituted TPE framework capable of detecting a range of anions with its sensitivity toward these anions directly influenced by the basicity of the anion. The second class of TPE-based sensors displays a unique sensitivity toward the presence of pyrophosphate anion and is the first known example of a neutral TPE-based pyrophosphate sensor that does not require a zinc cofactor as a requisite of detection.

Our interest in utilizing anions in the self-assembly of organic materials resulted in the synthesis of twelve N-halophenyl pyridinium salts that are capable of assembling the solid state as a direct consequence of a combination of hydrogen- and halogen-bonding intermolecular forces and their interaction with a halide counterion. In four examples, the abundance of iodine halogen-bond donors relative to counterion acceptors resulted in the formation of extended halogen-bonded networks in the crystal structures that proved to be sufficiently strong to avoid disruption by an abundance of competing hydrogen bond donors.

Five additional examples of TPE-based halopyridinium salts were analyzed via crystallographic methods to examine what role the counterion will play, if any, in the directed assembly of these materials with the aid of potentially strong halogen bond donors. Three examples feature the presence of a traditionally coordinating anion and two examples study the types of assembly motifs that may be encountered when the anion is noncoordinating. Conclusions from this study prompted the synthesis of TPE-based pyridinium- and imidazolium salts potentially capable of participating in anion recognition through solution phase halogen bonding. Though the results did not imply success, the potential to continue to refine our synthetic methodology and analytical techniques is being explored.

TABLE OF CONTENTS

LIST OF TABLES

LIST OF FIGURES

LIST OF SCHEMES

CHAPTER I

INTRODUCTION TO ANION COORDINATION AND ITS APPLICATIONS

1.1 Early Development of Anion Coordination Chemistry

Anions play a plethora of roles in biology, bioinorganic chemistry, organic chemistry and mineralogy. For example, an estimated 70-75% of substrates and cofactors involved in enzymatic processes are negatively charged species.[1] As such, the directed coordination of anions in molecular complexation and the development of synthetic receptor molecules represent a burgeoning field for supramolecular chemistry in solution phase recognition and solid-state crystal engineering.

In order for any material to be designed for the expressed purpose of sensing/recognition of anions or with the intention of incorporating them into their chemical framework, certain unique properties of anions must be considered. First, anions are considerably larger than most metal cations; F^-, the smallest common anion, has an ionic radius of 1.33 Å, only slightly smaller than that of the relatively mid-sized metal cation K^+ (1.38 Å).[2] Therefore, the subsequent design of receptors, particularly those receptors wishing to encapsulate or sequester anions, need to be considerably larger. Second, many anions have relatively high free energies of solvation (ΔG_{solv} (F^-) = -465 kJ/mol; ΔG_{solv} (Cl^-) = -340 kJ/mol)[3], and any designed receptor would need to be able to effectively compete with the surrounding medium for interactions with the anion. Third, unlike spherical metal cations, many common anions in inorganic, organic and biological chemistry assume a myriad of shapes and geometries (CO_3^{2-}, trigonal planar; PO_4^{3-} tetrahedral; PF_6^-, octahedral, etc.) in addition to the spherical halides. Fourth, many anions only exist within a relatively narrow pH range (i.e. $H_2PO_4^-$ is stable when pH is 3-5.5; HCO_3^- is stable between pH of 6.5 and 10) and their detection may partially rely upon interaction with a protonated receptor, which may itself only be stable within a narrow pH window. The challenges presented by the unique chemistry of anions may be numerous, but they are thankfully not insurmountable.

The study of anion coordination chemistry has grown from an area of purely academic interest to a well-established pillar of supramolecular chemistry offering a wide variety of applications over the past 50 years. These developments effectively began in the late 1960s when du Pont chemists Park and Simmons published NMR analyses of a series of *katapinate* (in Greek: swallow up, engulf) diammonium salts of various carbon chain lengths (7-10 carbons, Figure 1.1) complexed with halide ions.[4] Their findings concluded halides engaged in hydrogen-bonding interactions with the protonated species and encapsulation was later confirmed with X-ray crystallographic studies.[5]

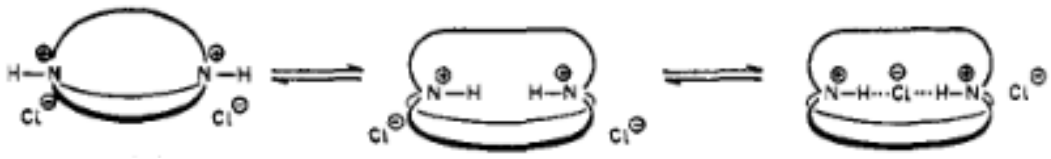

Figure 1.1. Katapinate diammonium salts with complexed and free chloride anion. Reprinted with permission from Park et al, copyright (1968) American Chemical Society.

Development of the earliest complexes was concerned mainly with the detection of spherical monoatomic halide anions but with time, more sophisticated receptors were developed. Recognition of molecular linear anions was first reported in the case of azide binding by a hexaprotonated derivative of macrobicyclic receptor **1.1** within the cavity of the host.[6] Development of subsequent receptors for polyatomic oxoanions such as nitrate (**1.2**)[7] and terephthalate (**1.3**)[8] were reported shortly thereafter with interior cavities tuned to the size of the anions.

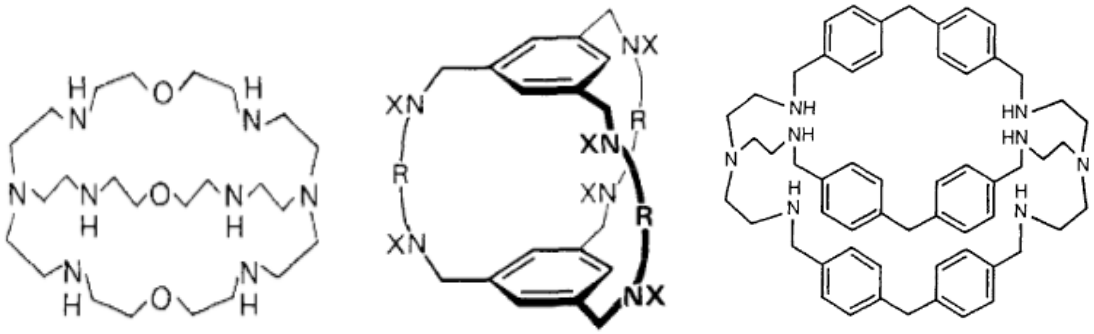

1.1 **1.2** **1.3**

Figure 1.2. Select macrocyclic anion hosts with noted affinities for azide (**1.1**), nitrate (**1.2** X= H), and terephthalate (**1.3**) anion. All inclusion complexes were confirmed by subsequent X-ray crystallographic studies.

1.2 Development of Modern Anion Receptors

Many of the first anion receptors were macrocyclic in nature and relied upon encapsulation of the anion. Many, if not most, relied upon the utilization of the amine moiety in varying stages of protonation (receptors **1.1** and **1.3** for example, were only capable of detecting their respective anion substrates in their hexaprotonated forms). As the desire for more selective and sensitive receptors increased, their sophistication and versatility correspondingly increased; Current methodologies for receptor synthesis rely upon the presence of 1) a binding site where the anion can interact/coordinate and 2) a reporter unit that can effectively signal when an anionic substrate has been incorporated.

Most modern anion receptors are designed in one of three ways; 1) receptors where the binding site and the reporter are covalently linked through a spacer; 2) receptors where the binding site is integral to the reporter and 3) receptors where the anion binding induces an irreversible reaction, which thereby activates the reporter.[9] This last approach describes the formation of a "chemodosimeter", which, rather than forming a supramolecular anion-receptor complex with an anionic substrate, is fundamentally altered by the presence/binding of the anion and typically this results in the formation of a new molecule with different optical properties.

The design of anion binding sites may take many forms. Some of the most ubiquitous receptors developed focus on the incorporation of chemical moieties that interact through the formation of hydrogen-bonding interactions. To this end, receptors that incorporate amine,[10,11,12] guanidinium,[13] amide,[14,15] pyrrole,[16] amido-pyrrole,[17] carbazole,[18,19] boronic acids,[20,21,22] urea[23,24] and thiourea[25,26] moieties have been among the most common and successful in their detection of anions. Some typical hydrogen bonding interactions are showcased in Figure 1.3 with dashed lines indicating accepted modes of interaction with an anion.

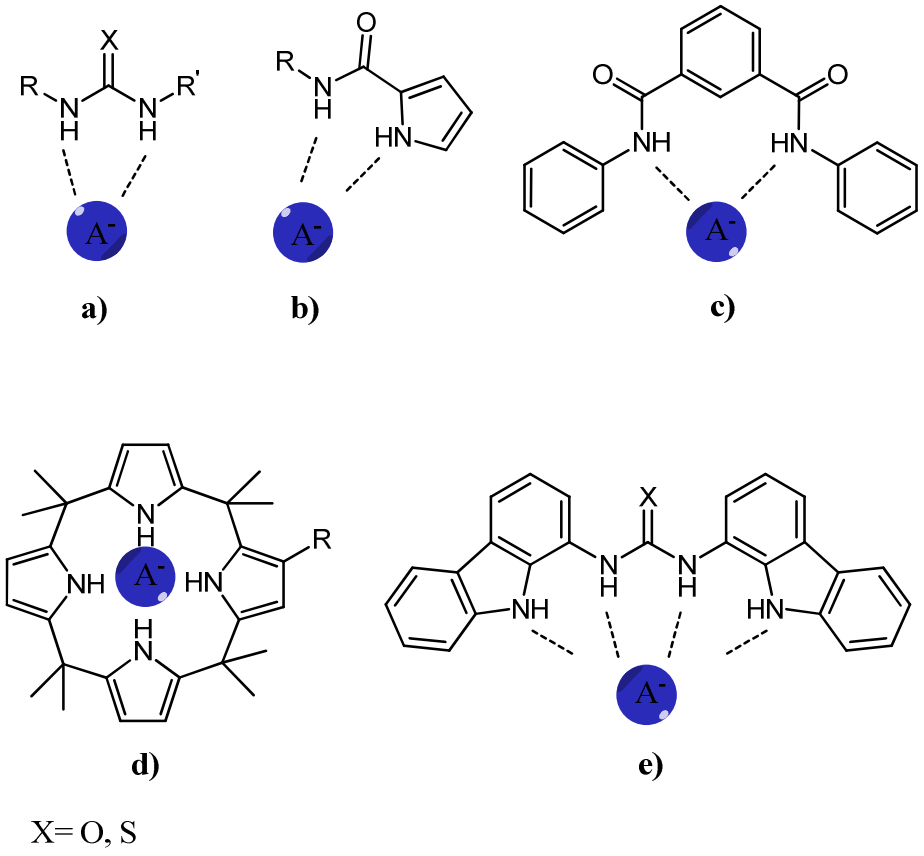

Figure 1.3. Select modes of anion coordination with various hydrogen-bonding anion receptor archetypes presented. a) ureas/thioureas b) amidopyrrole c) bisamido d) calix[4]pyrrole and e) urea/thiourea carbazoles.

In order for the sensors to display an adequate measure of selectivity and sensitivity, it can be assumed that most of the hydrogen-bonded interactions formed with the anion should be of a relatively strong nature, or at least strong enough to be able to effectively compete with the surrounding medium. Some anions, such as fluorine, are sufficiently basic that they are sometimes capable of deprotonating their intended receptors. However, this can be a key feature in the design of a given sensor. Gunnlaugsson[27] and Fabrizzi[28] were among the first to develop colourimetric sensors that relied upon deprotonation by fluoride to induce a color change in solution.

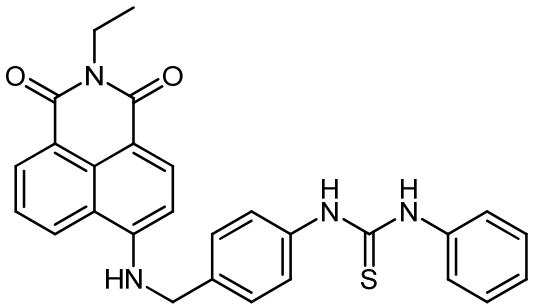

1.4

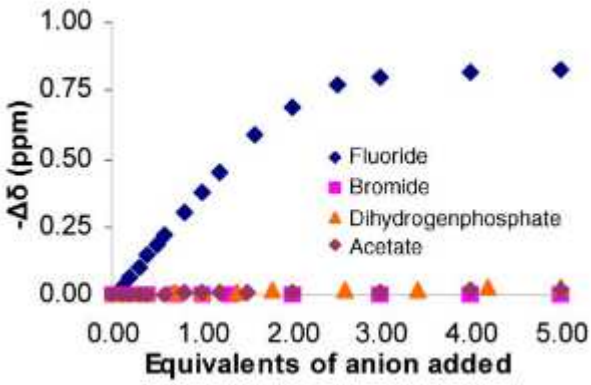

a)

b)

Figure 1.4. Gunlaugsson's thiourea-based receptor; a) plot of ^{1}H NMR chemical shift differences vs. equivalents of anion added; only F^- produces a measureable response. b) d^6-DMSO solutions of **1.4** in the absence (yellow) and presence (purple) of F^-.

Gunnlaugsson relied upon the incorporation of a thiourea appended with a derivative of the reporter 4-amino-1,8-naphthalimide, a highly fluorescent dye, to produce **1.4**. Fluorescence titration studies in d_6-DMSO demonstrated fluorescence quenching upon the addition of small amounts of fluoride, but when excess fluoride (> 2 equiv) was added, dramatic shifts in the absorbance were observed, resulting in color changes from light yellow to dark purple (Figure 1.4). It should be noted here that the quenching of fluorescence emission was also observed upon the addition of OAc^- and $H_2PO_4^-$ (attributed to their interaction with the thiourea moiety), but without the accompanying changes in absorbance. This behavior was later attributed to the deprotonation of the amino-NH by F^- NMR studies that monitored the disappearance of the amino-NH resonance and the formation of the stable $[HF_2]^-$ complex. Admittedly, the interaction of anions with the thiourea moiety was what the group had anticipated would

come about as a result of the interaction of fluorine with the sensor but the deprotonation observed in the presence of fluoride provided some valuable information about the limits of such systems.

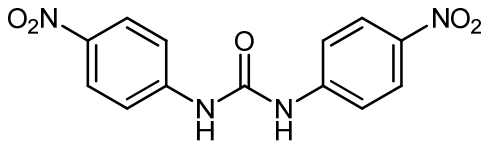

1.5

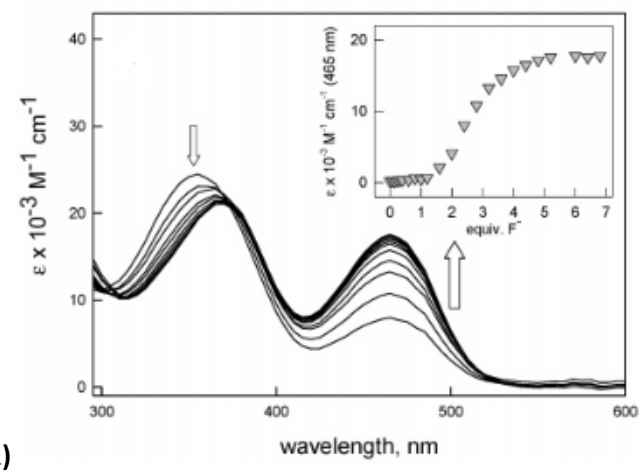

a)

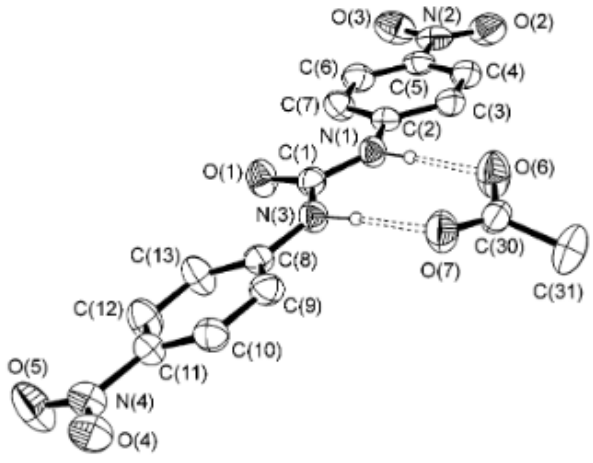

b)

Figure 1.5. a) UV-vis absorbance titrations of compound **1.5** (1 μM in MeCN) with F^-, added as a tetrabutylammonium salt, with inset monitoring the increase in absorbance at 475 nm, indicating the formation of the deprotonated receptor. b) ORTEP view of the [**1.5**-OAc^-] complex at 30% probability. Reprinted with permission from Fabrizzi et al, copyright (2004) American Chemical Society.

Fabrizzi demonstrated the propensity of simple monoureas such as **1.5** to undergo deprotonation by F^- through a series of UV-vis experiments in acetonitrile that showed considerable shifts in absorbance in solutions and ranged from pale yellow to deep red. Monitoring absorbance at 345 nm indicated the formation of a 1:1 complex of [**1.5**-F^-] at 345 nm and additional equivalents of F^- resulted in the appearance of a new peak at 475 nm, indicative of the deprotonated receptor **1.5** (Figure 1.5). Accompanying ^{1}H NMR experiments in DMSO-d_6 showed the formation of $[HF_2]^-$. The addition of other anions (OAc^-, NO_3^-, HSO_4^-, $H_2PO_4^-$, OBz^- and NO_2^-) resulted in the formation of hydrogen-bonded complexes with the urea (asserted by x-ray crystallographic evidence) but not the corresponding changes in absorbance.

1.3 Anion receptors as Chemodosimeters

Some anion receptors rely upon the interaction of the anion with a binding site to form a new molecule with modified optical properties. With respect to the identity of the anion and the nature of the signaling unit or mechanism, this process may encounter varying degrees of reversibility. A great variety of chemodosimeters have been developed and applied particularly successfully to the detection of CN^-.[29,30]

Sun and coworkers[31] were able to develop a colorimetric sensor **1.6** based upon the propensity of CN^- to participate in nucleophilic attack on carbonyl compounds to form the corresponding cyanohydrins. Their sensor detected CN^- to the exclusion of other inorganic anions; the addition of cyanide is stabilized by the formation of intramolecular hydrogen bonds and the highly electron-withdrawing nature of the nitro-groups on the aromatic ring further activates the amido-carbonyl group for nucleophilic attack by CN^- (Figure 1.6).

colorless

yellow

colorless

1.6

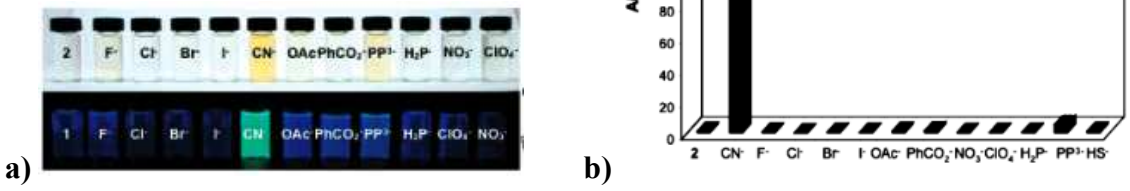

Figure 1.6. The addition of CN^- to **1.6** shows exclusive detection of the anion both a) colourimetrically and b) fluorometrically. Reprinted with permission from Sun et al, copyright (2006) American Chemical Society.

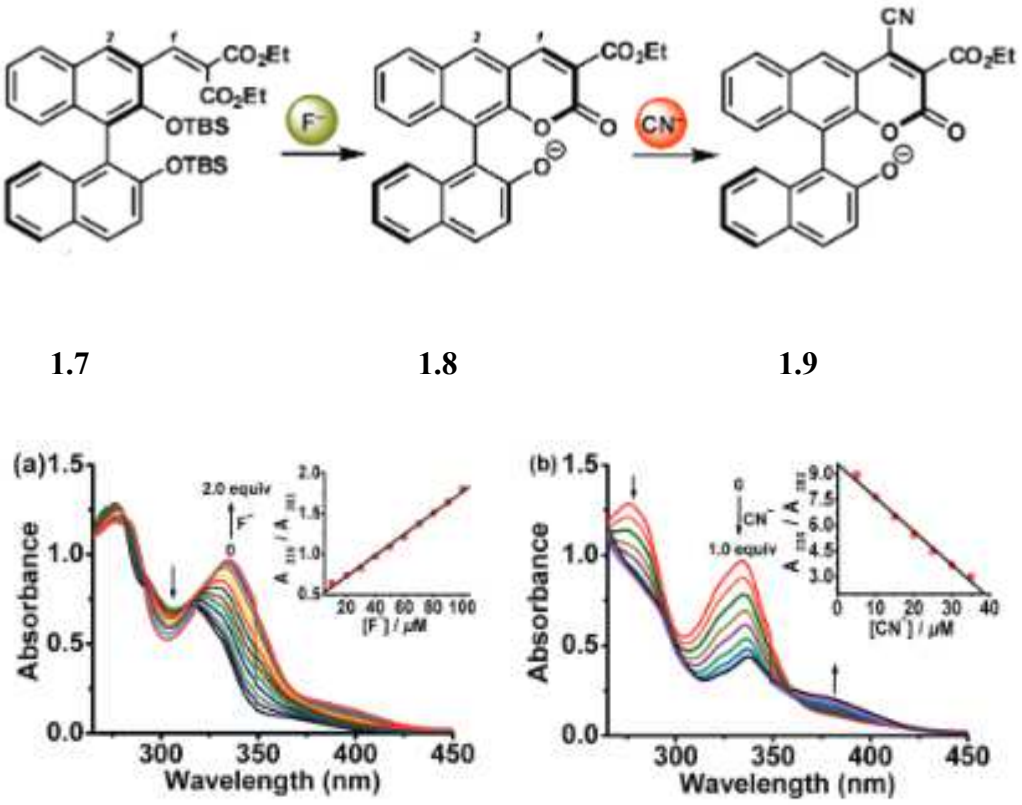

Figure 1.7. Sequential addition of F^- and CN^- to **1.7** results in coumarin derivative **1.8** and cyano-coumarin derivative **1.9**, respectively. a) UV-vis absorbance shows appearance of new peak at 335 nm with presence of F^- and b) disappearance of peak at 335 nm with CN^- with a moderate increase in absorbance at 382 nm (in MeCN). Reprinted with permission from Wang et al, copyright (2012) American Chemical Society.

Wang and colleagues[32] developed a sequential sensor **1.7** for F^- and CN^- based on a 1,1'-binaphthyl framework. Desilylation by the increased presence of F^- resulted in the formation of a coumarin derivative **1.8**, monitored by UV-vis aborbance and fluorescence emission spectroscopy (new peak emerges at 335 nm in UV spectrum, Figure 1.7a) with subsequent addition of CN^- producing a novel cyano-coumarin derivative **1.9** through Michael-type intermediate that loses a hydride with rearomatization as the driving force. (moderate increase in UV-vis absorbance at 382 nm, Figure 1.7b). This type of chemical system hints at the potentially powerful concept of anion relay recognition, which

emphasizes the possibility of using one versatile chemosensor to detect multiple anions in a sequence rather than utilizing sensors attuned to a specific anion.

1.4 Anion-Responsive Gels as Receptors

Gels are soft materials with many interesting physical and chemical properties and have attracted a great deal of recognition within the field of supramolecular chemistry in recent years. Generally, they consist of low-molecular-weight molecules that are held together by noncovalent interactions such as hydrogen-bonds, aromatic π-π stacking, metal coordination or other van der Waals forces, forming extensive assemblies of fibrous networks.[33] Typically, the formation of such gels has been influenced by external conditions, such as temperature, concentration of the substrate, and choice of solvent. However, recent advances have demonstrated that anions can act to stimulate sol-gel transitions, thereby demonstrating their potential as unique anion sensors, with particular interest in the tunable and reversible nature of the methodology.

de Mendoza[34] and colleagues synthesized a unique bicyclic diguanidinium chloride that was capable of forming gels in nonpolar aromatic solvents such as toluene, *p*-xylene and mesitylene. Tetrabutylammonium salts of various anions were added (AcO^-, NO_3^-, PF_6^-, BzO^-, Br^-, Cl^-, HSO_4^-) and after vigorous mixing as well as cycles of heating and cooling, they discovered that only chloride and bromide solutions lead to stable gels, whereas any other anion resulted in a disruption of the aggregation. Based upon these observations, they concluded that incompatible spatial and geometric differences among the respective anions were a key contributor to the breakup of aggregates; the spherical nature of chloride and bromide were sufficient to interact with the diguanidinium moiety and still preserve the gel aggregates.

Steed and coworkers[35] synthesized a class of gel-forming materials comprised of chiral di-urea monomers with even numbers of methylene spacer units (n = 2, 4, 6 and 8) between each urea moiety. Gels were formed in DMSO-H_2O and MeOH-H_2O mixtures. They noted that gel formation was considerably disrupted by the presence of OAc^- anion,

with anion titrations indicating the formation of discrete 1:1 gelator-anion complexes (determined by Job plot analysis). A binding affinity of 18,000 mol^{-1} dm^3 was calculated. They concluded that OAc^- effectively competes with dimerization of the di-urea chains as a necessary first step to gel formation, disrupting the hydrogen-bonded network formed between carbonyl groups and urea-NH hydrogens of successive oligomers (Figure 1.8). Subsequent titrations with Cl^-, NO_3^-, Br^- and BF_4^- showed comparatively little to no effect on formation of the gel network and the selectivity of the gel toward OAc^- may be attributed to the capacity of the anion to form discrete interactions with both NH groups of a urea moiety.

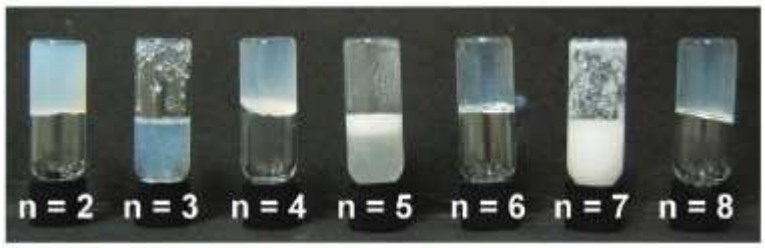

Figure 1.8. Steed's gelating ureas capable of forming with even numbers of methylene spacers. Reprinted with permission from Steed et al, copyright (2008) Royal Society of Chemistry.

Gel synthesis continues to be an area of intense interest with promising potential applications in drug delivery,[36] tissue engineering,[37] templated synthesis of nanoparticles, and pollutant capture and sequestration[38] and the ability of different anion binding interactions to tune the properties of such gels will doubtlessly continue to be an area of growing interest.

1.5 Anion-Mediated Catalysis in Organic Chemistry

With the prevalent use of several metal-based catalysts in organic synthesis, there is a growing concern about the environmental impact and the lack of sustainability in such methodologies (expense, difficulty of handling, toxicity, etc.). A considerable amount of research has explored the utility of natural enzymes in catalyzing industrial-scale organic reactions,[39,40] but there are considerable limitations, not least of which is the fact that most enzymes will not function in non-aqueous environments. Thus, biomimetic chemistry has come to the forefront of inquiry with considerable effort expended into developing artificial enzymes that act similar to their natural analogues to recognize anionic substrates (most cofactors for natural enzymes are anionic) through simple noncovalent interactions such as hydrogen-bonding, anion-π interactions and ion pairing electrostatic interactions.[41,42]

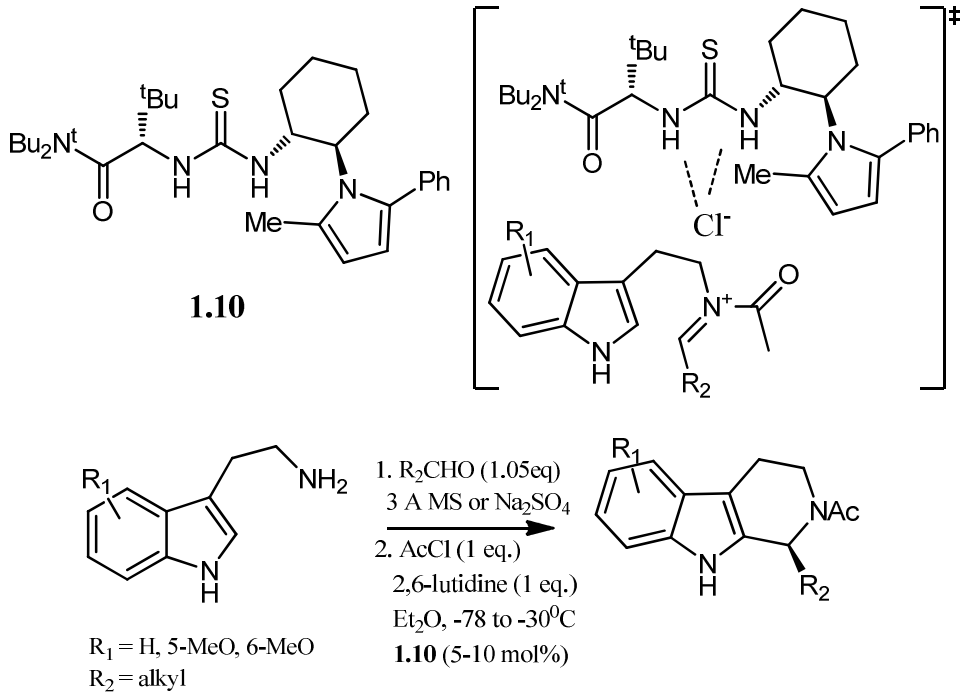

Figure 1.9. The presence of thiourea catalyst **1.10** facilitates Pictet-Spengler cyclizations by extracting the chloride, further activating the N-iminium substrate.

Some of the earliest efforts to develop methodologies for catalysis mediated by chloride binding were made by Taylor and Jacobsen,[43] who utilized the chiral bulky thiourea derivative **1.10** as a modified Brønsted acid catalyst for Pictet-Spengler cyclization reactions to form synthetically important tetrahydro-β-carbolines. Tryptamine substrates are derivatized to imines which are then subsequently activated with acetyl chloride. The hydrogen-bond donating thiourea acts to extract the chloride counterion of the N-acyl iminium salt, further enhancing the electrophilic character of the iminium moiety and resulting in the desired intramolecular ring closing (Figure 1.9). The use of such a chiral bulky thiourea catalyst also resulted in enantioenriched products under mild conditions.

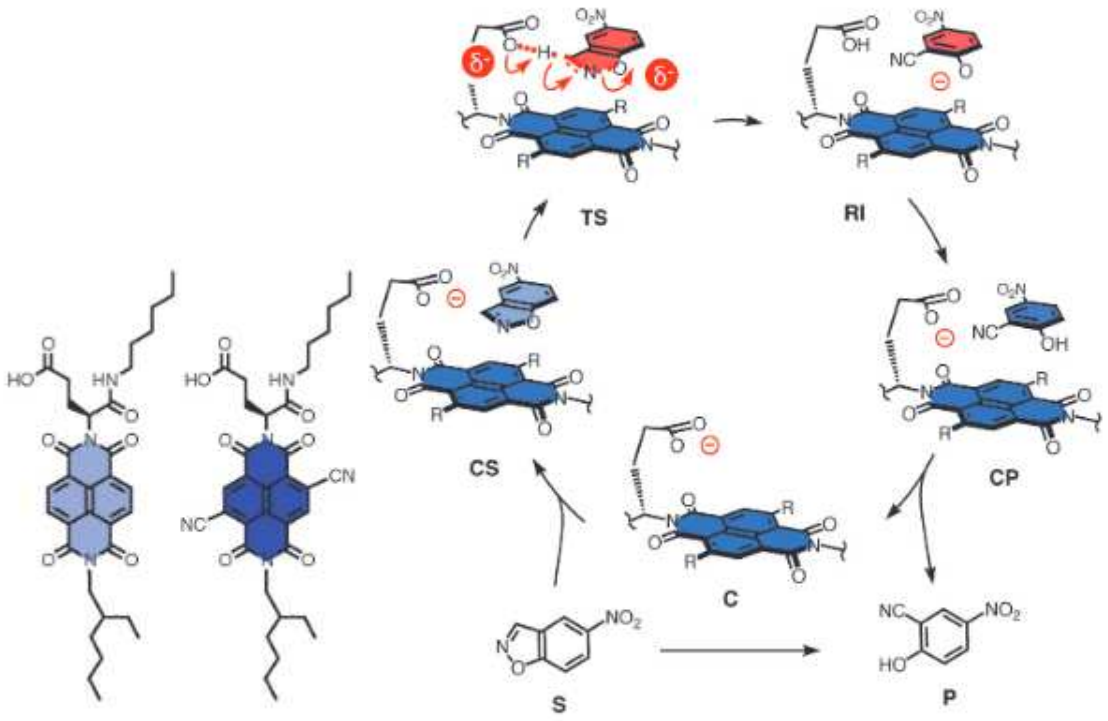

1.11 **1.12**

Figure 1.10. Schematic representation of a catalytic cycle for **1.11** and **1.12** facilitating Kemp elimination of benzisoxazole substrates (S); (CS) = catalyst/substrate complex; (TS) = transition state; (RI) = reaction intermediate; (CP) = catalyst/product complex; (P) = product. Reprinted with permission from Matile et al, copyright (2013) by Wiley & Sons.

While chloride and cyanide were among the first anionic substrates studied in organocatalytic processes,[44] interest gradually grew for utilizing carboxylates and other oxoanions. Carboxylates are some of the most common anions found in nature. Thus, the interest in developing organocatalytic systems incorporating carboxylates has been particularly strong.

While indeed carboxylate-mediated organocatalysis is highly sought after, not all catalysts draw from nature's inspiration; some interesting work came about from the Matile group,[45] who described some of the first organocatalytic systems to utilize carboxylates in anion-π interactions for the Kemp elimination of benzisoxazole. Their π-acidic naphthalenediimide catalysts **1.11** and **1.12** feature a covalently linked carboxylic acid moiety, which, upon deprotonation to the carboxylate acts to align the benzisoxazole

substrate along the face of the naphthalenediimide moiety (Figure 1.10). It is important to note that these substrates are not intended to be used for the purpose of detecting anions, but rather incorporate an active anion into their framework for the express purpose of detecting and interacting with an organic substrate. Computational analysis shows that cofacial aromatic π-π stacking interactions lend greater stability to the transition state and lead to a considerable acceleration of the elimination reaction, demonstrating the unique concept of anion-π catalysis, a motif not previously seen in nature, but of growing interest in the field.

1.6 Transport of Anions via Synthetic Channels

All living cells are surrounded by a phospholipid membrane that provides a barrier to the passive diffusion of large molecules and anions.[46] Rather than freely entering the cell, the transport of anions is tightly controlled by the actions of transport proteins embedded within the phospholipid membrane that act to ensure the intracellular concentration remains well-controlled. However, there are several diseases and disorders that affect these proteins and hence, their ability to regulate anion transport across the cellular membrane is either severely curtailed or completely absent. Such transport protein deficiencies have been linked to cystic fibrosis,[47] Dent's disease[48] and congenital chloride diarrhea,[49] among other serious ailments. Therefore, there has been considerable interest in the scientific community to develop synthetic substitutes for these insufficient transport proteins by synthesizing anion receptors that are capable of transportation of the anions across the phospholipid membrane. One proposed solution has been to implement methodologies to develop synthetic anion channels. The preponderance of substrates that have been developed for these studies is inspirational, though as of yet no *in vitro* studies have been undertaken with such substrates.[50]

These anion channels are intended to provide pores through a membrane through which an anion can travel; these structures can either be single molecules or membrane-spanning supramolecular self-assembled structures. For their synthesis, there are typically two strategies that are implemented; the design of "rigid rod" structures and the synthesis of cylindrical or tubular assemblies.

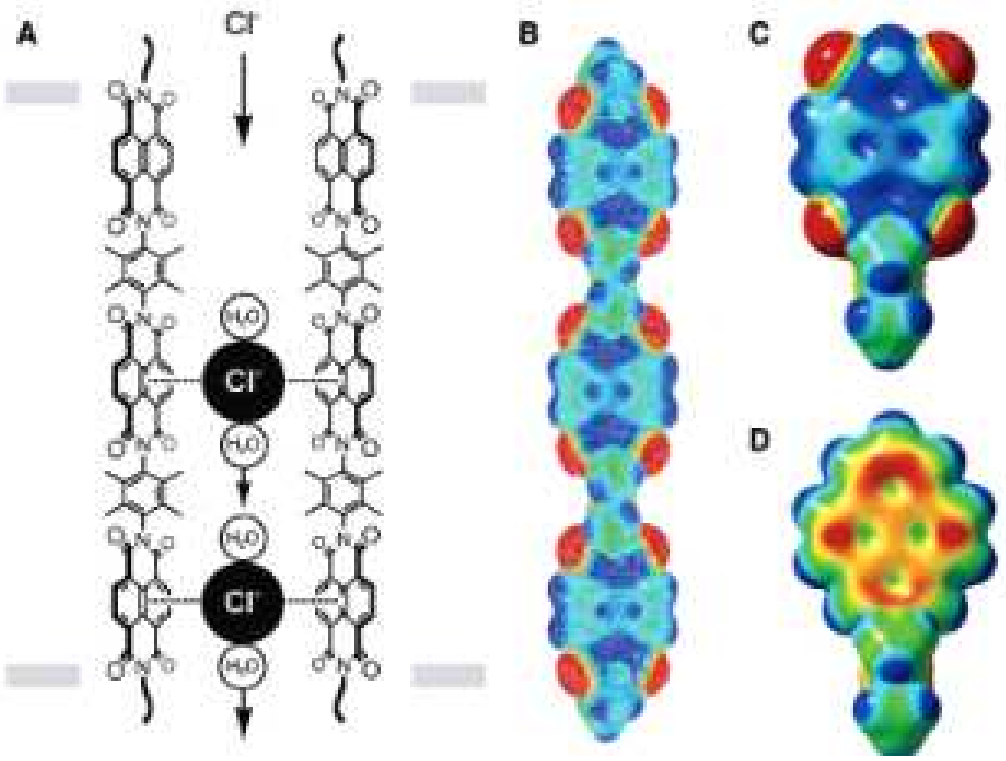

Figure 1.11. Matile's π-slides. Reprinted with permission from Matile et al, copyright (2007) Royal Society of Chemistry.

Some notable examples of the former involve work done by the Matile group[51,52] in their design of rigid rod structures spanning the membrane of egg yolk phosphatidylcholine (EYPC) membranes. Specifically, their efforts produced naphthalene- and perylenediimide (NDI,[51] PDI[52]) -based rigid rods that provided a π-acidic surface for anions to slide through the membrane via anion-π interactions (Figure 1.11). The electron-acceptor capability of NDI and PDI substrates is well-studied[53] and their face-to-face π-stacking interactions are among the highest ranked organic n-type semiconductors.[54] The group determined that their NDI and PDI channels displayed high selectivity for transport of anionic guests over cationic guests and a unique halide selectivity ($Cl^- > F^- >> Br^- > I^-$). This sequence of selectivity is a compromise between the Hofmeister bias ($I^- > Br^- > Cl^- > F^-$)[55], which determines selectivity for the channel exclusively by the cost of anion desolvation and the comparatively rare series ($F^- > Cl^- > Br^- > I^-$), where selectivity would be determined solely by the degree of anion binding to the channel. The results indicate that there is a specific balance between the stabilizing

effect of anion binding to the channel and the energetic cost of anion desolvation that must be taken into consideration.

There are numerous other examples of various anion-binding motifs implemented in rigid rod architectures, such as hydrogen-bonding interactions with hydrophilic polyalcohol chains supported on a polyarene backbone,[56] halogen-bonding interactions where anions can "hop" from one discrete binding site to another,[57] and charge-assisted binding in imidazole[58]- and benzimidazole-containing transporters.[59] All of which have demonstrated the versatility of this architecture and the plethora of synthetic strategies that can be brought to bear in this field.

Another approach to synthetic anion channels involves the use of cylindrical or tubular molecules and assemblies that provide pores large enough for anions to pass through the membrane. Much like the rigid-rod assemblies, these architectures are highly tunable and typically feature a balance between hydrophilic/ hydrophobic interactions and considerations of pore diameter, with well-explored examples like β-cyclodextrin derivatives[60] as relatively large and calix[4]arenes[61] as relatively small. Indeed, even metal-based ion channels,[62] which have typically displayed low selectivity for anions, are being explored for the tunability of the pore sizes.

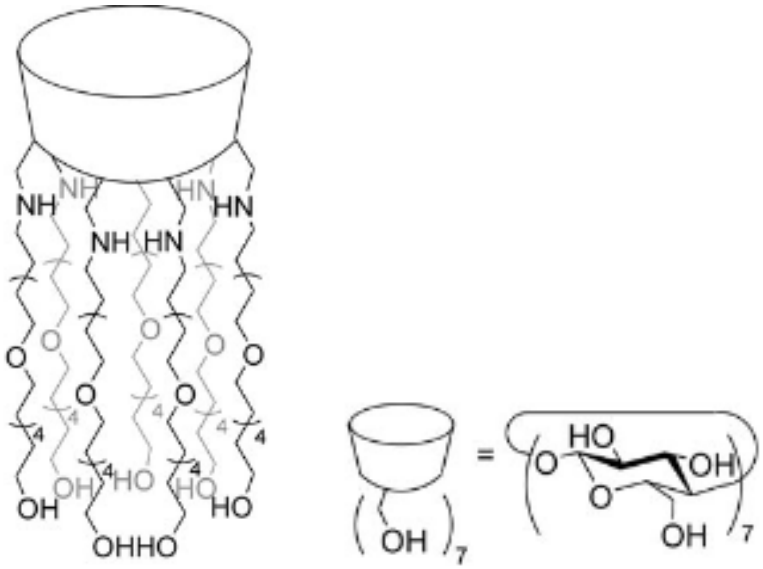

1.13

Figure 1.12. Schematic of β-cyclodextrin **1.13**. Reprinted with permission from Gin et al, copyright (2005) Wiley & Sons.

Gin and coworkers[63] developed an interesting ion channel by combining a β-cyclodextrin head group with oligoether chains attached to the primary face of the cyclodextrin through amine linkages (compound **1.13)**. The chains are sufficiently hydrophobic to allow the cyclodextrin to easily insert into a phospholipid membrane and the channel was demonstrated to selectively transport anions over cations- specifically, halide anions- as result of pH dependency, with acidic conditions (pH =5.6 and lower) resulting in protonation of the amino groups and electrostatic interactions with the halide anions preferable to interactions with cations. These channels follow the Hofmeister series ($I^- > Br^- > Cl^- > F^-$) of selectivity, where the more polarizable I^- anion enjoys a lower activation barrier to entry and a faster rate of transport through the hydrophobic interior of the channel.

1.7 Anion-Templated Synthesis and Formation of New Materials

The anion-driven assembly of supramolecular architectures has developed in recent years to move beyond simply another methodology for the detection and sequestration of anions, but also a method of assembling unique materials to be studied for their own particuar properties.

Jeong and coworkers,[64] looking to gain insight into the folding principles of natural molecules and create new bioinspired materials, explored the capacity of a select group of oligoindoles to participate in foldamer formation mediated by the presence of chloride anions. The indole NH-moieties act as hydrogen bond donors to stabilize the chloride anion within a binding cavity formed as a result of the formation of the foldamer **1.14** with near complete encapsulation of the anion. Evidence of foldamer formation was assessed with ^{1}H NMR studies with significant shifts observed for the resonances of indole N-H protons in the presence of chloride, added as a tetrabutylammonium salt (Figure 1.13).

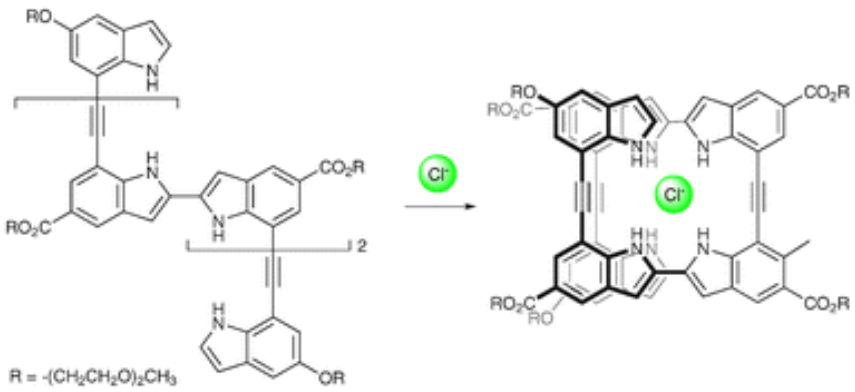

a) **1.14**

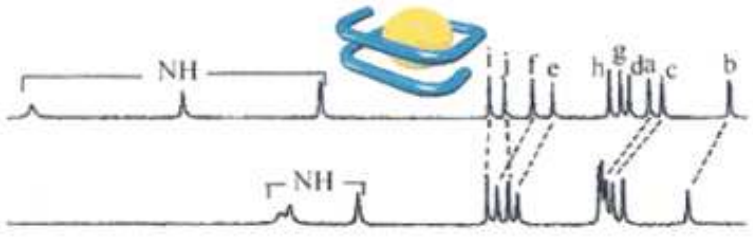

b)

Figure 1.13. a) Oligoindoles forming helical foldamer complex **1.14** upon the addition of Cl^- (b) ^1H NMR studies (in d^4-MeCN) showcasing significant changes in δ with the addition of 1 equivalent of Cl^-, added as tetrabutylammonium salt. Reprinted with permission from Jeong et al., copyright (2005) American Chemical Society.

While numerous examples of cation-induced formation of foldamer structures have been described in the literature,[65,66] the prevalence of anion-mediated assembly is relatively rare, though reports have been steadily growing over the last few years. [67,68]

Beer and his team have demonstrated numerous examples of anion-templated synthesis of increasingly complex mechanically interlocked molecules.[69,70] There are many potential applications for these complexes, ranging from the development of molecular motors and nanoswitches to biomimicry of several naturally occuring proteins, which completely encapsulate their anionic substrates in highly selective interactions through hydrogen-bonding networks buried deep within the protein structure.

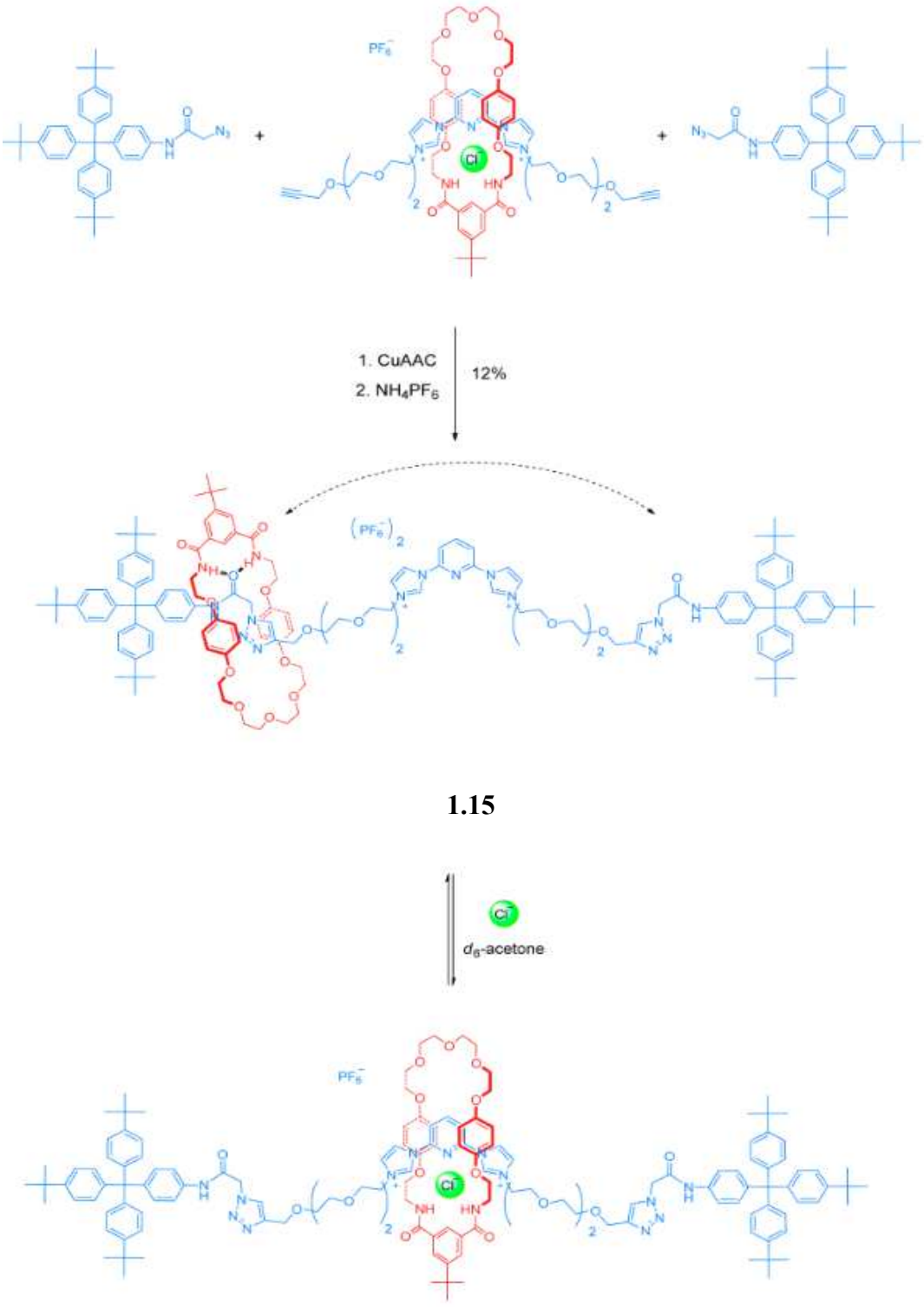

1.15

Figure 1.14. Chloride-templated synthesis of rotaxane complex **1.15** as PF_6^- salt. Subsequent addition of chloride results in translocation of the macrocycle across the thread of the 2,6-bisimidazolium pyridine axle.[71a] Reprinted with permission from Beer, et al, copyright (2013) American Chemical Society.

One particularly interesting example[71b] incorporating these ideas is the group's use of chloride as a template for the formation of a rotaxane structure by "threading the needle" of an isophthalimide macrocycle with a bis-alkynyl substituted 2,6-bisimidazolium pyridine moiety. Once threaded, the terminal alkynes are subsequently capped with bulky tetraaryl triazoles via Cu-catalyzed click chemistry and anion metathesis substitutes the chloride anion for the noncoordinating hexafluorophosphate analogue **1.15**. Solution NMR studies demonstrate that in the absence of chloride as a coordinating anion, the macrocycle resides primarily over one of the two triazole groups through stabilizing hydrogen bonding interactions between the isophthalimide NH-groups of the macrocycle and a carbonyl group of the triazole-imidazolium thread. However, the gradual addition of chloride facilitates molecular motion through shuttling of the isophthalimide macrocycle over the 2,6-bisimidazole pyridine moiety, with both components working to encapsulate the chloride via multiple hydrogen-bonding interactions. Evidence for the translocation of the isophthalimide macrocycle is primarily obtained by rationalization of ^{1}H NMR shifts and significant changes in the observed 2D ^{1}H-^{1}H NMR ROESY couplings.

1.8 Summary

Anion coordination chemistry is a large and ever-growing field that continues to inspire a great degree of ingenuity in finding solutions for modern problems ranging from their simple detection to their facilitated transport in biological/biochemical systems and their utility in organocatalytic systems. Whatever the chosen application or field of inquiry, interesting challenges are inherent in the synthesis of anion receptors that must be constructed to exploit the unique attributes of anions (shape, geometry, size, solvation energy, etc.). All of the applications previously explored rely on a combination of noncovalent intermolecular interactions (hydrogen bonding, anion-π interactions,

electrostatic interactions, halogen bonding, etc.) of the chosen receptors with the anion and accompanying unique physical properties to either facilitate a detection, a physiochemical change, a catalytic process, or a process of supramolecular assembly. Because of the variety of roles that they play in nature, the desire to continuously develop new materials capable of detecting, isolating, and transporting them continues to grow; concordantly, the roles that they may play in organocatalytics and templated assemblies of novel materials will doubtless be explored for many more years to come.

The role of anion chemistry in the development of several novel materials is discussed in the accompanying chapters with applications focusing on anion-directed behavior in both the solution phase and solid state. The second chapter focuses on the development of two classes of novel solution-phase anion sensors based upon the framework of tetraphenylethylene. The third chapter explores the utility of halide anions to participate in directing self-assembly of N-haloarylpyridinium substrates in the solid state. The fourth chapter features studies of the effects of coordinating and noncoordinating anions in the anion-directed assembly of tetraphenylethylene derivatives as well as attempts to synthesize additional novel solution-phase sensors based upon observations of behavior in the solid state. The final chapter will feature all of the experimental details and procedures of the preceeding chapters.

CHAPTER II

DEVELOPMENT OF UREA AND BIS-AMIDOPYRROLE-FUNCTIONALIZED TETRAPHENYLETHYLENES FOR APPLICATIONS IN ANION DETECTION

2.1 Introduction

Molecular recognition refers to a specific interaction between two molecules that may be brought about by non-covalent interactions. These interactions can range from hydrogen-bonding,[72] van der Waals forces of attraction, $\pi - \pi$ interactions,[73] halogen-bonding,[74] metal-coordination or simple electrostatic interactions. Molecular recognition plays a key role in a variety of biological systems and can also be harnessed in the development of designed materials in supramolecular chemistry that rely upon selective interactions between molecules.

In the development of molecular sensors or chemosensors, molecules are engineered for the express purpose of interacting with an analyte to produce a physical/chemical change that can be detected. Successful sensors will combine molecular recognition- the specific interaction of an analyte with a functionalized portion of the molecule- with the appending of a reporter molecule to detect the presence of the analyte.

The desire to detect anions and develop anion-binding materials is in large part due to the variety of roles that anions play in biological and environmental chemistry. Anions can be detected in numerous ways and many sensors that utilize colorimetry, chemodosimetry, fluorescent emission, molecular complexation, sol-gel formation and electrochemistry have been successfully developed. However, it is important to consider that the ideal sensor should be chemically robust, highly selective in its capacity for detection and reasonably sensitive to the presence of the target analyte.

2.2 Tetraphenylethylenes as "Turn-On" Fluorescent Sensors

Among engineered materials that detect an analyte via fluorescence emission, there are generally two types to be considered; those materials that detect an analyte through the mechanism of fluorescence quenching, and those materials that operate through a mechanism of fluorescence enhancement. These two types are referred to colloquially as "turn-off" and "turn-on" fluorescence, respectively. For solution-phase detection, turn-on fluorescence is comparatively underutilized and is particularly advantageous because it has the inherent potential for higher sensitivity to the presence of analyte.[75]

Aggregation-induced emission (AIE) is a special turn-on fluorescent phenomenon that is exhibited in several organic compounds.[76,77] In stark contrast to the vast majority of organic fluorophores, AIE-exhibiting compounds display little to no fluorescent response in dilute solutions but become considerably more fluorescent under conditions resulting in intermolecular aggregation. This can occur in the solid state or when the compounds are dissolved in poor solvents. This property can be useful in the development of fluorescent reporters capable of detecting or monitoring various binding events or chemical processes under conditions where emission from more traditional fluorophores would be quenched.

Tetraphenylethylene (TPE) possesses numerous features common to many AIE active organic molecules. TPE and its derivatives are generally non-emissive in solution as a result of the rotations of the phenyl rings along the =C-Ph axes and the conformational twisting of the C_{alkene}-C_{alkene} bond in the excited state. These operations serve as non-radiative relaxation pathways for the gradual decay of the excited state.[78] However, aggregation of the molecules leads to restriction of the essential bond rotations, resulting in a "turn-on" fluorescent response. It is these properties combined with the synthetic accessibility of TPE derivatives that have made these molecules particularly attractive as platforms for the design of novel materials capable of detecting targeted analytes such as metal ions,[79] small molecules,[80] biomolecules and explosives.[81]

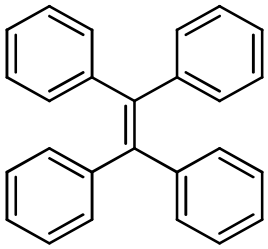

Figure 2.1. Tetraphenylethylene.

Figure 2.2 displays some examples where the "turn-on" fluorescent properties of TPE derivatives are utilized in the development of highly selective sensors. For example, B.Z. Tang and coworkers[82] developed a pyridine-substituted TPE derivative (**2.1**) that relies on the ability of trivalent metals such as Fe^{3+}, Cr^{3+} and Al^{3+} to undergo hydrolysis to form metal hydroxides and free protons which will then subsequently protonate the pyridine pendant on the TPE, displaying a unique colorimetric response.

Kato and coworkers[83] prepared a TPE derivative featuring lactose moieties installed via click-chemistry (**2.2**) that was nonfluorescent in buffered solutions, but exhibited significant fluorescence enhancement after the addition of influenza virus. It was speculated that the lactose groups were able to bind non-covalently to the viral protein coat and cause aggregation of the attached TPE units.

Chatterjee and coworkers[84] developed a TPE-phosphate sensor (**2.3**) designed for the selective detection of Pb^{2+} ions in aqueous solutions. The high affinity of phosphate for Pb^{2+} resulted in the formation of lead phosphate complexes, which would precipitate out of their solvent systems, forming a dispersed phase where aggregation occurs. The group surveyed numerous other divalent metals and discovered that their system was selective for Pb^{2+}.

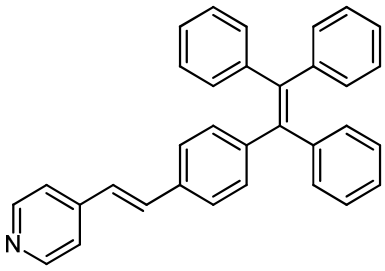

2.1

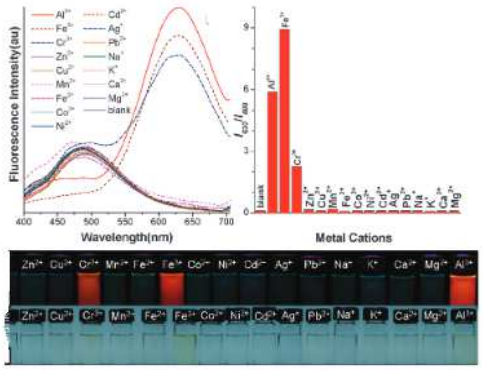

(a)

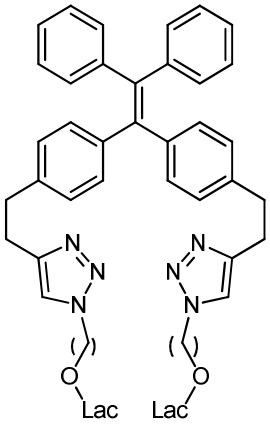

2.2

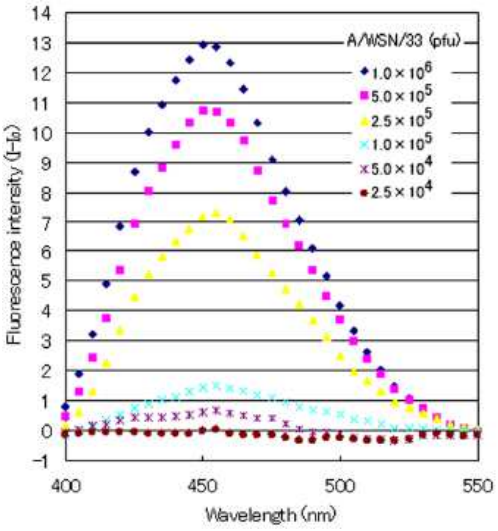

(b)

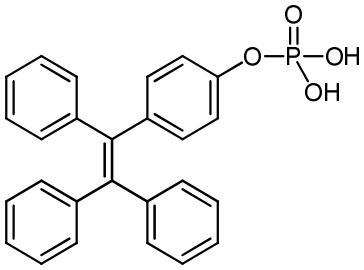

2.3

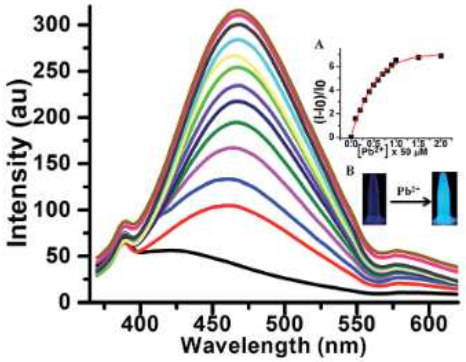

(c)

Figure 2.2. Assorted TPE derivatives employed as selective solution-phase sensors; (a) Compound **2.1** detecting trivalent metal cations. (b) Compound **2.2** with lactose units as detecting functionality for influenza virus A. (c) Compound **2.3** functionalized with phosphate for selective detection of Pb^{2+} ions.

The Pigge group has an active interest in exploring the versatility of tetraphenylethylene derivatives in supramolecular assemblies that has culminated in the development of robust TPE-based semiconductors comprising tetracarboxylated TPEs and bis(pyridines);[85] halo-benzoyl TPE esters that participate in supramolecular self-assembly through directed halogen bonding interactions;[86] and tetrapyridyl-substituted TPEs[87] that form extended 2D metal-organic networks with zinc salts and tunable halogen-bonding networks with iodoperfluoroarenes.

Current work has subsequently turned to attempting to utilize the AIE properties of tetraphenylethylene derivatives to develop robust and synthetically accessible solution-phase anion sensors.

2.3 Objectives

We recognized that the capacity of TPE derivatives to function as anion sensors was a concept that was relatively unexplored and have developed two classes of TPE-based compounds that incorporate urea and amido-pyrrole functionalities, respectively. We hypothesized that the operative mechanism of AIE in these systems would be enabled through hydrogen-bonding interactions of acidic hydrogen species within the urea and amido-pyrrole moieties with select anions in solution and the selectivity would likely be modulated by the relative basicity of the anions. While this predicted selectivity trend appeared to hold true for the urea-functionalized series, the amido-pyrroles behaved altogether differently; the amido-pyrrole based TPE sensors were initially developed with the intention of acting as selective sensors for dicarboxylate anions, as there have been reports in the literature[88] of such functionalized systems acting in such a capacity, though never in "turn-on" fluorophores or TPE-based systems. Surprisingly, we discovered that the amido-pyrrole functionalized TPEs displayed little to no fluorescent response toward select dicarboxylates but displayed considerable selectivity for pyrophosphate anions; while a handful of TPE-based pyrophosphate detectors are known, our series showcases sensors that are synthetically accessible, electronically neutral and do not require metal ions as cofactors in subsequent aggregation-induced emission.

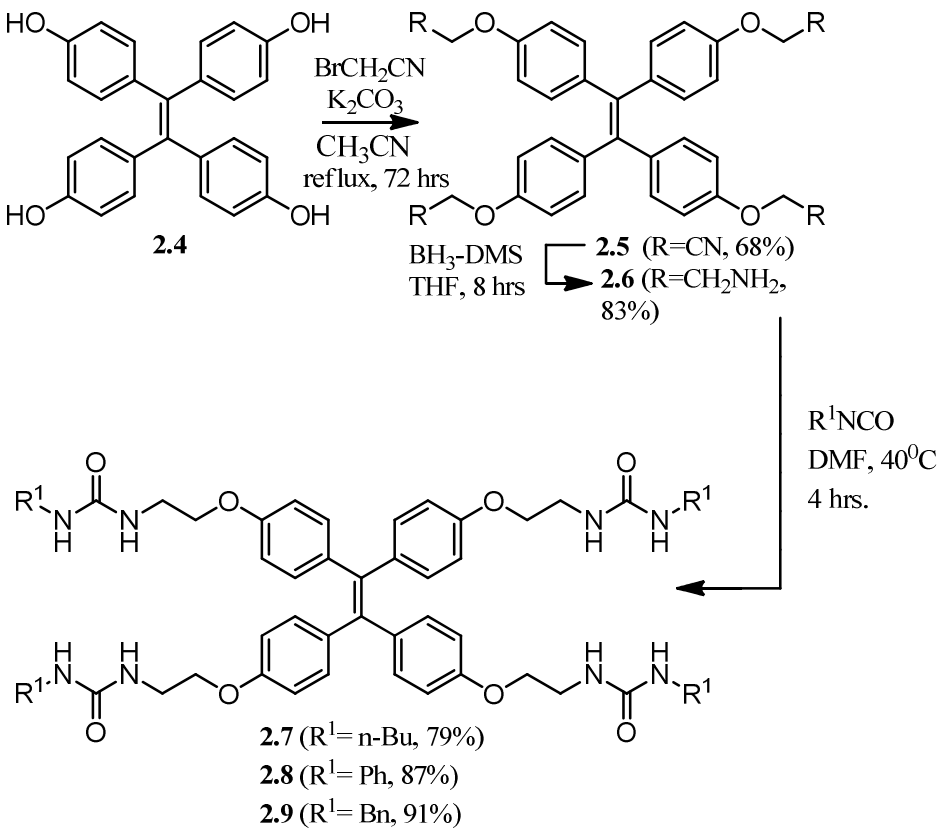

Scheme 2.1. Synthesis of TPE-urea derivatives **2.7**-**2.9**.

2.4 Results and Discussion

Synthesis of urea-functionalized tetraphenylethylenes (compounds **2.7**, **2.8**, and **2.9**) was accomplished in a simple and straightforward manner starting with the preparation of compound **2.4** from previously established methods.[89] Alkylation of **2.4** with bromoacetonitrile under basic conditions and gentle refluxing for 3 days afforded **2.5** in moderate yield. Reduction of the tetra(nitrile) with an excess of borane-dimethyl sulfide in THF over 8 hours afforded the tetra(amine) **2.6** in good yield. Treatment of **2.6** with an excess (8 equivalents) of n-butyl-, phenyl- and benzylisocyanate in DMF under mild conditions afforded the tetraureas **2.7**, **2.8** and **2.9,** respectively. The urea-functionalized TPEs are insoluble in water and only sparingly soluble in nonpolar organic solvents but they are easily isolated via evaporation of DMF and trituration of the solid products with cold THF. The ureas were subsequently characterized by NMR and HRMS.

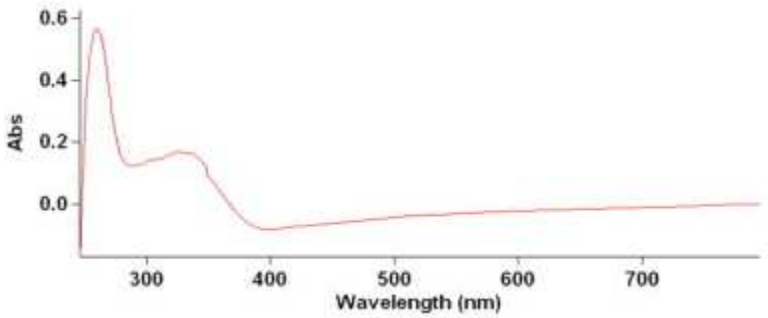

a)

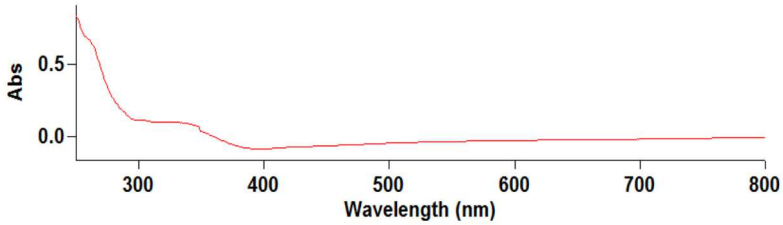

b)

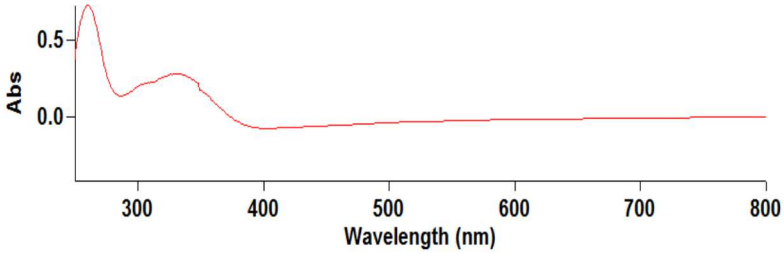

c)

Figure 2.3. UV-visible absorption spectra of tetra(urea) TPE compounds. All spectra were collected with compounds in THF solvent containing 0.15% v/v DMSO (a) Compound **2.7** (12.5 μM) (b) Compound **2.8** (8.0 μM) (c) Compound **2.9** (10 μM).

UV-visible absorption spectra were taken for the tetra(urea) TPEs and each were determined to have a broad absorption range with maximum absorption at ~350 nm (Figure 2.3). Fluorimetric studies were subsequently carried out for each of the three urea-TPE derivatives to qualitatively assess the degree of fluorescent enhancement when Bu_4N^+ salts of select anions were introduced. The urea derivatives were analyzed in solutions of THF with 0.15% v/v DMSO added for purposes of aiding solubility.

As has been a unifying characteristic of tetraphenylethylene derivatives, the urea-TPE derivatives are weakly fluorescent under dilute conditions in the previously

indicated solvent system, but fluorescence markedly increases upon the addition of water as an antisolvent, illustrative of the fluorescence enhancement of the aggregation process.

Stoichiometric amounts of Bu_4N^+ salts of select anions were added to each urea-TPE derivative in solution (Figure 2.4), as well as excess amounts (6 equivalents) to qualitatively assess the affinity of the TPE sensors and determine if the relative affinity for each anion was affected by their abundance (Figure 2.5). In each experiment, we discovered that the presence of added anion significantly enhanced the fluorescent emission relative to the respective controls (sensors in solution absent any added anions). The fluorescence enhancement is attributed to aggregation of multiple urea-TPE conjugates around the anion centers (AIE).

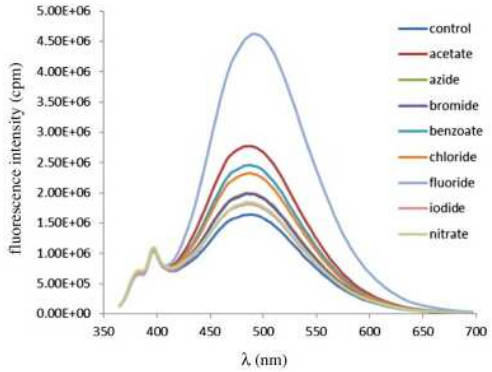

(a)

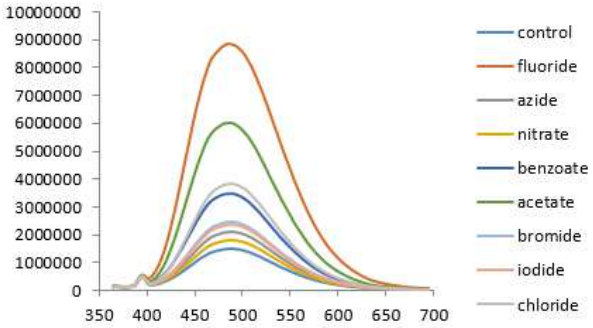

(b)

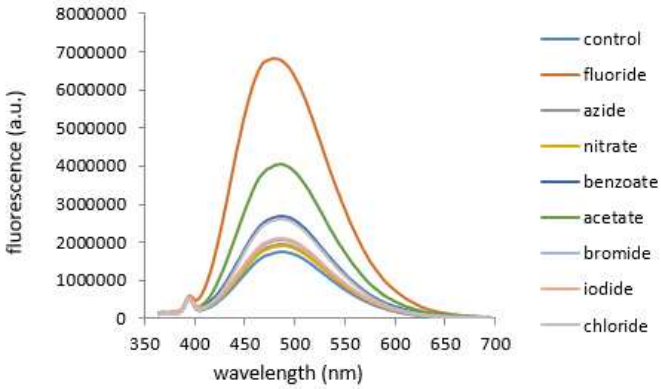

(c)

Figure 2.4. Overlay of fluorescent spectra urea-TPEs in the absence (control) and the presence of select anions (1 equivalent) added as $[Bu_4N]^+[X^-]$ salts. All fluorescence spectra were collected in THF with 0.15% v/v DMSO (a) Compound **2.7** (12.5 μM; λ_{ex} = 355 nm). (b) Compound **2.8** (11.6 μM; λ_{ex} = 355 nm). (c) Compound **2.9** (10.3 μM; λ_{ex} = 355 nm).

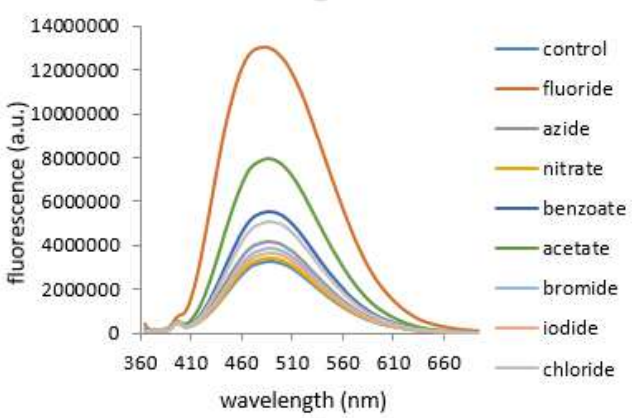

(a)

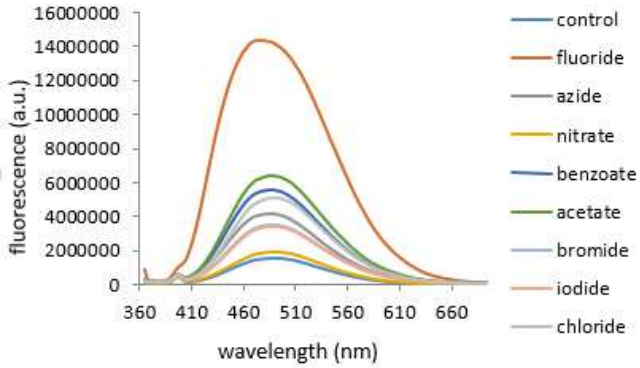

(b)

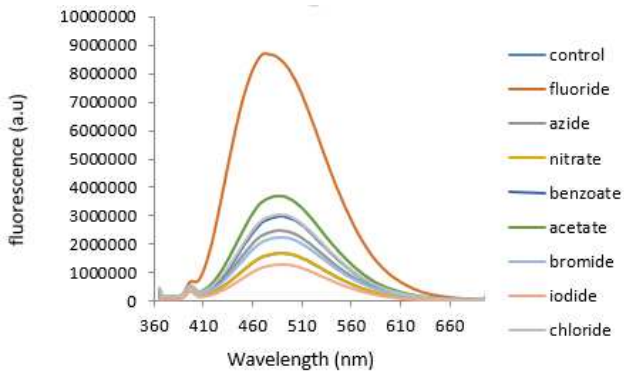

(c)

Figure 2.5. Overlay of fluorescence spectra of urea-TPEs in the absence (control) and the presence of select anions (6 equivalents) added as $[Bu_4N]^+[X^-]$ salts. All fluorescence spectra were collected in THF with 0.15% v/v DMSO (a) Compound **2.7** (12.5μM; λ_{ex} = 355 nm). (b) Compound **2.8** (11.6μM; λ_{ex} = 355 nm). (c) Compound **2.9** (10.3μM; λ_{ex} = 355 nm).

As Figures 2.4 and 2.5 also indicate, the magnitude of fluorescence enhancement varies as a function of anion, with fluoride providing the largest increase in fluorescence upon addition. In descending order, the anions that elicit the most response from the urea-TPE sensors are acetate, benzoate and chloride with azide, nitrate, bromide and iodide showing modest enhancement compared to the control, though decidedly more pronounced after the addition of 6 equivalents. The AIE response in the urea-TPE sensors correlates well with basicity and hydrogen-bonding capacity of the respective ions with the most basic anions eliciting the most profound responses. This observation also affirms our hypothesis that the urea-anion hydrogen bonding is the principal interaction leading to supramolecular aggregation.

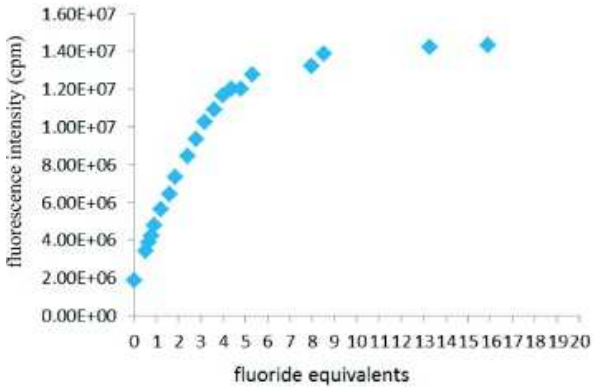

(a)

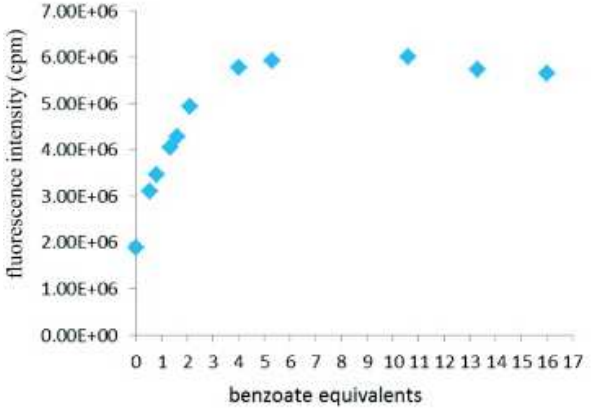

(b)

Figure 2.6. Plots of fluorescence intensity of **2.7** monitored at λ_{em} = 485 nm. Fluorescence titrations with addition of (a) fluoride and (b) benzoate anions with concentration of **2.7** remains constant at 12.5 μM; λ_{ex} = 355 nm.

As a further probe into the sensing potential of these compounds, fluorescence titration experiments were carried out with tetrabutylammonium salts of the fluoride and benzoate anions. Figure 2.6 depicts plots of fluorescence intensity of **2.7** monitored at λ_{em} = 485 nm as a function of increasing amounts of added anion (at a constant concentration of **2.7**).We discover that there is a sharp increase in the fluorescence intensity upon the addition of the first few equivalents of anion, but the intensity change quickly levels off around the 4-6 equivalent addition point. We surmise that the TPE-sensor approaches saturation at this point and the limit of aggregation is reached. Fluoride is a considerably

more basic anion than benzoate and is spherical in nature, yet we discover that basicity and anion shape has little to no bearing on the sensing capacity of these sensors.

As an additional probe into the mechanism of anion-binding and subsequent aggregation in the urea-TPE sensors, ^{1}H NMR titration experiments were carried out on compounds **2.7**, **2.8** and **2.9** in d_6-DMSO with monitoring of the urea N-H resonances in the presence of increasing amounts of TBAF and TBACl as depicted in figures 2.7 and 2.8, respectively.

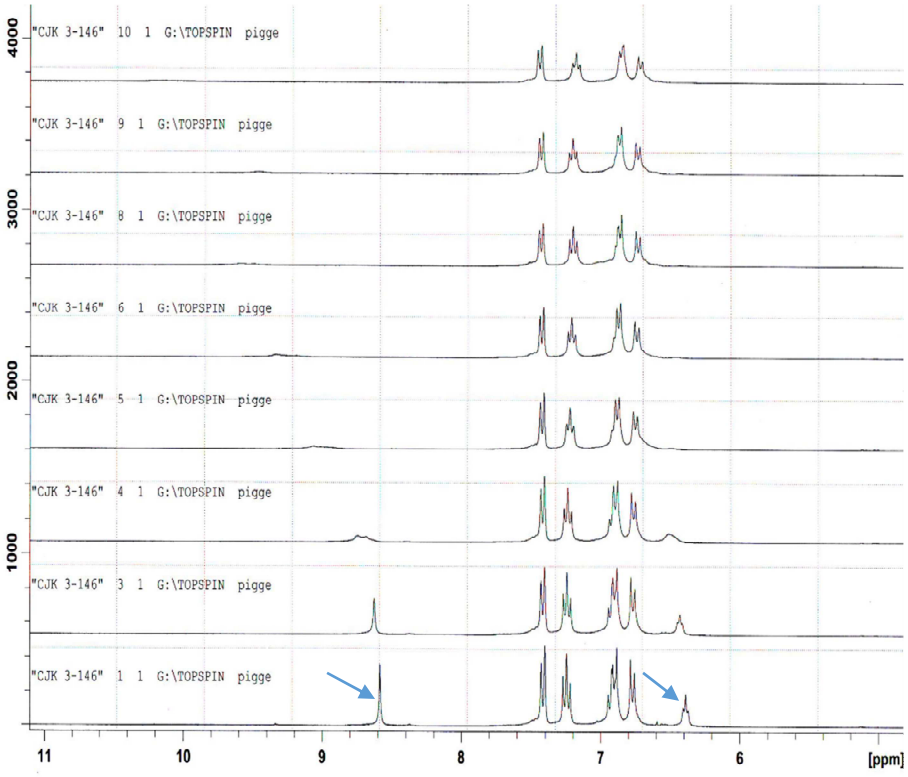

Figure 2.7. ^{1}H NMR (300 MHz, DMSO-d_6, δ in ppm) titration spectra of compound **2.9** first in the absence (control) and presence of increasing equivalents of TBAF (prepared in THF). From bottom to top, recorded spectra show results after the addition of 0 (control), 0.1, 0.2, 0.4, 0.5, 0.7, 1.0 and 1.3 equivalents, respectively. N-H peaks of interest are indicated with blue arrows.

To test our hypothesis that the operative mechanism of AIE for the urea-TPEs was the hydrogen-bonding interactions between each anionic species and the relatively acidic N-H bonds of the urea moieties, a set of NMR experiments was devised to monitor characteristic N-H resonances of these systems after the addition of increasing amounts of anion. The urea-TPE sensors were analyzed in d_6-DMSO with TBAF in THF added to the NMR tube. As Figure 2.7 shows, the resonances observed shift considerably far

downfield with increasing amounts of TBAF added to the NMR sample tube and nearly coalesce after the addition of more than 0.5 equivalents to the urea-TPE sensor. Initial concerns over the potential of such a strongly basic anion as fluoride to deprotonate the sensor via the acidic N-H moiety were stemmed by the lack of a distinctive bifluoride (HF_2^-) peak in the ^{19}F NMR spectrum (measured relative to TBAF as a F^- standard at -98 ppm; bifluoride appears at -148 ppm)[90] and the lack of any distinguishing changes in the fluorescence emission spectrum.

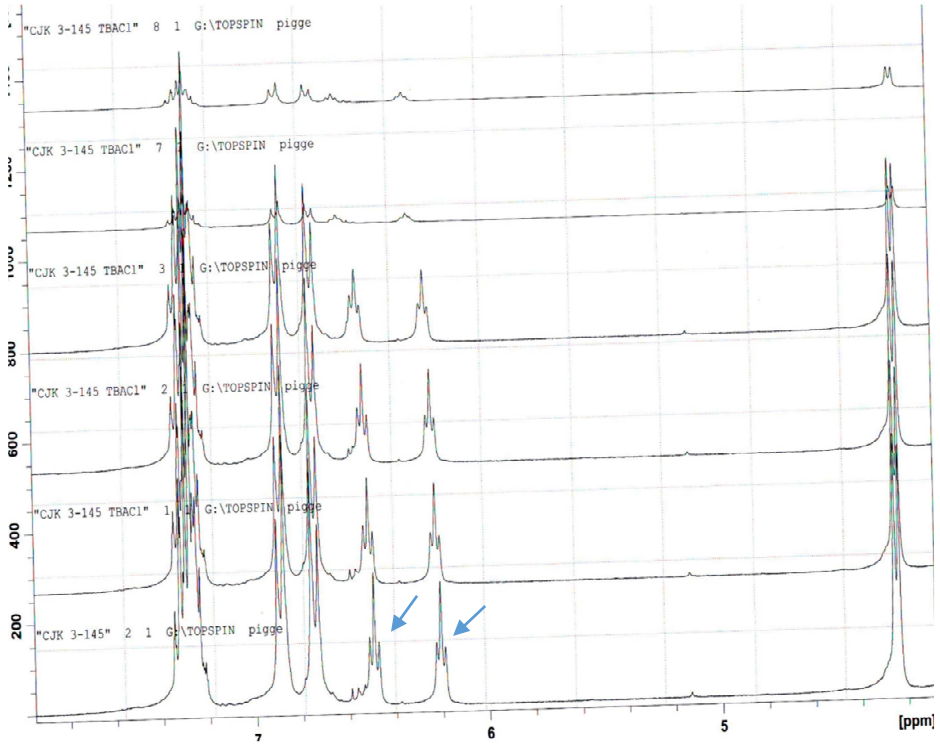

Figure 2.8. ^1H NMR (300 MHz, DMSO-d_6, δ in ppm) titration spectra of compound **2.8** first in the absence (control) and presence of increasing equivalents of TBACl (prepared in THF). From bottom to top, recorded spectra show results after the addition of 0 (control), 0.2, 0.4, 0.5, 0.7, 1.0 equivalents, respectively. N-H peaks of interest indicated with blue arrows.

Similar titration experiments were performed using TBACl as an anion source with the salt dissolved in THF and added to d_6-DMSO solutions of urea-TPE sensors in an NMR tube. Figure 2.8 depicts the N-H resonances of the urea moiety in **2.8** shifting downfield upon increasing addition of TBACl. As with the titrations using TBAF, the resonances shift noticeably downfield, though the effect is considerably less pronounced

than that observed with the addition of TBAF. We attribute these observations to the lower basicity of the chloride anion relative to fluoride anion. The NMR titrations serve to further confirm our hypothesis that interaction of the anion with acidic H-bond donors of the urea moieties in the TPEs is the operative mechanism of detection and subsequent AIE effects.

2.5 2-amido pyrrole-functionalized TPE sensors- synthesis

2-amidopyrrole-functionalized TPE sensors were developed according to Scheme 2.2. Compounds **2.10**[91] and **2.11**[92] were prepared according to literature methods. These compounds were then subjected to radical halogenation to yield brominated derivatives **2.12** and **2.13**. Starting from these compounds, divergent synthetic pathways were followed to yield the desired products

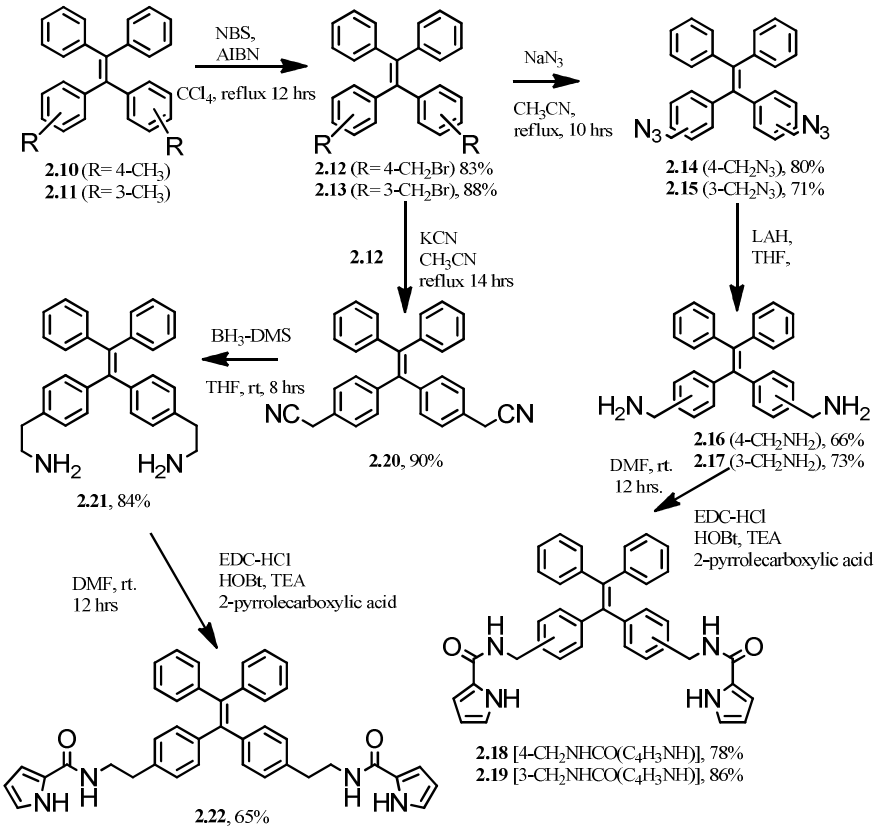

Scheme 2.2. Synthetic pathways to a new class of amido-pyrrole functionalized TPE sensors.

First, compounds **2.12** and **2.13** underwent azide substitution to yield **2.14** and **2.15**, which were then subsequently reduced by excess lithium aluminum hydride to produce amines **2.16** and **2.17**. These compounds underwent EDC-HCl-mediated coupling with 2-pyrrolecarboxylic acid to produce 2-amido-pyrrole substituted TPE sensors **2.18** and **2.19**, with each bearing a different substitution pattern off of the core TPE structure (4-substituted **2.18** and 3-substituted **2.19**).

Compound **2.12** underwent S_n2 substitution with cyanide nucleophile to yield **2.20** in good yield. This compound was subsequently reduced with borane-dimethyl sulfide complex to yield **2.21**. The amine was then subjected to EDC-HCl-mediated coupling with 2-pyrrolecarboxylic acid to afford the desired 2-amido-pyrrole substituted TPE in moderate yield.

Compounds **2.18**, **2.19** and **2.22** were originally synthesized with the intention of probing the utility of the 2-amidopyrrole moiety in TPE frameworks for "turn-on" sensing of dicarboxylates, which are of considerable importance in chemical and biological systems. Caballero and coworkers[93] developed a unique class of sensors that utilized ditopic 2-amidopyrrole receptors separated by an aromatic spacer with an appended fluorophore such as dansyl or acridine. Their results demonstrated "turn-off" fluorescence responses in their sensors in the presence of dicarboxlates. While sensors for these classes of compounds are in demand there are relatively few classes of sensors that have been developed with "turn-on" fluorescence response and to our knowledge, none that are based on the TPE framework as an operant fluorophore.

Interestingly, we discovered that these sensors afford little to no fluorescence response in the presence of dicarboxylates, but they were notably selective to the presence of pyrophosphate anions. While a couple of TPE-based pyrophosphate sensors have been reported,[94,95] the compounds described herein are electronically neutral, arguably more synthetically accessible, and do not require the presence of metal cofactors to exhibit the AIE fluorescence response.

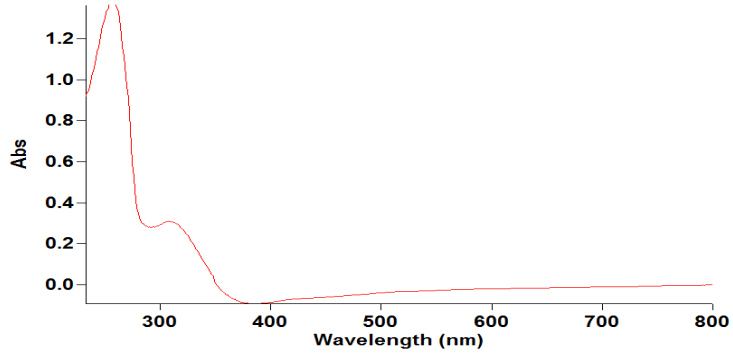

(a)

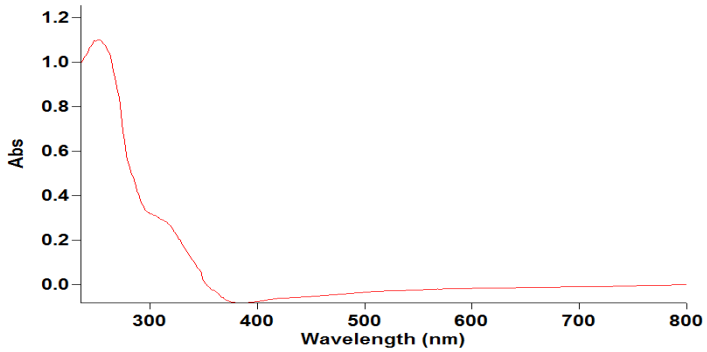

(b)

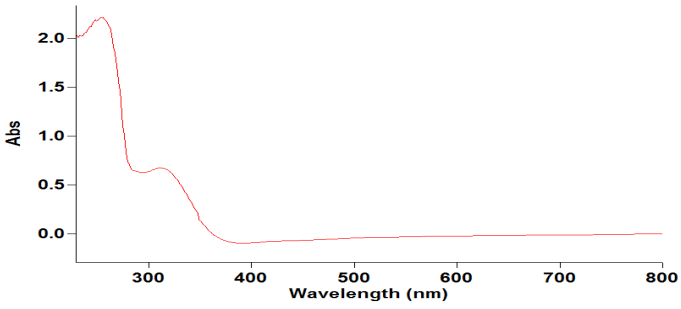

(c)

Figure 2.9. UV-visible absorption spectra of bis(amido-pyrrole) TPE compounds. All spectra were collected with compounds in THF solvent containing 0.15% v/v DMSO (a) Compound **2.18** (12.5 µM) (b) Compound **2.19** (17.4 µM) (c) Compound **2.21** (25.2 µM).

2-amidopyrrole-functionalized TPE sensors have very similar absorption spectra compared to the previously mentioned urea-TPE sensors, with the longest wavelength absorbance responses in the 300-340 nm range (Figure 2.9). The compounds are sparingly soluble in nonpolar organic solvents and moderately soluble in solvents such as DMF, acetonitrile and THF.

Fluorimetric experiments were conducted in a similar manner as previously described in this chapter, with Bu_4N^+ salts of select anions added to a fluorescence cuvette containing an amidopyrrole-TPE sensor in THF. With the exception of pyrophosphate, which possessed tributylammonium as its counterion, all other anion sources had tetrabutylammonium as the counterion. Tetrabutylammonium salts of malonate, succinate, and glutarate were synthesized according to previously published procedures.

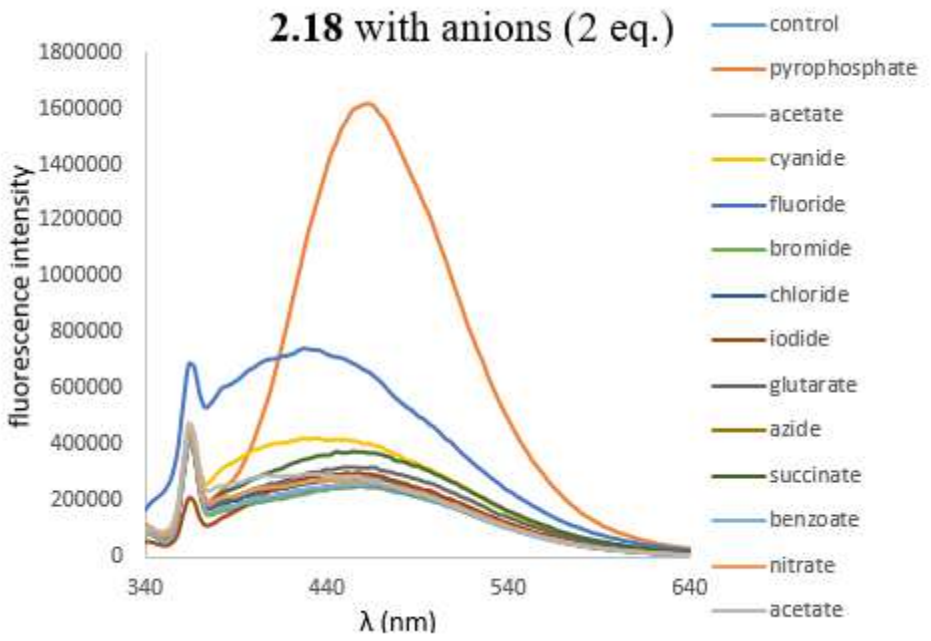

(a)

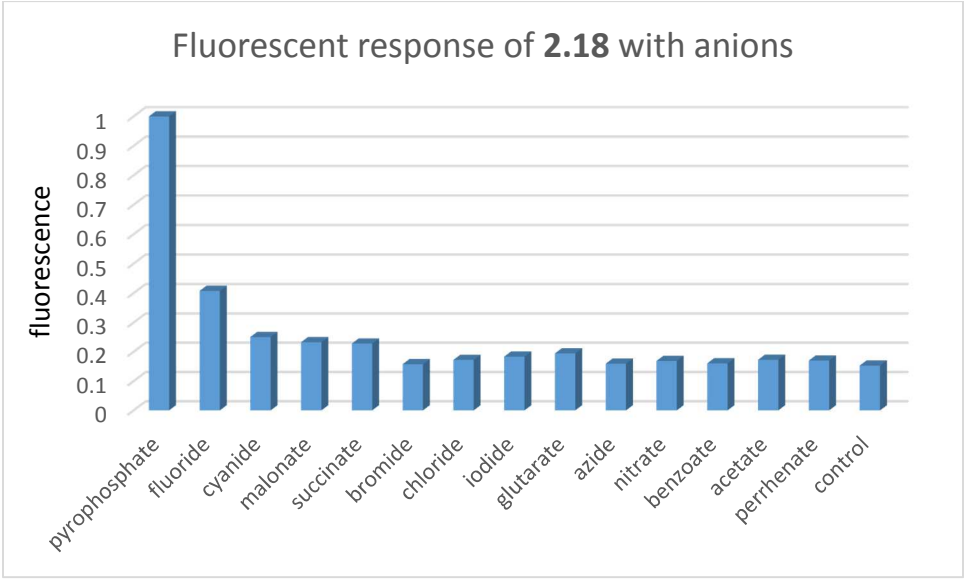

(b)

Figure 2.10. (a) Overlay of fluorescence spectra of **2.18** in THF in the absence of (control) and presence of select anions (2 equivalents) (b) relative fluorescence intensity at λ_{em} = 454 nm of **2.18** in the presence of various anions anions and control. [**2.18**] = 12.5 μM; λ_{ex} = 330 nm.

The fluorescence responses of **2.18** in solution in the presence of select anions is depicted in Figure 2.10. Dicarboxylate anions such as glutarate, malonate and succinate displayed a modest amount of fluorescence enhancement after addition of 2 equivalents, but there was little difference between the dicarboxylate anions and spherical anions such as bromide and chloride, and similarly monocarboxylates anions such as acetate or benzoate. The sensor does appear to be relatively selective for pyrophosphate. While there is a considerable fluorescent response for fluorine, the experimental results show a hypsochromic shift in emission λ_{max} from 454 nm to 430 nm. We hypothesize that the fluoride anion is sufficiently basic to deprotonate the pyrrole-TPE sensor, with the pyrrole N-H hydrogen possessing a pKa value of ~21. ^{19}F NMR monitoring of the sensor in the presence of increasing amounts of TBAF show an emerging signal at -148 ppm (F^- as an internal standard; -98 ppm) which is indicative of the formation of bifluoride anion HF_2^-. ^1H NMR monitoring under these conditions also shows the stark disappearance of amido and pyrrolic N-H resonances with the addition of TBAF in THF. It should be noted that the previously discussed urea-TPEs exhibit considerable downfield shifting and broadening in the urea N-H resonances, but do not completely coalesce.

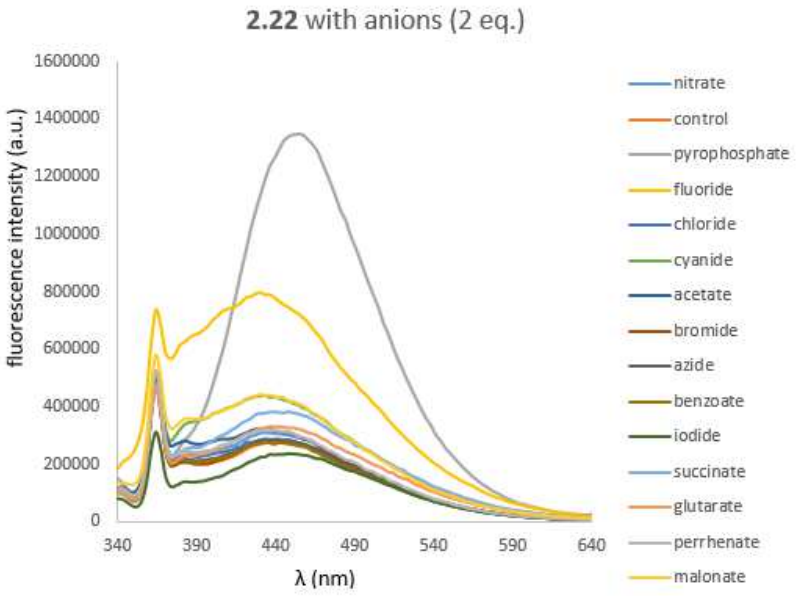

(a)

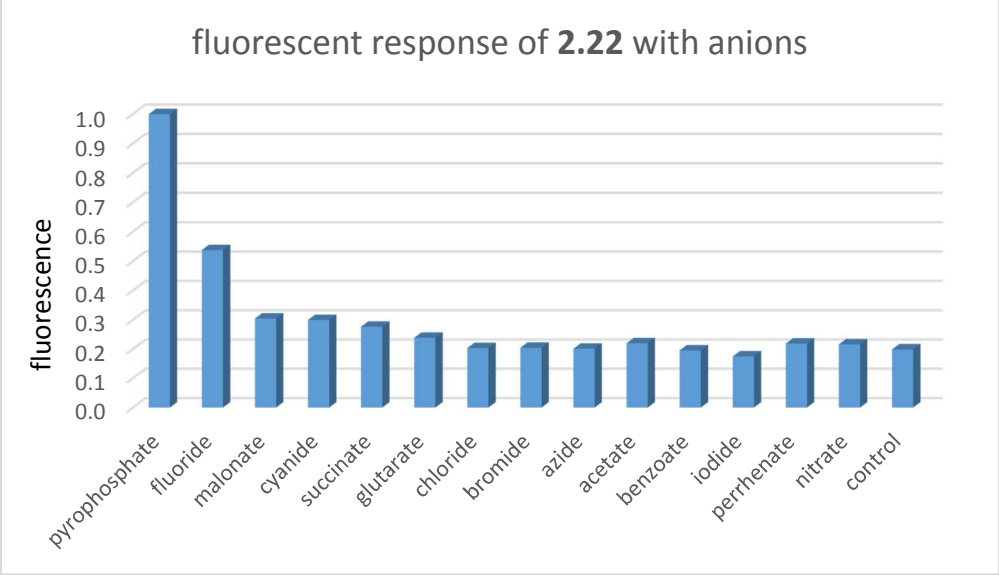

(b)

Figure 2.11. (a) Overlay of fluorescence spectra of **2.22** in THF in the absence of (control) and presence of select anions (2 equivalents) (b) fluorescence intensity at λ_{em} =454 nm of anions added to **2.22** (normalized to pyrophosphate) and control. [**2.22**] = 25.2 μM; λ_{ex} = 330 nm.

Fluorimetry results for anion tests with **2.22** display similar results to **2.18** with the sensor displaying notable selectivity for pyrophosphate anion and a similar hypsochromic shift in emission λ_{max} for fluorine (shift from 454 nm to 430 nm). The chain length of one extra carbon on each arm of the amidopyrrole-TPE sensor does not

appear to affect the sensitivity of this sensor to the presence of pyrophosphate as the fluorescent responses of **2.18** and **2.22** to pyrophosphate are approximately similar (fluorescent enhancement of ~5 times compared to respective control experiments.

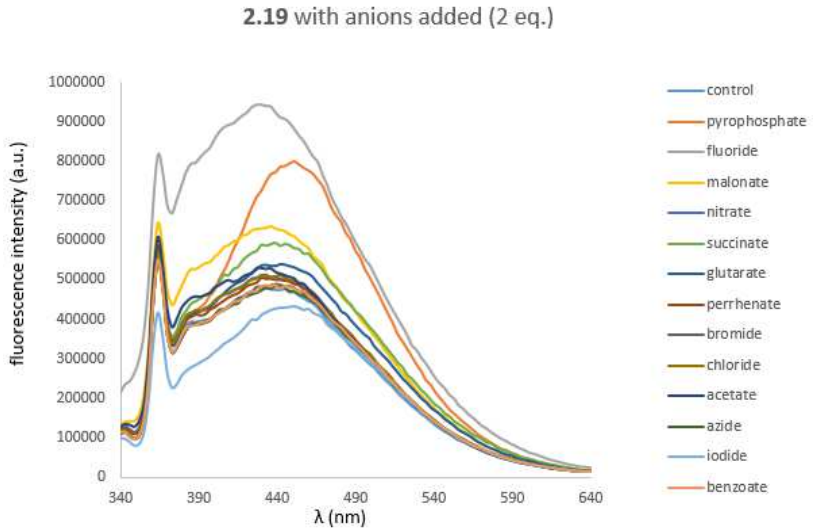

Figure 2.12. Overlay of fluorescence spectra of **2.19** in THF in the absence of (control) and presence of select anions (2 equivalents). **[2.19]** = 17.4μM; λ_{ex} = 330 nm.

Figure 2.12 depicts fluorescence data for compound **2.19** with the anion series. Again, the fluorescent responses of the anions are very similar to the compounds previously described. However, it should be noted that the fluorescent responses are relatively muted compared to **2.18** and **2.22**, indicative of a lower sensitivity of **2.19** for these anions. For example, pyrophosphate displays fluorescence enhancement of only ~2 times compared to fluorescence recorded in control experiments and the addition of F^- results in the greatest response from the sensor, which is still hypothesized to represent a deprotonation event, consistent with our observation of a hypsochromic shift at ~ 20 nm.

We hypothesize that the difference in the substitution pattern of the 2-amidopyrrole receptor arms attached to the TPE core (3,3', compared to 4,4' for **2.18** and **2.22**) may be responsible for this observation; the accepted mechanism of AIE in tetraphenylethylene derivatives requires the constraint of phenyl ring rotations around the =C-Ph bonds. In solution, the phenyl rings can rotate freely about this bond and substituents in the –para position are largely unaffected by this rotation. Substituents in

the –meta positions of the phenyl rings of the TPE core are however largely affected by this rotation and the sensitivity of prospective sensors toward select analytes may largely be blunted in the face of considerably higher entropic barriers

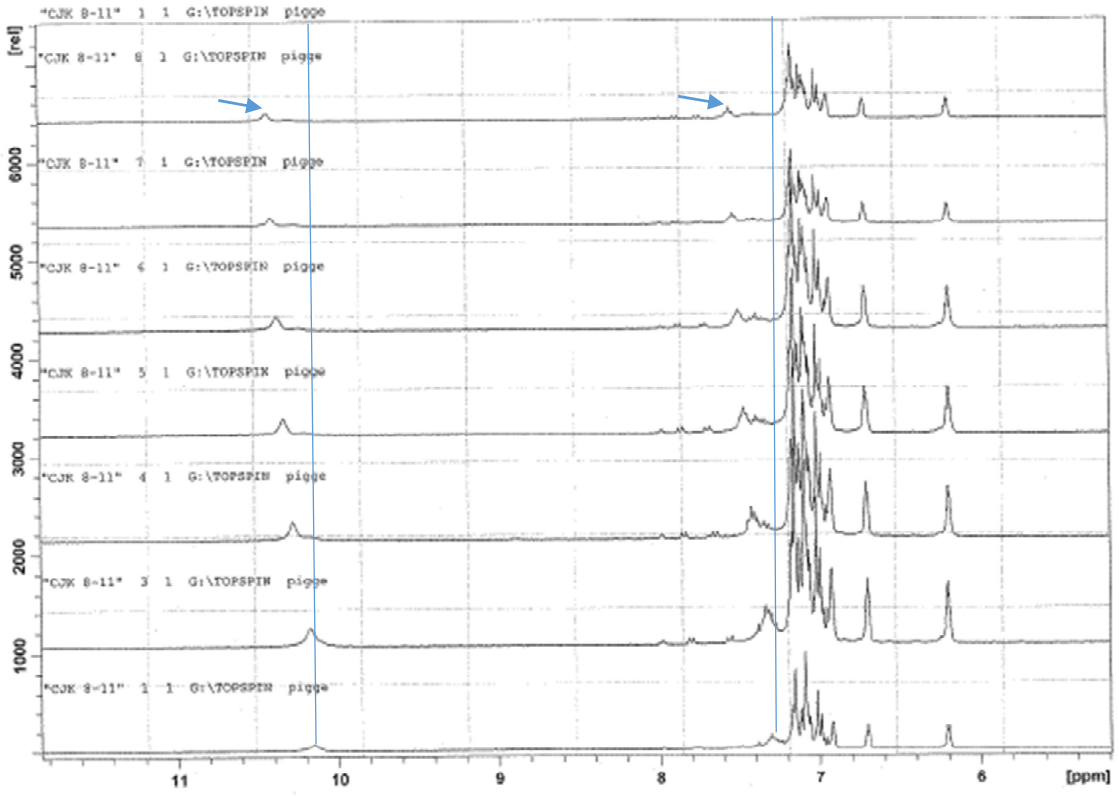

Figure 2.13. ^{1}H NMR (300 MHz, CD_3CN, δ in ppm) titration spectra of compound **2.18** first in the absence (control) and presence of increasing equivalents of $H_2P_2O_7^{2-}$ (prepared in CD_3CN, added as a tributylammonium salt). From bottom to top, recorded spectra show results after the addition of 0 (control), 0.1, 0.2, 0.3, 0.4, 0.5, 0.6 equivalents, respectively. N-H peaks of interest are indicated with blue arrows and blue lines of demarcation indicate how far each signal shifts.

As with the tetra-substituted urea-TPE sensors **2.7**-**2.9**, we set out to elucidate the method of anion coordination that the amido-pyrrole-TPEs will utilize to recognize pyrophosphate through a series of NMR titrations. Figure 2.13 depicts the movement of the pyrrole N-H (at 10.18 ppm, initially) and the amido-NH (at 7.40 ppm, initially) downfield in the presence of increasing amounts of pyrophosphate. We attribute the

movement of both of these resonances to be indicative of a binding event to pyrophosphate.

2.6 Summary

Two new classes of TPE-based anion sensors have been developed. The two classes are divided into urea-based TPE sensors and 2-amidopyrrole-based TPE sensors with interactions of the anions with relatively acidic N-H resonances within the sensors serving as the proposed mechanism leading to "turn-on" AIE responses for each class of sensors.

The urea-based TPE sensors[96] display a sensitivity to anions that largely reflects their relative basicity with fluoride producing the greatest response and anions such as azide and nitrate producing the smallest response. The sensors developed are synthetically accessible, robust and versatile and can be reasonably compared to similar TPE-based materials that have since been developed.[97]

The 2-amidopyrrole-based TPE sensors display a notable selectivity for pyrophosphate anions in solution analysis and represent the first class of TPE derivatives to utilize 2-amidopyrrole moieties as a selective anion sensor. These compounds also represent the first known example of TPE-based pyrophosphate sensors that are electronically neutral and do not require metal cofactors to elicit the "turn-on" fluorescent response.

CHAPTER III
CHARGE-ASSISTED HALOGEN BONDING IN BROMO-AND IODOPHENYLPYRIDINIUM CHLORIDES

3.1 Introduction to Halogen Bonding

The study of halogen bonding interactions has been of great interest in the field of supramolecular chemistry because of their remarkable capacity to facilitate molecular recognition and self-assembly processes in the solution phase[98,99] and the solid state.[100,101,102] While knowledge of their utility in these processes has been growing steadily over the past 15 years, their niche in supramolecular chemistry is relatively small compared to that of studies involving hydrogen bonding interactions.

While the ability of halogens to form well-defined adducts to electron donor species has been well-known for more than a century,[103,104] it was only after the development of more detailed theories of electron donor-acceptor complexes and intermolecular attractions that the concept of halogen bonding had a proper framework.

In 1954 Hassel's group published an X-ray crystallographic study of a halogen bond interaction that revealed a 1:1 adduct of 1,4-dioxane with bromine.[105] The O-Br distance in the crystal was measured to be 2.71Å, approximately 81% of the sum of the van der Waals radii of O and Br (3.35Å) with the O-Br-Br bond angle approaching linearity (near 180^0, Figure 3.1) . Thus, this was the first visual example that displayed the characteristic properties of a halogen bond; short interatomic distances and near-linear angles of interaction.

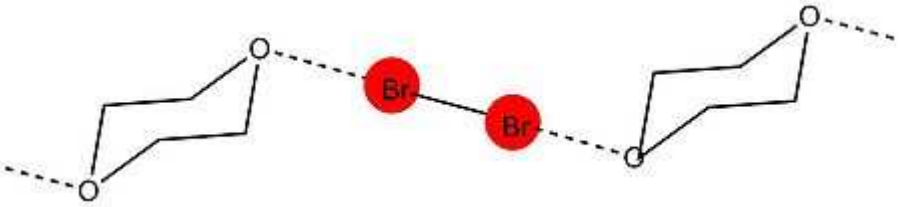

Figure 3.1. Molecular bromine (Br_2) halogen bonding interactions with 1,4-dioxane indicated with dashed lines

In the simplest sense, halogen bonding can be considered as an electrostatic attraction between an electrophilic halogen bond donor and a Lewis base halogen bond acceptor.[106] Extensive computational studies and experimental confirmations have shown that organohalogens have a halogen bond donor ability that follows the order of RI> RBr > RCl >> RF that follows as a direct consequence of the increasing polarizability of the heavier, more electron-rich halogens.[107,108] Many organohalogens feature an uneven distribution of electron density about the halogen that presents a region of positive electrostatic potential opposite the C-X bond axis. This electrostatic potential can be enhanced by increasing the s-character of the carbon hybridization, i.e. $Csp^3 < Csp^2 <$ Csp,[109] by incorporating electron-withdrawing substituents on the molecule,[110,111] or introducing a positively charged heteroatom adjacent to the XB donor.[112] Potential donors without these modifications are typically considered "unactivated."

The substitution of tetrafluoromethane with increasingly strong halogen bond donors outlined in Figure 3.2 showcases the prominence of an increasingly positive electrostatic potential along the C-X bond axis (designated as a "σ-hole") with electron-rich halogen bond acceptors forming associations via $n \rightarrow \sigma^*$ interactions.[113] The highly directional nature of this interaction implies that strong halogen bonding interactions between donors and acceptors tend to approach linearity with respect to the C-X bond on the halogen bond donor (180^0).

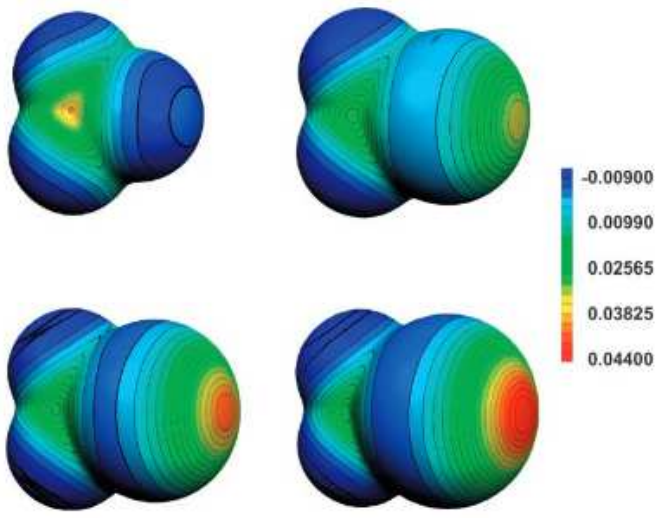

Figure 3.2. Surface potential of halogen-bond donors as a function of halogen substitution of CF_3X, represented in hartrees; (a) X =F; (b) X= Cl; (c) X = Br; (d) X=I

While relatively simple unactivated organohalogens are not particularly noteworthy XB donors, perfluoro-iodoarenes,[114] perfluoro-iodoalkanes[115] and iodo-alkynes[116,117] are recognized as among the best halogen bond donors. This is attributed to two principal factors; the inclusion of iodine as a halogen bond donor and the position of electron-withdrawing fluorine substituents, thereby enhancing the halogen bond donor capability of iodine. Architectures incorporating these elements have proven to be particularly effective in the directed assembly of materials in the solid state and are noted for their wide degree of applicability.

Resnati and coworkers[118] have successfully incorporated perfluoro-iodoarene tectons into solid state organic synthesis by utilizing perfluoro-iodoaryl ethers as halogen bond donors to template assembly of *trans*-1,2-bis(4-pyridyl)ethylenes as halogen bond acceptors through the lone pair electrons of the nitrogen atom. The bispyridyl ethylenes are aided in their assembly by intramolecular π-π stacking interactions of perfluoro-iodo aromatic rings with distances ranging from 3.55 Å to 3.92 Å. The intermolecular I···N distances range from 2.80 Å -2.82 Å (~21% the sum of the van der Waals radii of iodine and nitrogen; 3.53 Å) indicative of fairly strong halogen bonding interactions. The strength of halogen bonds often is indicated using a ratio, denoted "R", which is the ratio of the distance between two potentially interacting atoms and their van der Waals radii. Typically, the lower this value, the greater the strength of the halogen bond. The combination of intermolecular halogen bonding and intra- and intermolecular π-π stacking interactions allow for synthesis of tetrakis (4-pyridyl)cyclobutane via 2+2 photodimerization reactions (Figure 3.3).

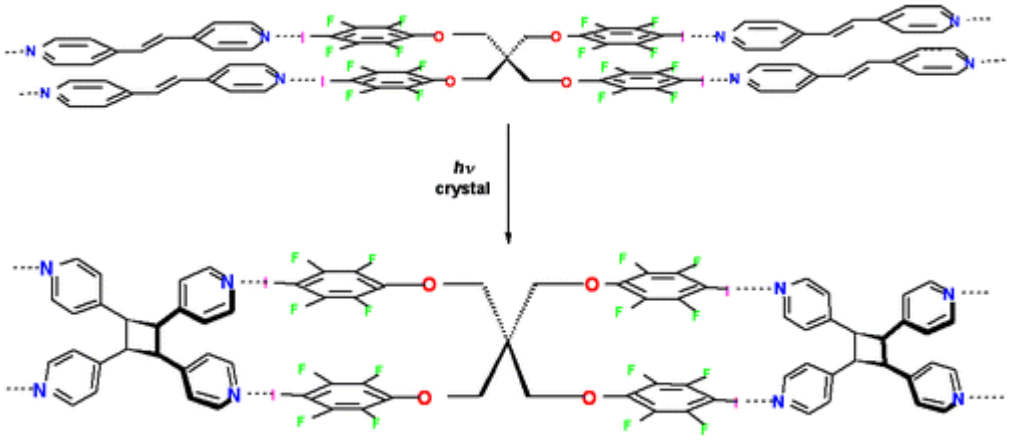

Figure 3.3. Incorporation of perfluoro-iodo arene tectons in directed assembly of *trans*-1,2-bis(4-pyridyl)ethylenes and subsequent [2+2] photodimerization to synthesize tetrakis(4-pyridyl)cyclobutane in the solid state. Reprinted with permission from Resnati et al, copyright (2004) by the American Chemical Society.

Perfluoro-iodoarenes can also be reliably incorporated into self-assembly of organic materials where the potential for competing intermolecular hydrogen-bonding interactions becomes a concern. Åakeroy and coworkers[119] examined this in their study of a series of co-crystals incorporating 1,4-diiodotetrafluorobenzene (DITFB) and 2-aminopyrazine. Through a combination of halogen- and hydrogen-bonding interactions, a network of 1D chains are assembled through self-complementary dimerization of the aminopyrazines via N-H···N hydrogen bonding and I···N halogen bonding where the halogen bonding interaction must be able to compete with secondary N-H···N interactions to form the expected network (Figure 3.4). These types of studies lend a great degree of insight into the variety of interactions that will either compete with or complement halogen-bonding in the engineering of ever more complex materials.

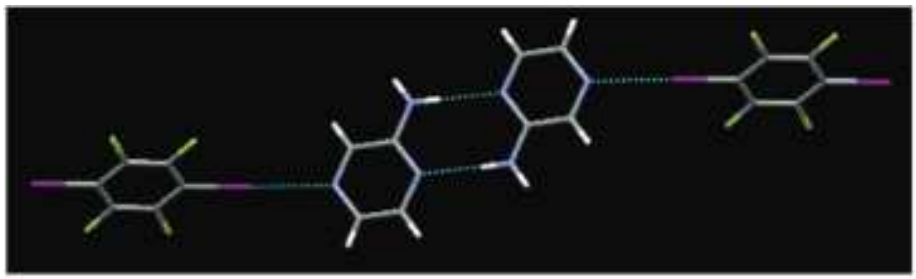

Figure 3.4. Formation of 1D network in a cocrystal of DITFB and 2-aminopyrazine through a combination of I···N halogen bonding and hydrogen-bonding-mediated dimerization of 2-aminopyrazine. Reprinted with permission from Åackeroy et al, copyright (2011) American Chemical Society.

While the utility of perfluoro-iodoarenes and alkanes has been well-studied, there is considerable difficulty in incorporating these moieties into increasingly complex molecules with the intention of directing self-assembly. Therefore, it is important to identify more synthetically accessible pathways to viable halogen bond donors that can exhibit structure directing effects in a reliable and predictable way.

3.2 Objectives

While the halogen-bond donor potential of halopyridinium[120,121] and haloimidazolium[122,123] salts has been well documented in a number of studies, the noted increase in halogen bond donor capability is in large part due to the presence of a positively-charged heteroatom on the same ring as the relevant carbon-halogen bond. To further probe the versatility of charge-assisted halogen bonding in facilitating directed assembly of supramolecular architectures, it is beneficial to explore more synthetically accessible targets. To this end, we explored the utility of N-halophenylpyridinium cations as halogen bond donors that could be easily accessed via the derivatization of pre-existing pyridine rings. While these compounds would differ from previously established halopyridinium donors in that the relevant halogen would not be directly attached to the pyridine ring, we believed that the presence of an immediately adjacent pyridinium ring would still be sufficient to activate the halogen toward halogen-bonding interactions. This expectation is indirectly supported by studies examining the solid state halogen bonding interactions in positively charged haloanilinium salts ($XC_6H_4NH_3^+$; X= Br, I).[124] Our results in this area imply that any molecule possessing a peripheral pyridine substituent could be converted to a viable halogen bond donor.

3.3.1 Results and Discussion

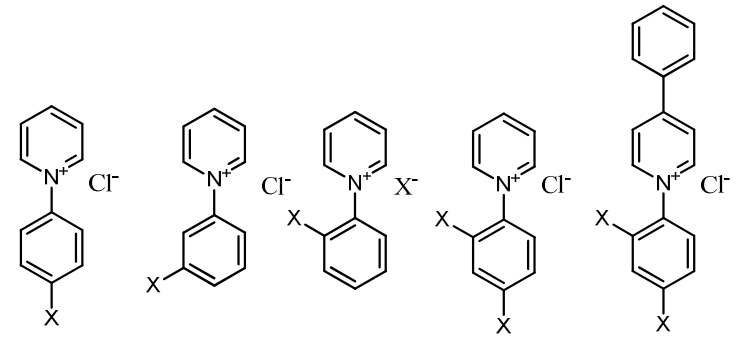

3.3 (X = I) **3.5** (X=I) **3.7** (X= I, X^- = I^-) **3.9** (X= I) **3.11** (X =I)
3.4 (X=Br) **3.6** (X=Br) **3.8** (X=Br, X^- = Cl^-) **3.10** (X= Br) **3.12** (X= Br)

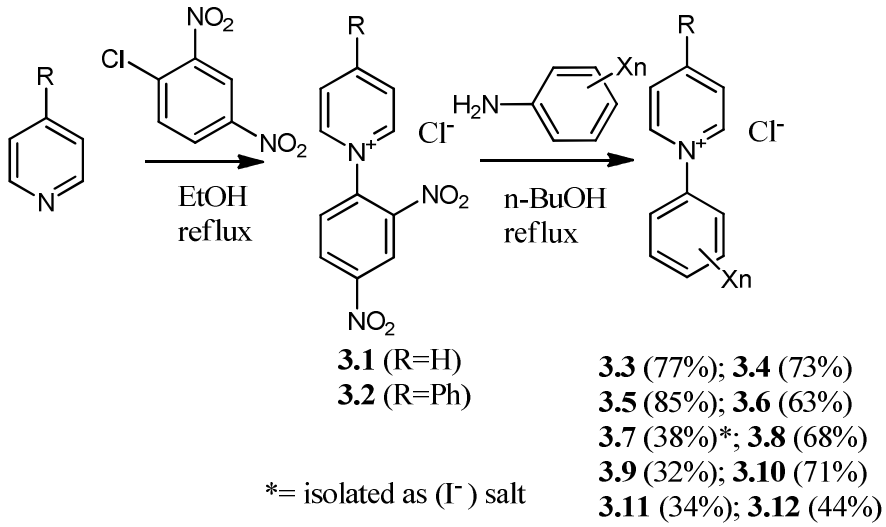

3.1 (R=H)
3.2 (R=Ph)

3.3 (77%); **3.4** (73%)
3.5 (85%); **3.6** (63%)
3.7 (38%)*; **3.8** (68%)
3.9 (32%); **3.10** (71%)
3.11 (34%); **3.12** (44%)

Scheme 3.1. Ten N-haloarylpyrdinium salts synthesized for this study and the general synthetic outline for salts **3.3-3.12.**

The synthesis of N-halophenylpyridinium halides **3.3-3.12** was accomplished via the well-known Zincke reaction[125,126] using the general route outlined in Scheme 3.1. Pyridine and 4-phenylpyridine were first converted to their corresponding N-dinitrophenylpyridinium salts **3.1** and **3.2**. These salts were isolated and then were treated with the appropriate halo- or dihaloaniline in refluxing n-BuOH. The desired N-halophenyl pyridinium chlorides were obtained in moderate to good isolated yields with the exception of **3.7**, which was obtained as the iodide salt. It is believed that the iodoaniline and/or a portion of the 2-iodophenylpyridinium cation underwent a dehalogenation/ substitution under the reaction conditions to afford the iodide anion

observed in the crystalline salt. None of the other salts displayed any evidence of this dehalogenation/substitution process.

Each salt was characterized by ^{1}H and ^{13}C NMR spectroscopy as well as high-resolution ESI mass spectrometry. X-ray quality single crystals were grown by a slow evaporation of a 1:1 mixture of MeOH/acetone solution over 1-2 days. Crystalline samples were characterized by single-crystal X-ray diffractometry and PXRD for bulk samples.

The electron-withdrawing nature of the pyridinium substituents was expected to help activate the halophenyl groups toward halogen bonding interactions with the strength of these interactions largely based on the identity of the halogen-bond donor (Br or I), the substitution pattern (*o, m, p*), and the availability of donors (mono- or di-substituted analogues) with the halide counterion serving as the halogen bond acceptor. The ability of halide anions (e.g., Cl^-, I^-) to act as halogen bond acceptors is well documented, so it was expected that any observed halogen-bonding interactions would be expected to be charge-assisted. While **3.3-3.12** are devoid of any conventional hydrogen-bond donors, the possibilities of solid state aryl and pyridinium C-H···X^- interactions to participate in competitive hydrogen bonding need to be considered. Additionally, the use of polar MeOH:acetone mixtures in crystallization experiments afforded the possibility of hydrogen bonding solvates (methanol, opportunistic H_2O) to be present, especially considering the relatively high free energy of solvation of Cl^- (ΔG_{solv} = -340 kJ/mol),[127] this possibility proves to be quite probable. Indeed, variations of these types of interactions are observed for most of the structures presented, yet many of the expected halogen-bonding interactions are also observed.

Figure 3.5. Asymmetric unit in **3.3**. Chloride anion shown as green sphere. I···Cl^- *d* = 3.436 Å, R_{XB} = 0.91, C–I···Cl^- angle = 166.27^0.

The structure of 4-iodophenylpyridinium chloride (**3.3**) represents many of the interactions previously considered. The ion pair crystallizes in the centrosymmetric space group $P2_1/c$ with one ion pair and two water molecules of solvation comprising the asymmetric unit (Figure 3.5). A halogen bonding interaction is observed as indicated by the ratio of the observed I···Cl^- distance (3.436 Å) over the sum of the relevant van der Waals radii (3.79 Å); $R_{XB} = 0.91$. Additionally, the C-I···Cl^- angle is relatively close to linear (166.27^0). The Cl^- ion is solvated with two water molecules interacting via hydrogen bonding and is part of an extended network of solvated chloride ions (Figure 3.6).

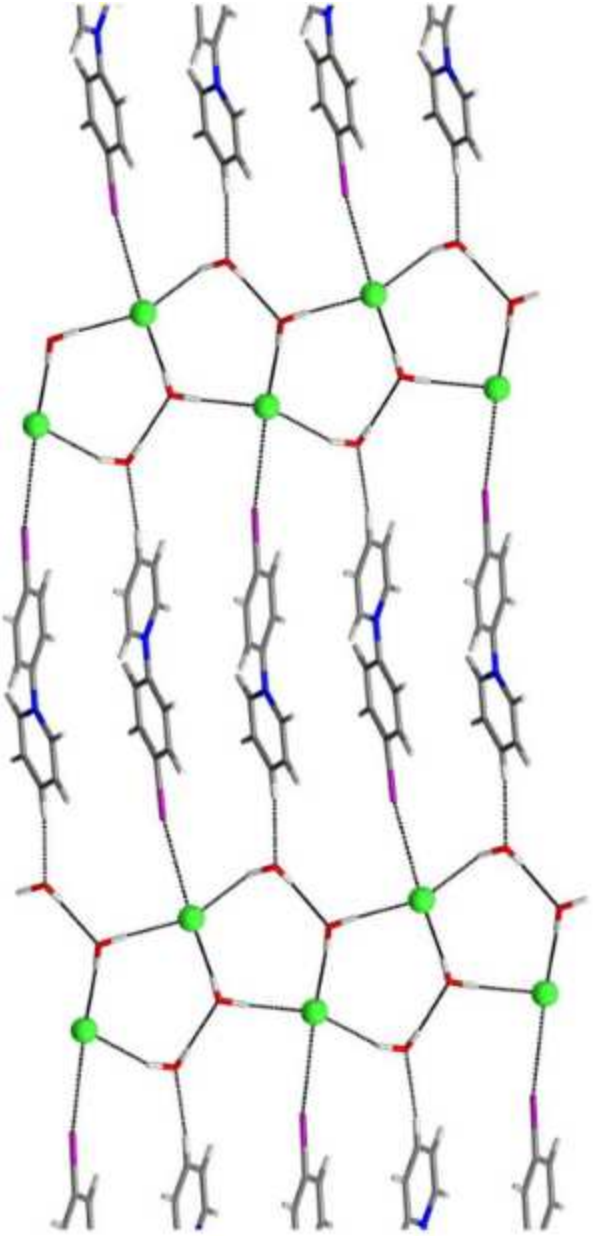

Figure 3.6. XB interactions and chloride ion solvation in **3.3**.

Extensive hydrogen bonding between chloride ions and water solvates produces fused cycles joined by iodophenylpyridinium cations via I···Cl^- halogen bonding and pyridinium C-H···OH_2 hydrogen bonding giving way to 2D layers. The iodophenylpyridinium cations are stacked in an anti-parallel fashion consistent with alignment of the dipoles. Between the layers, aromatic stacking is prominent with centroid-centroid distances between stacked iodophenyl and pyridinium rings at 3.783 Å,

well within the range of conventional π-π stacking interactions. Not visible in the figure is the additional pyridinium C-H···Cl^- hydrogen bonding interactions joining the layers and allowing for slightly offset stacking between those layers.

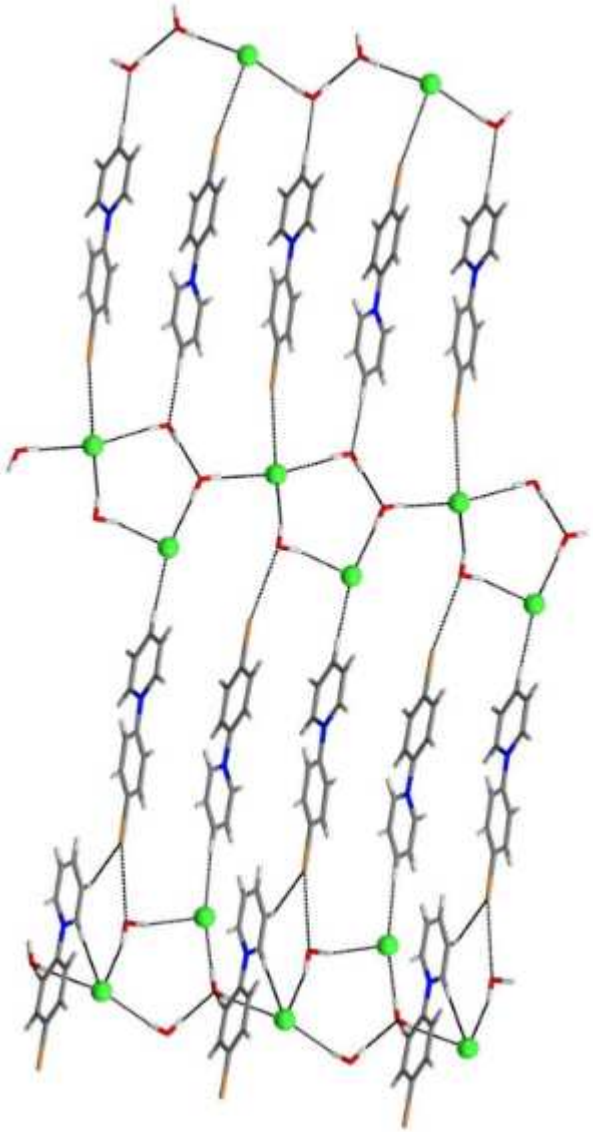

Figure 3.7. Halogen and hydrogen bonding interations in **3.4**.

The structure of 4-bromophenylpyridinium chloride **3.4** differs from the iodo analogue **3.3** in a few ways. First, the crystal analyzed presents in the non-centrosymmetric space group $P2_1/n$ with two unique pyridinium cations displayed in the

asymmetric unit. Only one of these cations is actually engaged in Br···Cl^- halogen bonding (Figure 3.7), and in a comparatively weaker fashion when measured against the iodo analogue (Br···Cl^- distance; 3.490 Å, R_{XB} = 0.95). The second cation features an aryl bromide serving a dual role as a halogen bond donor to a water solvate molecule (Br···O 3.271 Å, R_{XB} = 0.97, C-Br···O angle 163.53^0) and a hydrogen bond acceptor to a pyridinium C-H donor (C-H···Br distance 3.016 Å, C-Br···H angle 142.36^0). In a similar fashion to **3.3**, the chloride counterions participate in the formation of cyclic hydrated networks joined with bridging bromphenylpyridinium cations via Br···Cl^-/ OH_2 halogen bonding and pyridinium C-H···Cl^-/ OH_2 hydrogen bonding to form 2D layers that are stacked in an offset fashion displaying pyridinium cations separated by hydrated networks of water and chloride. In addition, the individual stacks of cations adopt favorable antiparallel dipolar arrangements with arene-arene ring separations ranged from 3.786 to 3.914 Å

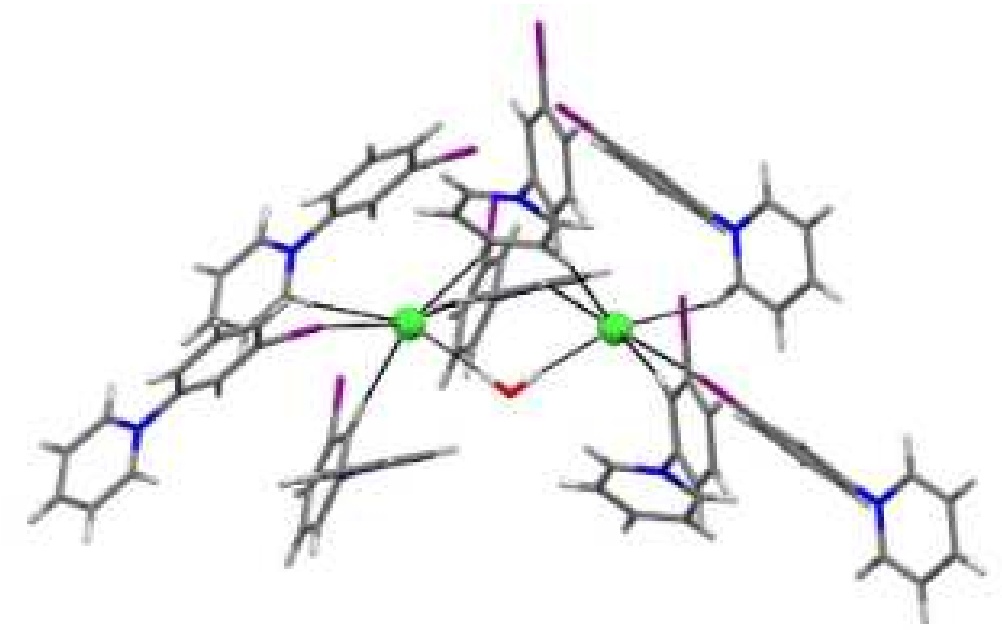

Figure 3.8. Intermolecular interactions of chloride ions in **3.5**.

The crystal of 3-iodophenylpyridinium chloride **3.5** features an ostensibly more complicated structure; one ion pair and a 0.5 H_2O solvate molecule feature in the asymmetric unit. The coordination sphere of each chloride anion is octahedral in nature

with six intermolecular contacts, one of which is a relatively strong halogen bond to an iodoarene moiety ($I\cdots Cl^-$ distance 3.249 Å, $R_{XB} = 0.86$, C-I$\cdots Cl^-$ angle 168.01^0). Hydrogen bonds from a chloride-bridging water molecule and four additional pyridinium C-H bonds complete the coordination sphere (Figure 3.8). Unlike in the previous structures **3.3** and **3.4**, there are no stabilizing intermolecular π-π stacking interactions observed. Despite this, the halogen bonding interaction between the iodoarene donor and the chloride ion acceptor is quite strong and is even shorter than that of the essential interaction in **3.3**.

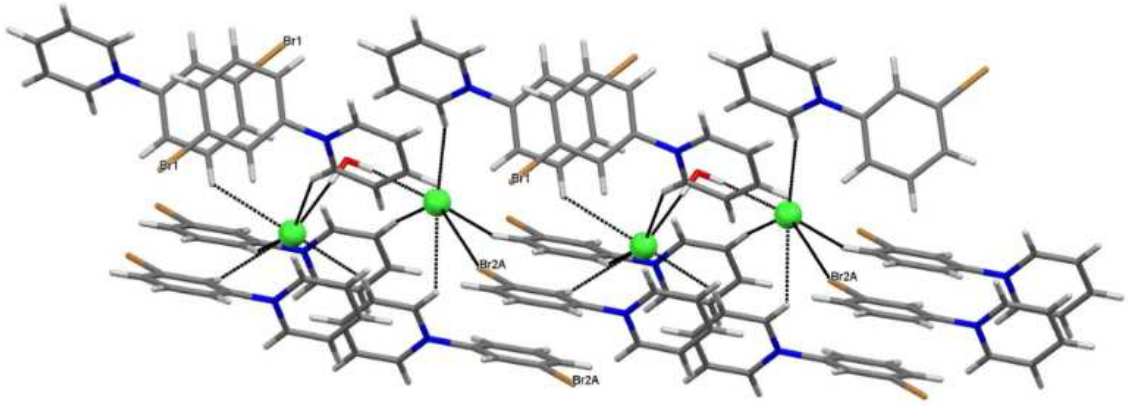

Figure 3.9. Coordination environment of chloride ions in **3.6**.

In contrast, the amount of halogen bonding interactions exhibited in 3-bromophenylpyridinium chloride **3.6** is considerably curtailed. Indeed, in a similar fashion to **3.4**, the asymmetric unit displays two unique ion pairs with a water molecule of solvation. The first bromophenyl unit (designated Br1 in Figure 3.9) does not participate in any significant intermolecular contacts. As was the case with the structure of **3.5**, chloride ions in **3.6** are arranged in pairs via hydrogen bonding from a bridging water molecule with each anion displaying a roughly octahedral coordination sphere defined by O-H and C-H hydrogen bond donors, along with a single Br$\cdots Cl^-$ halogen bond with the second bromophenyl moiety (designated Br2A in Figure 3.9). Further, the nature of the halogen bond itself is quite weak and directionality deviates relatively far from linearity (Br$\cdots Cl^-$ distance 3.543 Å, $R_{XB} = 0.97$, C-Br$\cdots Cl^-$ angle 161.13^0). Another

distinctive feature of this structure involves the self-assembly of unique pyridinium cations into distinct linear chains through dipolar stacking of pyridinium and bromophenyl rings.

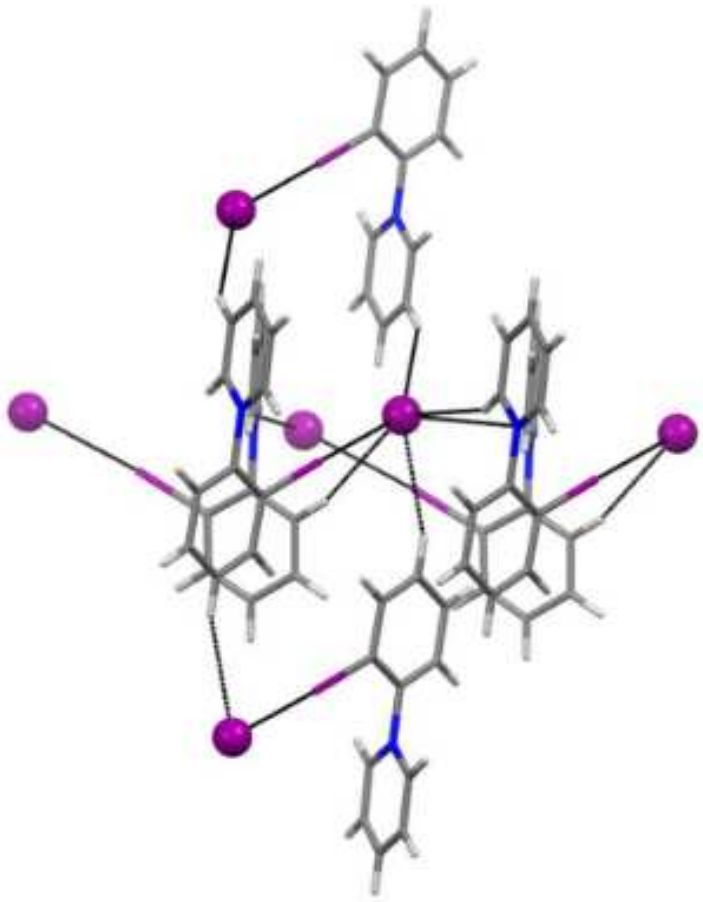

Figure 3.10. ArI···I$^-$ halogen bonding and the coordination sphere around iodide in **3.7** (iodide shown in purple).

The structure of **3.7** involves the presence of an iodide counterion rather than chloride (Figure 3.10). Interestingly, the crystals of **3.7** contained no water solvate molecules, perhaps as a result of the decreased hydrophilicity of iodide compared to chloride (ΔG_{solv} = -275 kJ/mol for iodide, compared to -340kJ/mol for chloride).[127] One ion pair is featured in the asymmetric unit with the iodoarene engaged in strong halogen bonding to an iodide anion (I···I$^-$ 3.576 Å, R_{XB} = 0.86, C-I···I$^-$ angle 170.47^0). A similar

type of interaction was reported by Gray and Jones[124] in crystals of 3-iodoanilinium iodide although their reported halogen bond distance is noticeably larger (R_{XB} = 0.88). Each iodide anion displays six close intermolecular contacts; in addition to the halogen bond, there are three pyridinium C-H···I^- hydrogen bonds, a hydrogen-bond donor emanating from an iodophenyl C-H donor. The distances for these interactions range from 2.855 to 3.141 Å (I^-···H vdW distance = 3.26 Å). Additionally, each anion approaches the face of a pyridinium ring (d = 3.669 Å) to complete the iodide coordination sphere.

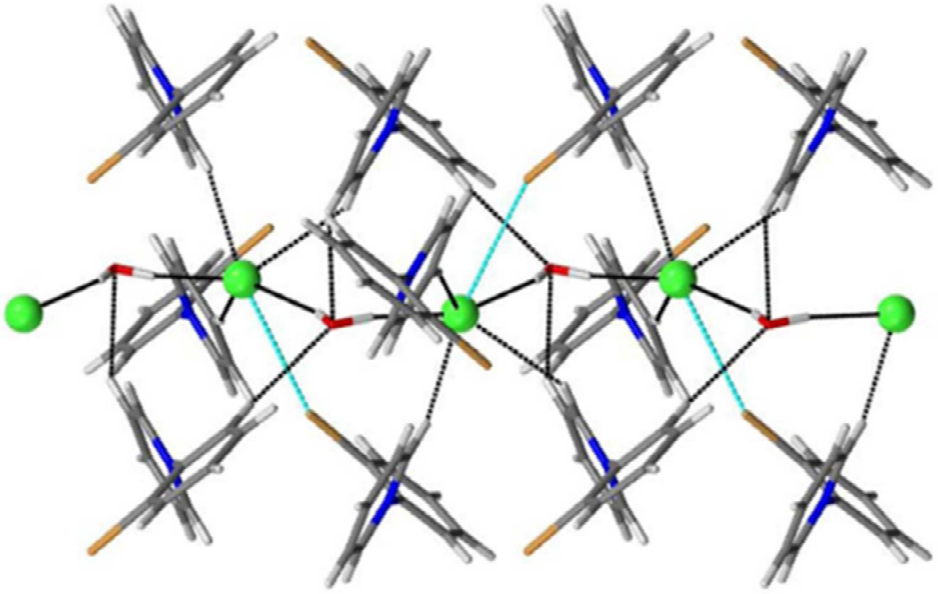

Figure 3.11. Noncovalent interactions surrounding the chloride ion in **3.8.** the halogen bond indicated in light blue is approximately equal to the sum of the Br···Cl^- vdW radii.

The structure of 2-bromophenylpyridinium chloride **3.8** showcases essentially no halogen bonding. Rather, chloride anions are organized in staggered chains with bridging water solvate molecules interacting via hydrogen bonding (Figure 3.11). There are some additional interactions involving pyridinium C-H···Cl^- hydrogen bonding interactions are also evident. The "halogen bond" observed is very weak and its classification as a halogen bond is debatable; the distance is essentially equal to the sum of the van der Waals radii (d = 3.626 Å, R_{XB} = 0.99) and the C-Br···Cl^- angle is 158.02^0, quite far from linearity.

The dihalophenylpyridinium chlorides **3.9-3.12** were selected for this study to explore the propensity to generate halogen bond-mediated networks. With the introduction of a second halogen substituent in these substrates, an excess of halogen bond donors is produced relative to chloride halogen bond acceptors; namely, a 2:1 ratio. The chloride ions may therefore participate in halogen bonding with multiple halogen bond donors to generate extended networks and/or 0D oligomers (e.g. dimers, trimers, etc.). The diiodophenylpyridinium derivatives **3.9** and **3.11** do indeed display this behavior in the solid state, and the dibromophenyl pyridinium analogues present their own interesting characteristics.

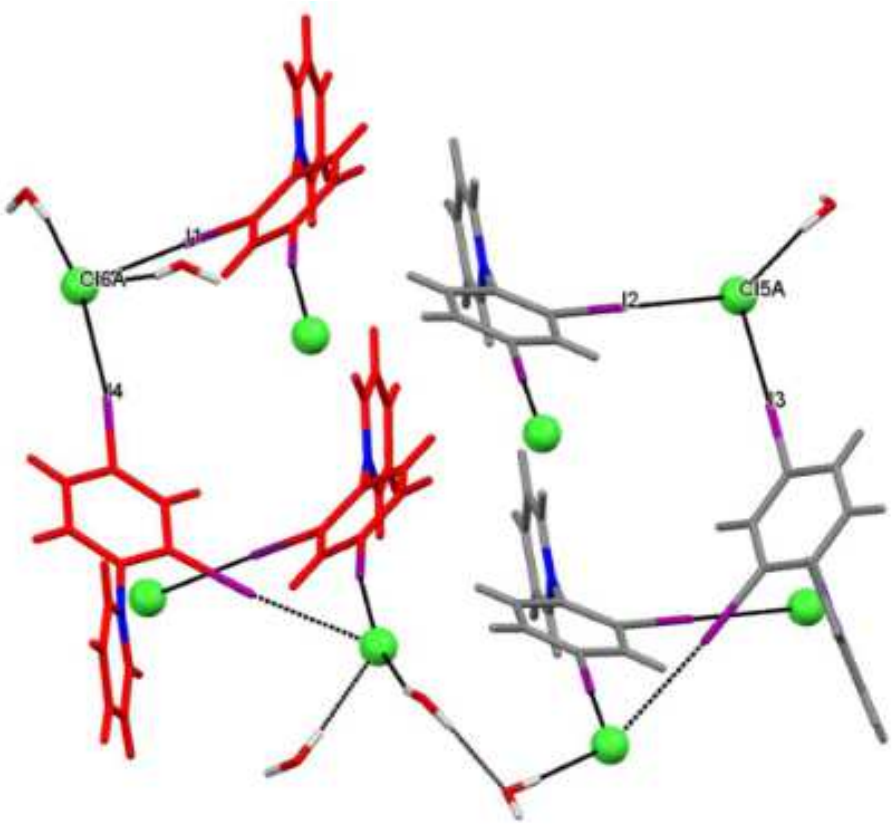

Figure 3.12. Extended halogen bonding networks in helical assemblies found in **3.9**. Helices are derived from unique diiodophenylpyridinium cations are color-coded in red and gray.

Two unique ion pairs and three solvate water molecules are featured within the asymmetric unit of **3.9**. The extended packing features the two unique arylpyridinium chlorides segregated into individual, helical constructs mediated by bridging ArI···Cl^-··· IAr halogen bonds (Figure 3.12). The presence of both left-handed and right-handed helices is noted and the essential metrics of halogen-bonding interactions vary slightly when the two helices are compared to one another. The metrics of each of the key interactions are described in the following table:

Interaction	*Distance*	R_{XB}	*Angle*
C-I1···Cl6A$^-$	3.140 Å	0.83	173.69^0
C-I4···Cl6A$^-$	3.563 Å	0.94	172.06^0
C-I2···Cl5A$^-$	3.230 Å	0.85	176.37^0
C-I3···Cl5A$^-$	3.318 Å	0.88	177.22^0

Table 3.1 Summary of the key interactions, distances and angles displayed in **3.9**.

Each halogen bond indicated in Figure 3.12 approaches linearity with C-I···Cl^- angles ranging from 172.02^0 to 177.22^0. The chloride ions are bridging via a 4-iodo substituent from one pyridinium cation and a 2-iodo substituent from a second pyridinium cation. The two helical assemblies link to one another through their respective chloride ions via bridging water molecules. Additionally, pyridinium C-H···Cl^- hydrogen bonding involving the most deshielded, polarized hydrogen atoms (immediately adjacent to the nitrogen) also feature in the commingling of the two helical halogen-bonded networks (Figure 3.13).

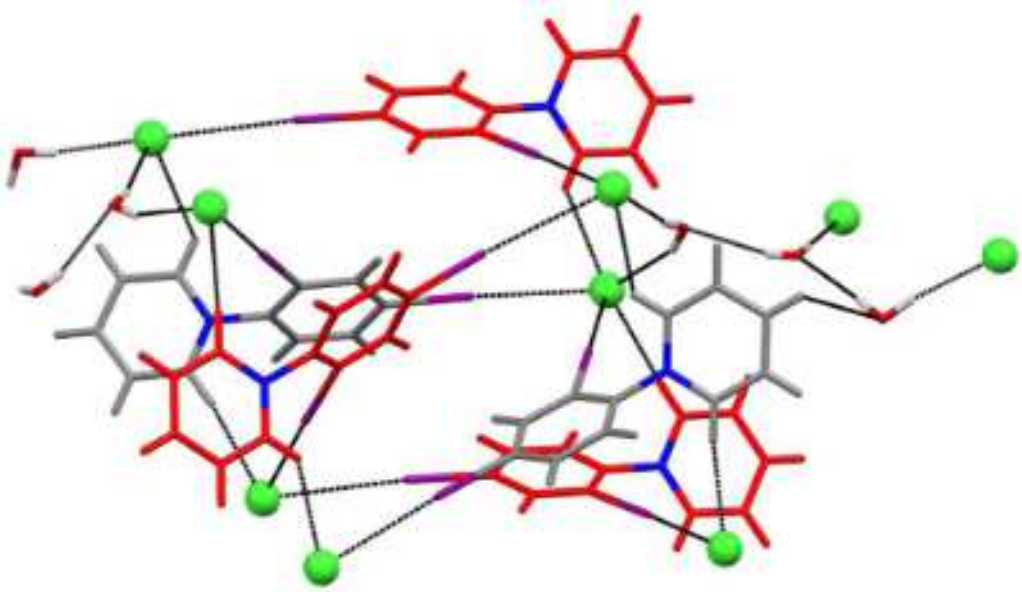

Figure 3.13. Bridging of two helical networks in **3.9** through chloride ions and water solvates with pyridinium C-H···Cl^- hydrogen bonding.

In stark contrast, the structure of N-dibromophenylpyridinium chloride **3.10** differs significantly from its diiodo analogue **3.9** in both the topology of the crystalline network and the degree of halogen bonding. In fact, only the 2-bromo substituent of each phenylpyridinium cation displays any halogen bonding interaction, though not with the chloride anion; a neighboring bromophenyl ring features in the interaction with a distance near 3.143 Å (Figure 3.14). The 4-bromo substituent does not participate in any measureable intermolecular interactions and the coordination environment of each chloride anion is occupied by hydrogen bonding to two water solvates and two C-H groups from surrounding pyridinium rings. The water molecules act to bridge adjacent chloride counterions and the anions are themselves layered between phenylpyridinium cations to afford well-defined hydrophilic and hydrophobic regions within the extended structure.

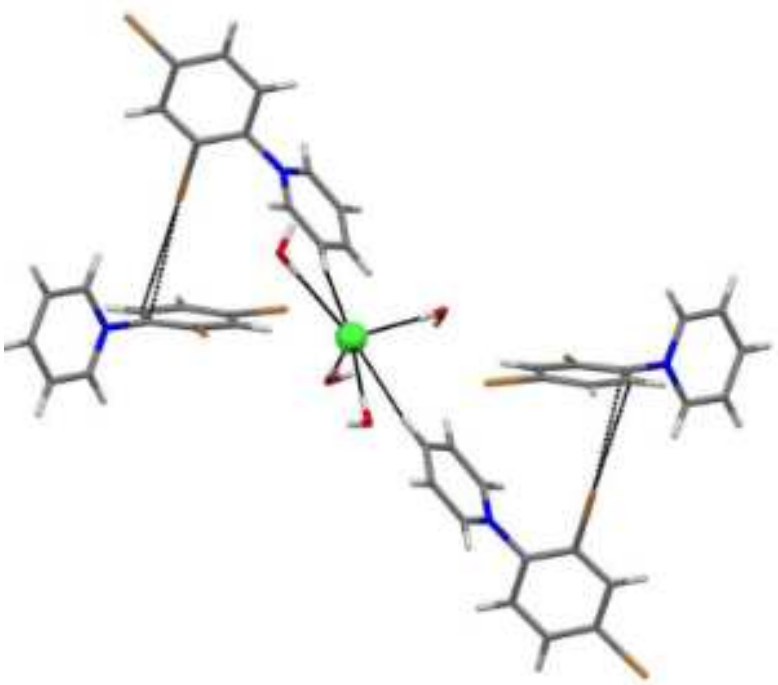

Figure 3.14. Coordination environment around chloride anions in **3.10** and the distinct absence of Br···Cl^- halogen bonds.

In a similar fashion to **3.9,** the 4-phenyl-N-diiodophenyl pyridinium chloride salt **3.11** demonstrates halogen-bonding interactions through both the 4-iodo and 2-iodo substituents via ArI···Cl^-···IAr bridging interactions. However, in this structure, the coordination sphere of the chloride ion features no solvate molecules. This may be a consequence of both the relatively strong halogen bonding interactions and the increased hydrophobicity of the 4-phenyl substituent of **3.11** relative to the unsubstituted pyridinium analogue **3.9**. Moreover, the halogen bonding network in this structure does not produce infinite helical chains of ion pairs, but instead results in the formation of discrete halogen-bonded dimers that are arrayed in 2D layers (Figure 3.15). The dimers formed as a result of halogen bond-mediated dimerization feature two distinct and fairly strong halogen bonds with C-I···Cl^- angles approaching linearity (I1···Cl^- = 3.232 Å, R_{XB} = 0.85, 169.39^0 and I2···Cl^- = 3.101 Å, R_{XB} = 0.82, 172.63^0). The I···Cl^-···I angle is 81.44^0. The chloride ions forming the vertices within these dimers are separated by 10.788 Å.

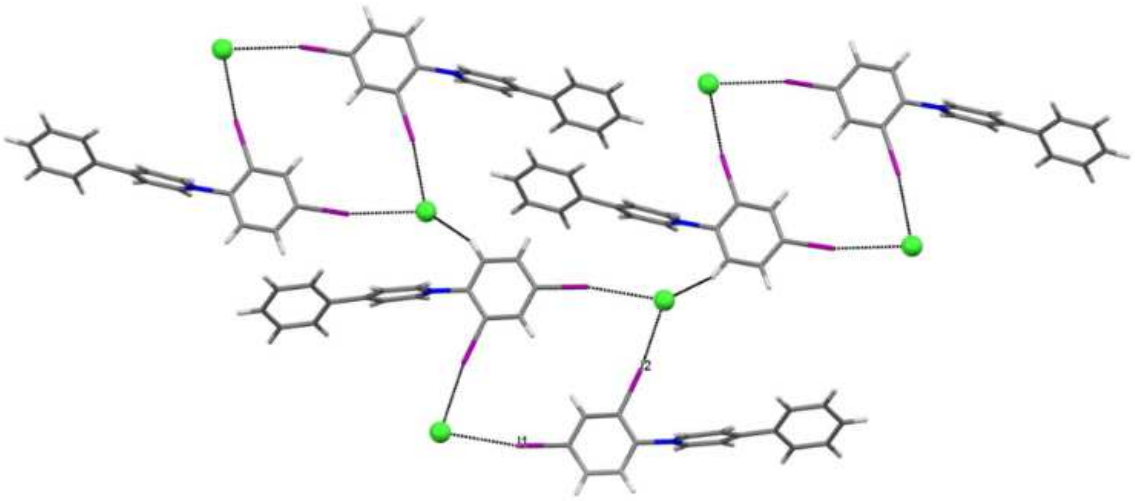

Figure 3.15. Halogen-bonded macrocyclic dimers observed in **3.11**.

2D Halogen-bonded dimers are arrayed in the *bc* plane and are connected via pyridinium C-H···Cl^- hydrogen bonding (d = 2.575 Å) and dipole-assisted π-π stacking interactions between the 4-phenyl substituents (centroid-centroid distance = 3.879 Å) Halogen-bonded layers in this plane stack in an ABAB pattern that are linked through pyridinium C-H···Cl^- and C-H···I hydrogen bonding (Figure 3.16). In addition, it should be noted that **3.9** and **3.11** have halogen-bond donors arrayed identically (2,4-diiodophenylpyridinium) with identical halogen bond acceptors (chloride anions), though they display very different halogen bonding networks. Thus, the presence of water solvate molecules in **3.9** and their absence in **3.11** appears to play a critical role in the observed halogen bonding motifs.

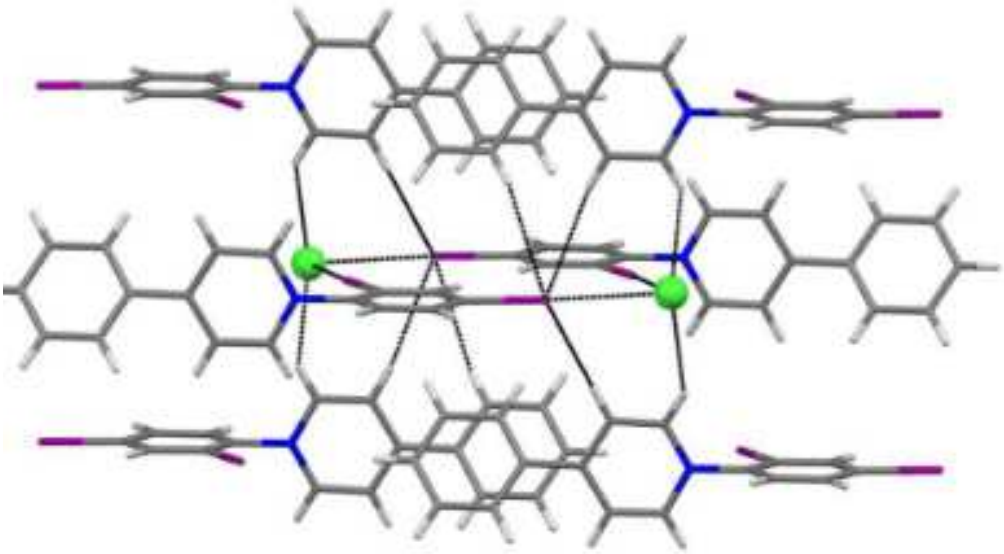

Figure 3.16. Stacking of layers within **3.11** displayed in ABA fashion.

While there are certain solid state features found in the crystal structure of **3.12** similar to those found in its diiodo analogue **3.11**, there are some significant differences. First, each chloride ion is associated with one water molecule of solvation in **3.12**, whereas **3.11** exhibits no solvated molecules. The presence of these solvated chloride anions takes the form of chloride dimers bridged by water molecules with O-H···Cl^- hydrogen bonding. Two 4-phenyldibromophenylpyridinium cations form a similar macrocyclic assembly to those observed in **3.11**, with the combined bridging OH_2···Cl^- dimers forming the vertices of the larger supramolecular assembly (Figure 3.17). However, only the 2-bromo substituent engages with a chloride ion in halogen bonding (d = 3.286 Å, R_{XB} = 0.90, C-Br···Cl^- = 175.62^0), while the 4-bromo substituent interacts with the oxygen of H_2O as a surrogate Lewis base halogen bond acceptor (Br···O d = 3.040 Å, R_{XB} – 0.90, C-Br···O = 167.94^0). Additional pyridinium C-H···Cl^- interactions form the remainder of the chloride coordination sphere. The crystal structure displays some positional disorder between the chloride ions and water molecules, with a split positional occupancy between them.

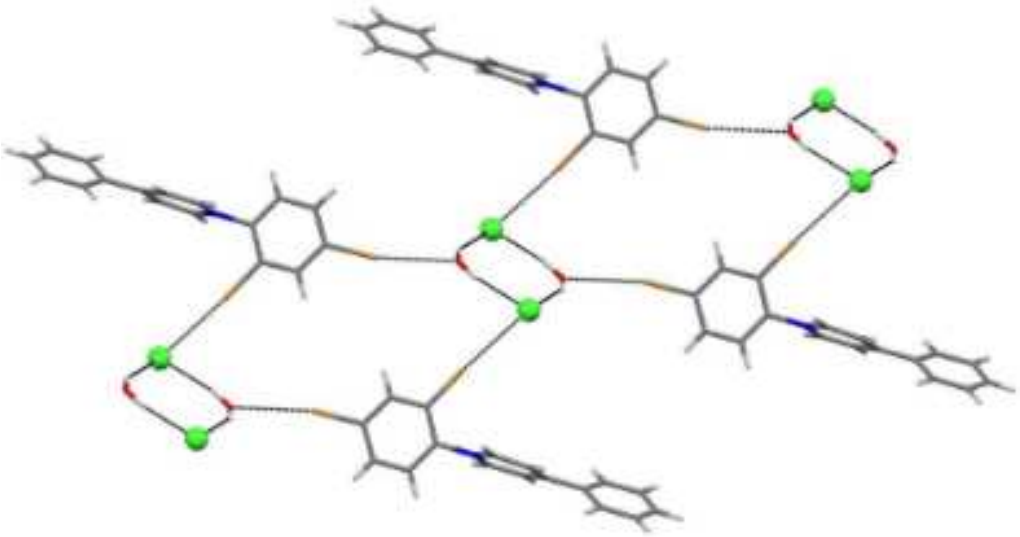

Figure 3.17. Main hydrogen/halogen bonding network in **3.12**.

This series of ten halophenylpyridinium salts was studied with the intention of assessing their capability to participate in charge-assisted halogen bonding with halide anion acceptors and to further probe the utility of these types of interactions in facilitating formation of discrete halogen bonding interactions. Given the fact that iodine is considered to be a better halogen bond donor than bromine, the observation that iodine-substituted phenyl-pyridinium chlorides display a greater capacity for halogen bonding interactions than their bromine-substituted analogues in the studied series is not particularly surprising. There are, however, significant differences in the type, extent, and magnitude of solid state halogen-bonding interactions. Specifically, every iodophenyl group in the examined series participates in solid state halogen bonding with chloride (or iodide in **3.7**) anions. As the sole halogen bond donors, these groups are expected to interact with the anions, as the anions are the best halogen bond acceptors. In the cases of the bromo-substituted analogues in this series, the expected halogen-bond interaction with the chloride counterion is either severely weakened (R_{XB} = 0.95-0.99 for Br···Cl^- interactions), or entirely obfuscated by competing interactions of the counterion with water solvates and aryl/pyridinium C-H hydrogen bond donors, with several structures incorporating ArBr residues that do not engage in any significant intermolecular contacts.

In contrast, the iodo-substituted analogues provided ArI···X^- interactions that all display R_{XB} of ~0.90 or less with C-I···X^- angles approaching linearity. The presence of two halogen bond donors relative to one halogen bond acceptor anion in each ion pair also affords the possibility of the formation of halogen-bonded networks, which the iodo-substituted analogues readily form, while the bromo-substituted analogues have any potential network disrupted by solvated chloride ions.[128]

The cationic pyridinium ring proves to be an integral feature in these studies. The incorporation of this ring system provides the basis for enhanced halogen bond donor ability of the attached N-halophenyl groups via electron withdrawing inductive effects. It is these same inductive effects, however, that provide enhanced hydrogen-bond donor capability of pyridinium C-H groups, and specifically, those groups immediately adjacent to the nitrogen. Therefore, in nearly every structure studied, the prevalence of pyridinium C-H···X^- interactions in directed solid state assembly, is notably significant. In some cases, these interactions occur at the expense of expected ArBr···Cl^- interactions. This may be an indication that the H-bond donor ability of these C-H groups is equal to or surpasses the halogen bond donor ability of the aryl bromines, but is less than the halogen bond donor ability of the analogous iodoarenes. To a lesser extent, the presence of dipolar head-to-tail π-π stacking interactions between layers of phenylpyridinium cations may factor in the directed solid state assembly of these structures, but given its observed presence in only half of the molecules within this study (**3.3-3.4**, **3.6**, **3.8**, and **3.11**), it may be considered a noncovalent interaction of a generally lesser importance than solid state halogen bonding and hydrogen bonding.

3.3.2 Results and discussion for amido-substituted N-diiodophenylpyridinium salts

Analysis of the results from the previously noted series of salts **3.3-3.12** afforded the opportunity to consider the effects of additional moieties on the pyridinium ring that could potentially coordinate with the anion through hydrogen-bonding interactions. These types of interactions have the potential to disrupt the formation of halogen-bonded networks with strong competing interactions. Our interest in the study of such interaction

led to the synthesis and characterization of two additional pyridinium salts derived from nicotinamide and isonicotinamide starting materials.

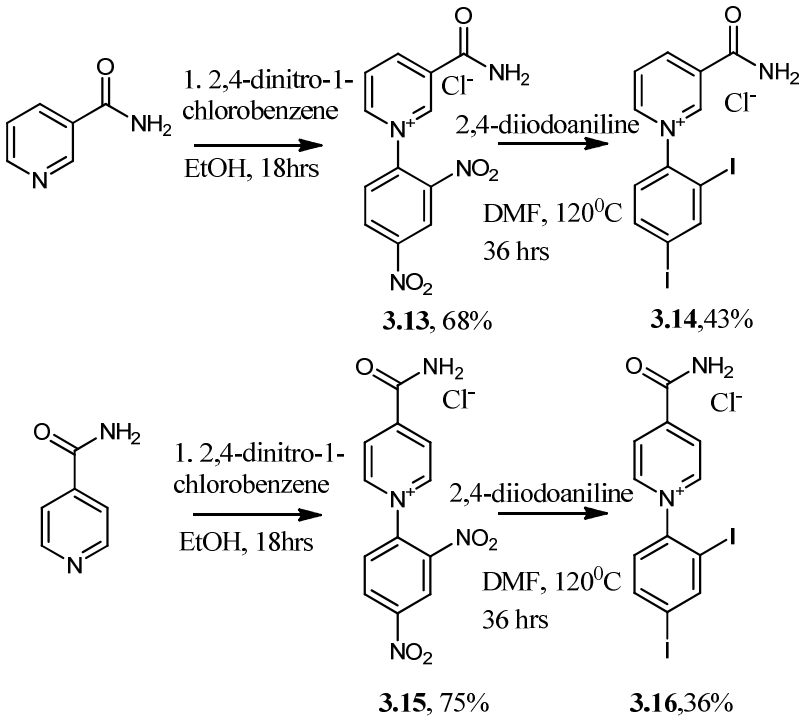

Scheme 3.2 Synthesis of amido-pyridinium salts **3.14** and **3.16** derived from nicotinamide and isonicotinamide, respectively.

A slight modification of the reaction conditions that afforded salts **3.3-3.12** provided salts **3.14** and **3.16** in modest yield; The Zincke salt precursors **3.13** and **3.15** were derived from nicotinamide and isonicotinamide, respectively, and utilized DMF rather than n-BuOH as a solvent for purposes of greater solubility (Scheme 3.2). 2,4-diiodoaniline was selected as a reactant to produce substrates that could form halogen-bonded networks similar to those discussed in the previous section. Given that previous results have indicated that pyridinium C-H groups can contribute significantly to the coordination sphere of the anion, the addition of the amido-NH_2 moiety to the pyridinium framework affords the presence of an abundance of viable hydrogen-bond donors relative to halogen-bond donors for potential competing interactions.

Crystals suitable for single crystal x-ray diffraction were grown by slow evaporation of a 1:1 MeOH:Acetone mixture over 2-3 days.

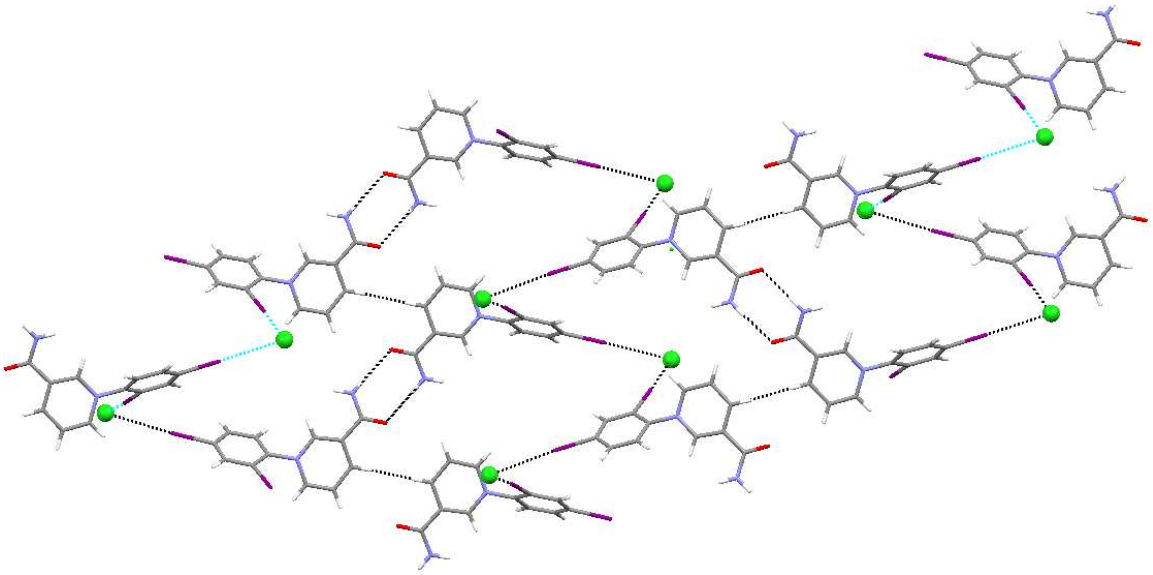

Figure 3.18 The helical assemblies resulting from I···Cl$^-$···I interactions with bis-amido dimer backbones, viewed along the *b* axis.

Compound **3.14** crystallizes in an orthorhombic cell and features a C_2 screw axis similar to what was observed in the structure of **3.9** with the formation of helical assemblies of the 3-amido-N-2,4-diiodophenylpyridinium cations mediated via chloride bridged interactions. The helical assemblies in the crystal structure between the iodine donors and the chloride acceptors are exclusively of the right-handed variety with bis amido-(NH-H···O=C) backbones formed as centrosymmetric dimers, as viewed along the *b*-axis in the extended structure (Figure 3.18).

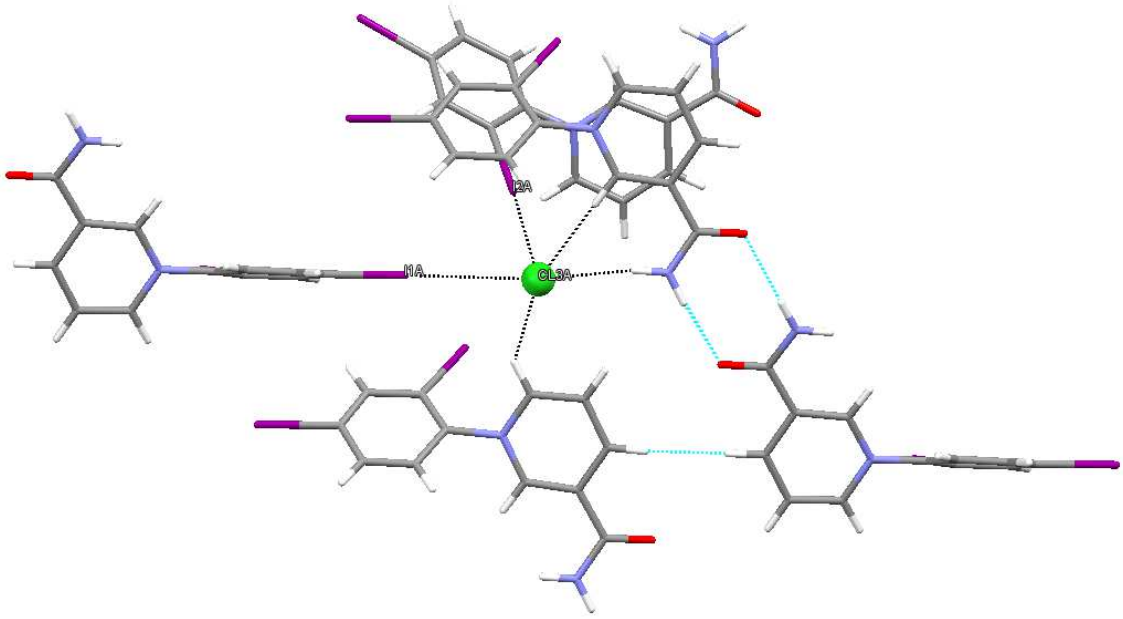

Figure 3.19 Coordination environment of the chloride anion in **3.14**.

The halogen bonding interactions observed in **3.14** are reasonably strong and approach linearity (I1A···Cl3A$^-$ = 3.483 Å; R_{XB} = 0.92 ; I2A···Cl3A$^-$ = 3.322 Å; R_{XB} = 0.87; C-I1A-Cl3A$^-$ = 172.05^0; C-I2A-Cl3A$^-$ = 169.95^0 ; I1A-Cl3A$^-$- I2A = 70.57^0) with the chloride anion coordinating two additional pyridinium cations through pyridinium C-H···Cl$^-$ interactions (d = 2.552 Å) and one amido N-H group that is otherwise engaged in dimer formation in an adjacent unit (Figure 3.19).

While the analysis of the structure of **3.14** indicates an amido-NH_2 moiety participating as a hydrogen bond donor to the chloride anion, the relative strength of the halogen bonding interactions indicate no significant disruption of the network; the dimerization of the amido-moieties of adjacent coplanar cations is a common supramolecular motif that has been noted in previous works[129] and provides a backbone for the halogen-bonded helical assemblies in a manner vaguely reminiscent of the role of the deoxyribose-phosphate backbone in the formation of helical DNA.

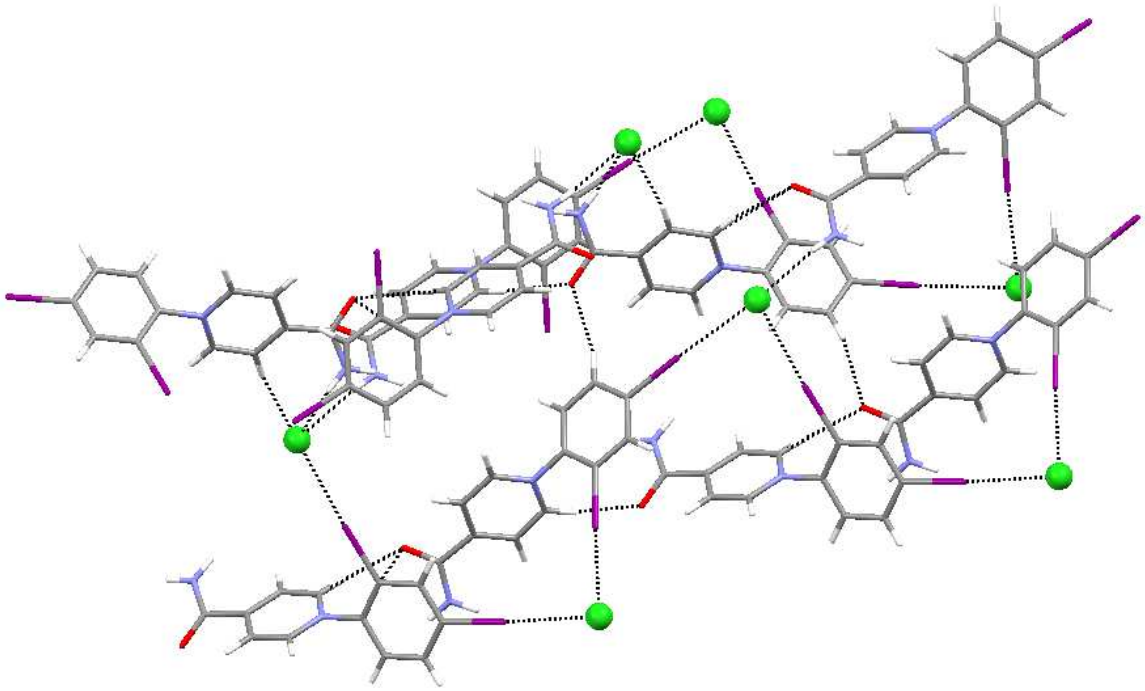

Figure 3.20. Extended structure of **3.16** with halogen-bonded network in a sawtooth formation.

The crystal structure of the 4-amido-N-2,4-diiodophenylpyridinium chloride salt **3.16** features an extended network of iodine-chloride interactions in a zigzag sawtooth formation (Figure 3.20). The coordination sphere of the chloride is trigonal bipyramidal in nature, with one iodine and a pyridinium C-H group contributing to the axial plane, and the second iodine joined by two amido-N-H interactions in the equatorial plane. The featured halogen bonds to chloride are relatively strong in the face of two separate amido-N-H donors to the coordination sphere (I1···Cl1$^-$ = 3.328 Å, R_{XB} = 0.87; I2···Cl1$^-$ = 3.193 Å, R_{XB} = 0.84; I1-Cl1—I2 = 80.11^0; C-I1···Cl1$^-$ = 176.33^0; C-I2···Cl$^-$ = 176.34^0) with the I-Cl-I interaction nearly perpendicular (Figure 3.21).

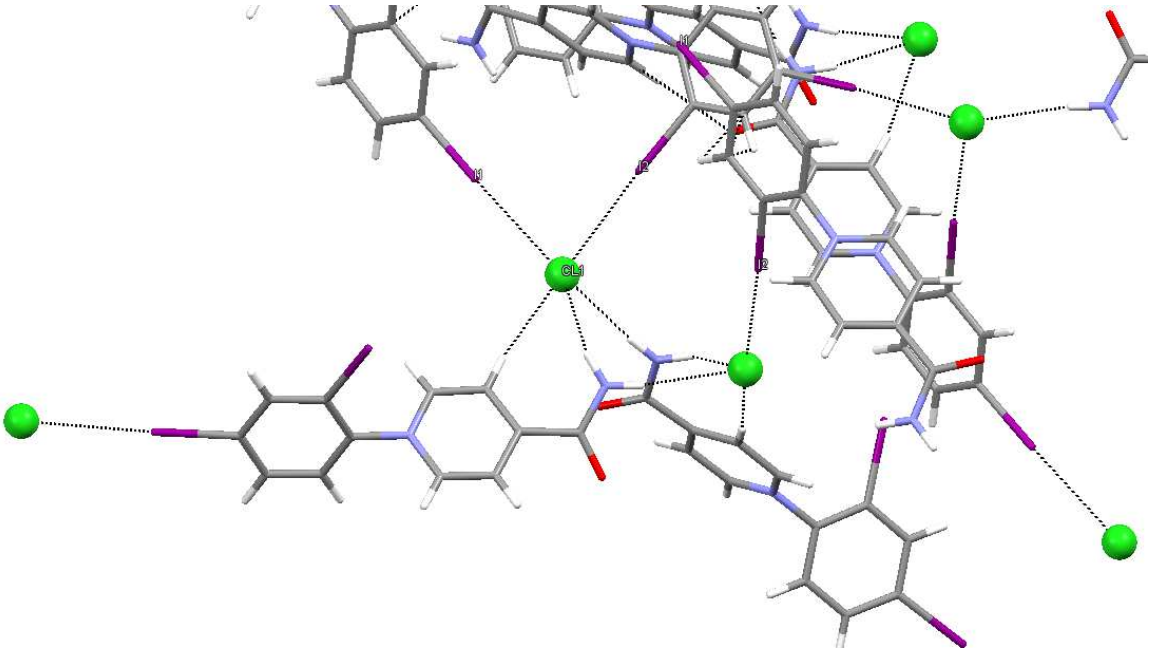

Figure 3.21. Coordination sphere of the chloride anion in **3.16**.

When compared to **3.14** the extended structure of **3.16** is relatively tightly packed with amido moieties of one cation resting over the face of a diiodophenyl ring of an adjacent cation with an amido-centroid distance of ~3.55 Å. Interactions of the carbonyl groups with pyridinium C-H donors effectively disrupts the dimerization of the amide groups of adjacent molecules, as was seen for the structure of **3.14**. Interestingly, however, in addition to bridging interactions between iodine donors, each chloride ion also acts to bridge adjacent amido-NH_2 groups, forming dimers in bifurcated arrays (N-H···Cl···H-N = 67.18^0) with chloride-chloride separation of 5.158 Å (Figure 3.21).

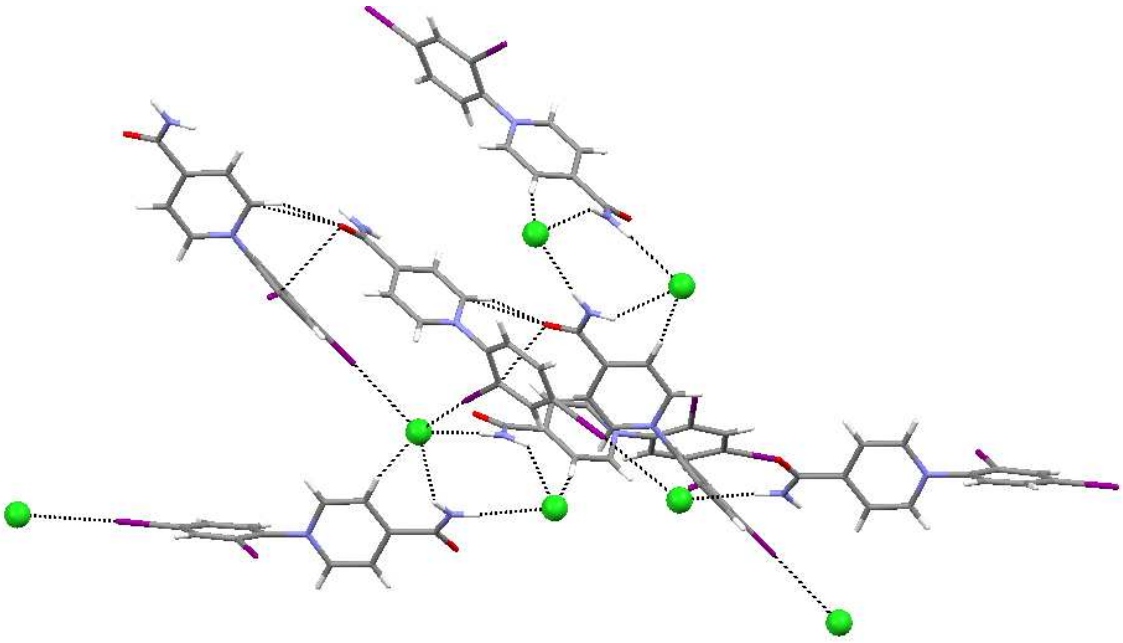

Figure 3.22. Alternative view of the extended structure of **3.16** showcasing chloride-bridged amido-NH_2 dimers in bifurcated arrays.

The abundance of additional hydrogen-bond donors in **3.14** and **3.16** relative to the first series of compounds **3.3**-**3.12** presented the possibility of competing interactions that could undermine the integrity of the halogen-bonded network. Instead, the halogen-bond interactions remain largely unaffected, and are of a strength comparable to the interactions observed in **3.9** and **3.11**, on the basis of their respective bond distances and highly linear angles of interaction.

Future efforts will focus on maintaining these halogen-bonded networks in the face of ever more complex substrates with hydrogen-bond donor groups of varying H-acidity and abundance, relative to available halogen bond donors. In time, these anion-mediated self-assembled structural motifs may be regarded as sufficiently robust and versatile to be utilized in wider applications of anion-templated assembly in crystal engineering.

3.4 Summary

Within this series, the reliability of halogen bonding between N-haloarylpyridinium cations and halide anions in crystalline ion pair assemblies was assessed. Examination of the crystal structures in this series revealed the universal occurrence of ArI···X^- (X = Cl or I) halogen bonding, with the occurrence of analogous ArBr···Cl^- halogen bonding interactions comparatively infrequent and weaker overall. The differences observed in the two series of pyridinium salts may be related to inherent differences in halogen bond donor ability between the two halogens such that activated bromoarene halogen bond donors are unable to compete with hydrogen bond donors such as water solvate molecules and/or pyridinium C-H groups for the chloride anion acceptors. Examination of disubstituted iodoarene substrates possessing halogen bond donor:acceptor ratios of 2:1 demonstrate the capacity of such systems to participate in generating halogen-bonded networks and discrete dimers through bridging Cl^- interactions.

Conclusions from the first series of ten samples studied led to the synthesis of two simple amido-substituted diiodophenyl pyridinium salts with added potential to disrupt halogen-bonded networks with potentially competing hydrogen bond. In the face of these donors, the networks remain largely unaffected and many structural motifs, including a helical assembly and the formation of chloride-bridged dimers are seen preserved from one studied set of pyridinium salts to the other.

The relatively simple synthetic methodology that afforded the studied substrates also underscores a unique versatility; any molecule possessing an unactivated pyridine ring can theoretically be converted into a suitable substrate for further studies of these important solid-state directing interactions. Further studies will attempt to examine the potential to preserve the observed halogen-bonding motifs in the presence of increasingly complex substrates with more potential hydrogen-bond donor competitors and varied anionic halogen bond acceptors.

CHAPTER IV

ANION-DIRECTED ASSEMBLY OF TETRAPHENYLETHYLENE-DERIVED BIS (3-HALO)PYRIDINIUM SALTS AND INVESTIGATIONS OF TETRAPHENYLENE-DERIVED BIS (2-IODO) IMIDAZOLIUM SALTS AS POTENTIAL SOLUTION PHASE ANION SENSORS

4.1 Introduction

The previous chapter explored the propensity of relatively simple N-halophenylpyridinium halides to participate in anion-mediated self-assembly in the solid state. Pyridinium-substituted iodoarenes and bromoarenes served as halogen bond donors and chloride anions (and in one case, iodide) functioned as halogen bond acceptors. In this chapter our efforts to expand the assembly strategy of charge-assisted halogen bonding to tetraphenylethylene-based functional materials are described.

The Pigge research group has a long-standing interest in exploring the applications of tetraphenylethylene(TPE)-based materials while controlling their assembly. Such efforts have led to the development of solid state semi-conducting assemblies mediated by hydrogen-bonding between a TPE-based tetracarboxylic acid and several bis(pyridine) components,[85] as well as an exploration of halogen bonding interactions within a series of neutral TPE-based halobenzoyl esters.[86]

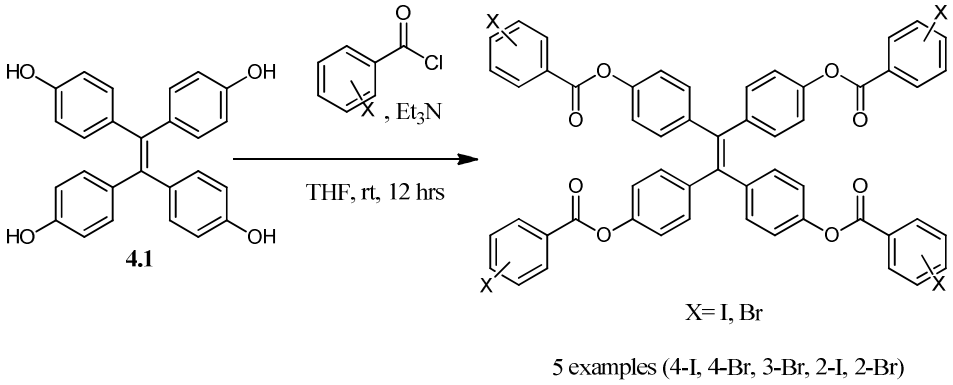

Scheme 4.1. acetylation of **4.1** with appropriate halobenzoyl chlorides to produce tetra-substituted TPE-based halobenzoyl esters.

The latter study in particular explored the self-assembly of iodo- and bromo-substituted benzoyl esters attached to a TPE framework derived from 1,1',2,2'-tetra(4-hydroxy)phenylethylene **4.1** (Scheme 4.1). After acetylation with an appropriate halobenzoyl chloride and a base, single crystals were grown from slow evaporation of DMF/pyridine solutions. Crystallographic studies of the materials revealed some common halogen bonding motifs/synthons(C-X···O=C and C-X···π_{arene} for 4-I, with one pyridine solvate in the asymmetric unit, Figure 4a; C-X···O=C and C-X···π_{arene} for 4-Br, with one pyridine solvate in the asymmetric unit, Figure 4b; C-X···π_{arene} and orthogonal C-X···X-C for 2-Br, Figure 4c) that partially guided their assembly in the solid state. The presence of C-X···O=C and C-X···π_{arene} interactions in many of the studied examples was not surprising, given the abundance of carbonyl- and arene-moieties in the substrates, but the relative lack of observed C-X···X-C interactions (only one example, Figure 4c) was a surprise to the authors, who expected this particular motif to be more prevalent, given their studies of similar halobenzoyl ester-containing materials.[130,131] The trends indicated that ortho- and para- substituted halo esters afforded more halogen-bonding interactions in the solid state relative to those of their meta-substituted analogues, likely an attribute of the relatively electropositive nature of the halogen-bond donor in these positions, yet the disparity between expected and observed halogen bonding motifs and their overall lack of presence relative to other packing patterns (e.g. π-π stacking of aromatic rings, C-H···O=C hydrogen bonding, etc.) likely resulted from a combination of the unique steric effects of these materials and the relatively modest halogen bond donor capability of the halide substituents.

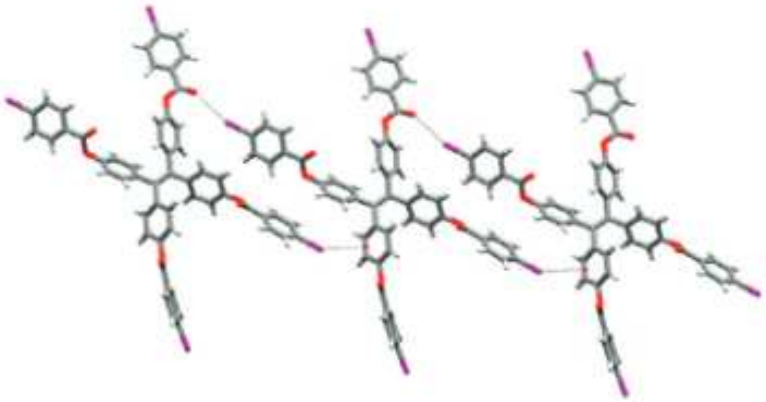

a)

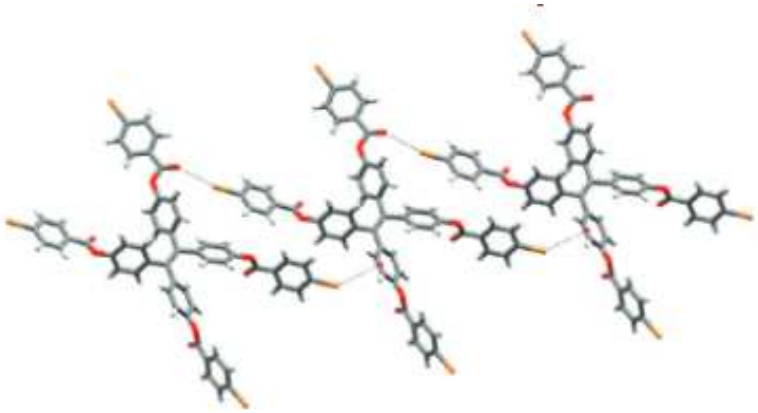

b)

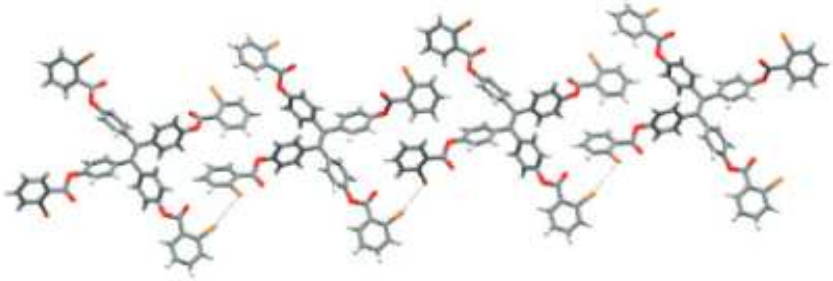

c)

Figure 4.1. packing in 1D chains of (a) 4-I with one pyridine solvate (b) 4-Br with one pyridine solvate (c) 2-Br; all solvates omitted for clarity.

4.2 Objectives

The objectives of the work featured in this chapter are two-fold and will be explored in two separate parts; first, we are interested in enhancing the halogen-bond donor capability of halide-substituted TPE derivatives through the use of charge-assisted halogen bonding. To this end, we have developed five bis-halopyridinium substituted TPE derivatives **4.2**-**4.6** with the intention of exploring their assembly in the solid state in the presence of potentially coordinating and noncoordinating anions and also to explore what additional influence, if any, the anions will have on the packing motifs of these materials; second, our study of these materials led us to consider whether it would be possible to utilize them or similar materials as novel TPE-based solution phase anion sensors with halogen-bonding interactions as the expected mechanism of anion-recognition.

4.3 Synthesis and Crystallographic Studies of TPE-bis(3-halo)pyridinium salts

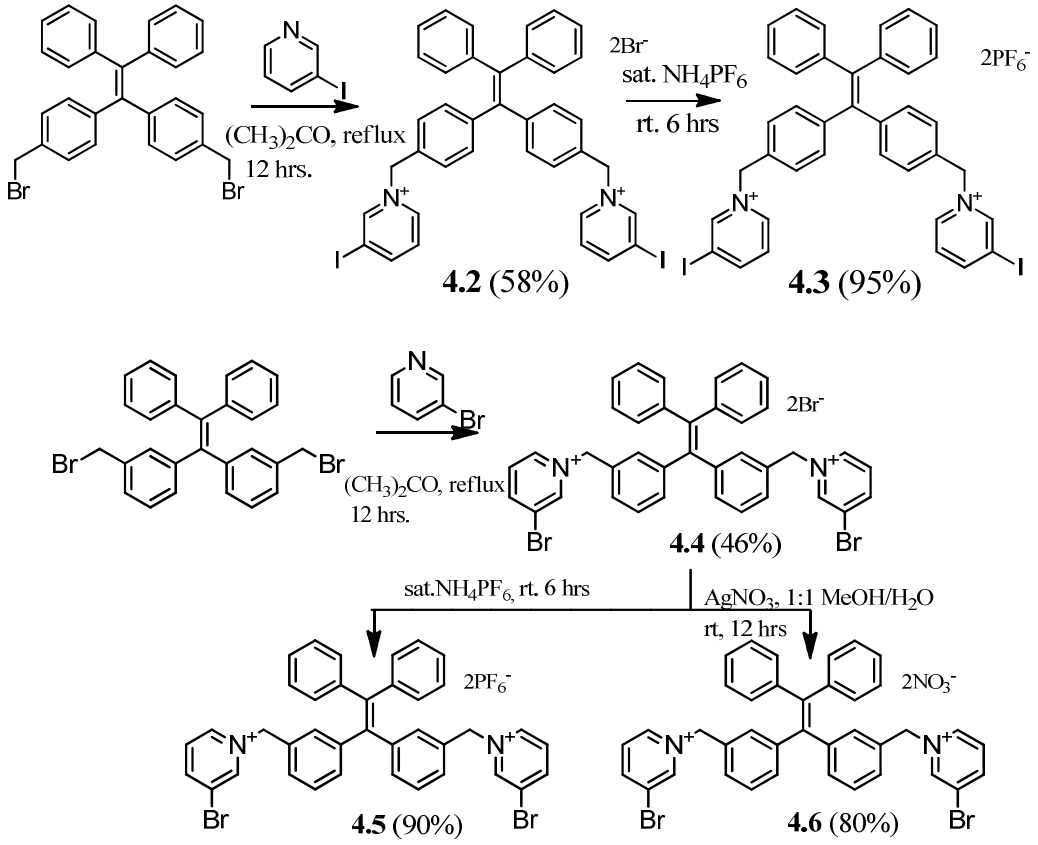

Scheme 4.2. Synthetic route to TPE-bishalopyridinium salts **4.2-4.6**.

TPE-bis(3-iodo)pyridinium salts **4.2** and **4.3** were prepared from a 4,4'-bisbromomethyl TPE precursor while the 3-bromopyridinium derivatives **4.4**, **4.5** and **4.6** were obtained from a 3,3'-bis(bromomethyl)analogue. Simple refluxing conditions in acetone for 12 hours afforded the appropriate halopyridinium salt with a bromide counterion (**4.2** and **4.4**). The bromide counterion was exchanged for hexafluorophosphate by stirring the bromide salt in an aqueous saturated solution of NH_4PF_6 for 6 hours at room temperature and then the products were extracted into EtOAc and the solvent dried to afford **4.3** and **4.5** in good yields. A nitrate salt **4.6** was obtained via anion metathesis with $AgNO_3$ in a gently stirring 1:1 MeOH:H_2O solution over 12 hours. After a filtration step to remove precipitated AgBr, compound **4.6** was obtained in

good yield. X-ray quality crystals were grown through slow evaporation of the appropriate salt in 1:1 MeOH/acetone mixtures over 1-2 days.

4.4 Results and Discussion

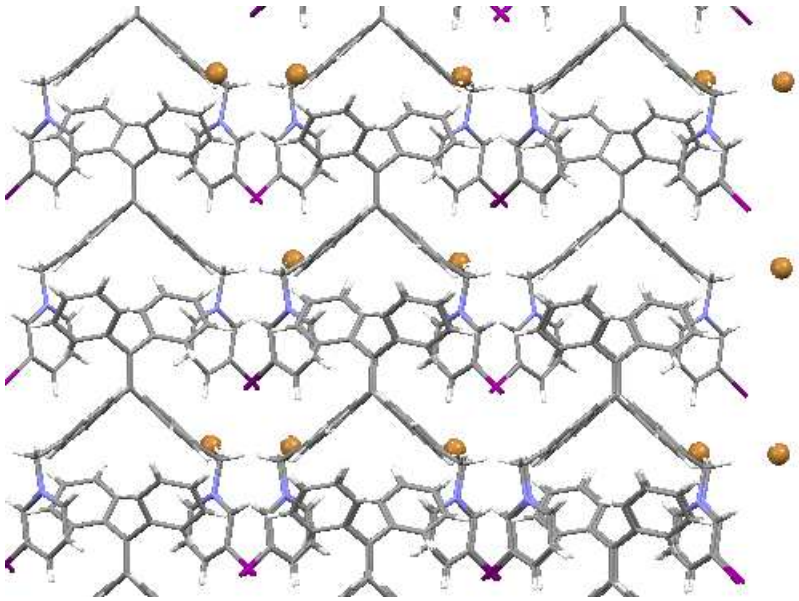

a)

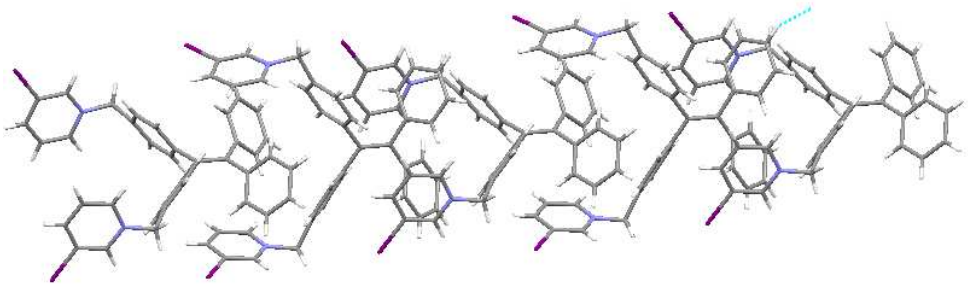

b)

Figure 4.2. (a) tight packing of 2D sheets of **4.2** viewed along *b* (b) extended chain (bromides omitted for clarity).

The extended structure of **4.2** features highly ordered packing (Figure 4.2a) displaying a fourfold screw axis (4_1) with relatively tight packing of the 4,4'-bis(3-iodopyridinium) TPE cations (intramolecular pyridinium-pyridinium cavity = 9.514 Å), somewhat resembling successive links in a chain (Figure 4b). The bromide anion participates directly in the assembly of the cations with contributions to its coordination

sphere from halogen and hydrogen bond donors. A relatively strong halogen bonding interaction (C-I1A···Br2A$^-$ = 3.283 Å; R_{XB} = 0.86, C-I1A-Br2A$^-$ = 166.35^0) is complemented by C-H hydrogen bonding from two methylene -CH_2 moieties (d = 2.820 Å) and additional contributions from the unsubstituted phenyl rings of the TPE cation (H18A···Br2A$^-$ = 2.903 Å) (Figure 4.3). An interesting triangular halogen-bond/hydrogen bond C-I···X$^-$···H-C synthon arises with the bromide, an iodine and a methylene C-H group each defining the vertices (I1A-Br2A$^-$ $^-$H7AA = 59.65^0)

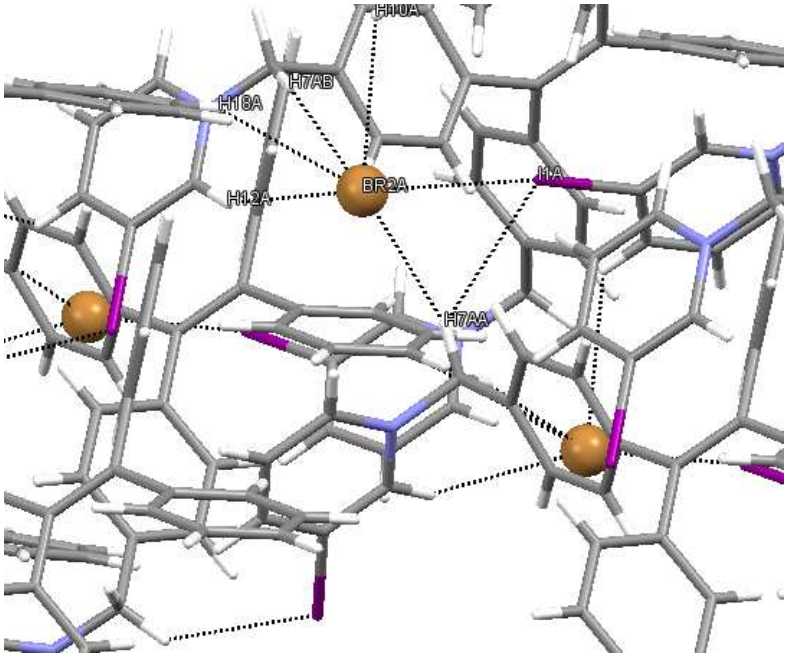

Figure 4.3. Coordination sphere of bromide anion in **4.2**.

The crystal structure of **4.3** features traditionally non-coordinating hexafluorophosphate as a counterion to evaluate the strength of the iodine substituents of the pyridinium rings as halogen bond donors and their capacity to influence the packing of these materials absent any influence from a potentially coordinating counterion

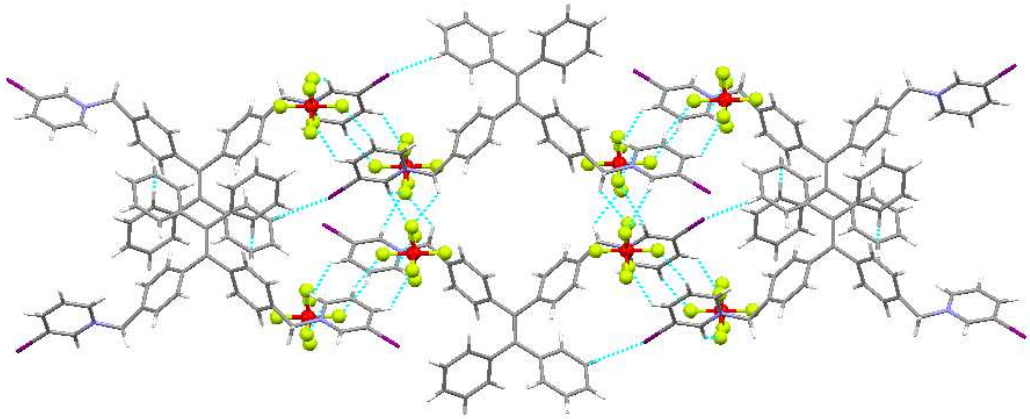

a)

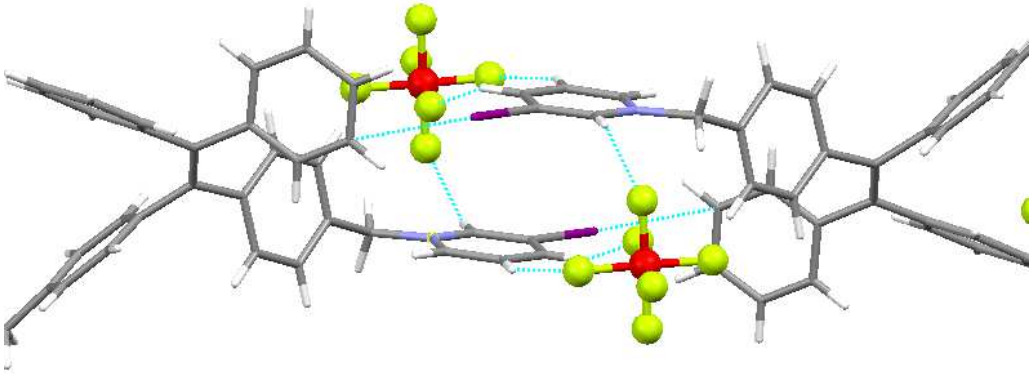

b)

Figure 4.4. (a) Extended packing showing *aba* stacking of layers in **4.3** down *c* (b) macrocyclic dimers of the cations with antiparallel edge-to-face π-stacking of iodopyridinium rings.

Compound **4.3** crystallizes in the monoclinic centrosymmetric space group C_2/c and features little to no interaction of the PF_6^- counterion with the iodine halogen-bond donor. Indeed, the extended packing of **4.3** reveals that the primary interactions in the solid state involve antiparallel edge-to-face π-stacking interactions ($d_{\pi\text{-}\pi} = 3.775$; Figure 4.4a) forming centrosymmetric macrocyclic dimers with additional interaction stemming from halogen bonding effects through C-I···π (over aryl carbon) synthons (C-I···C_{arene} = 3.546 Å, $R_{XB} = 0.96$; C-I-$C_{arene} = 168.99^0$). These C-I···C_{arene} distance and interactions are comparable with similar systems that have been studied by Pigge[130] and others.[132] The PF_6^- counterion appears to participate in only weak hydrogen-bonding interactions with acidic pyridinium-C-H groups (d = 2.512 Å).

It should be noted that the lack of adventitious solvent in the packing of crystals **4.2** and **4.3** likely arises from the tightly packed structure and the lack of any distinct porous channels through which solvent can travel. It should also be noted that a nitrate salt was obtained under similar experimental conditions to those listed for obtaining salt **4.6**, but crystals suitable for x-ray diffraction studies could not be successfully grown, though the presence of nitrate could be verified by a broad N-O stretching frequency range of 1300-1500 cm^{-1} in the IR.

Compounds **4.4-4.6** were obtained using 3-bromopyridine and a 3,3' bisbromomethyl TPE precursor. The bromide salt **4.4** was obtained with one methanol and one water solvate in the asymmetric unit. The salt crystallizes in an orthorhombic cell with space group Pccn and forms 2D arrays in alternating fashion with respect to the orientation of the dication. A view along the *b* axis reveals this array with Br^- counterions demarcating porous networks of channels, which the water solvates occupy (omitted for clarity, Figure 4.5a)

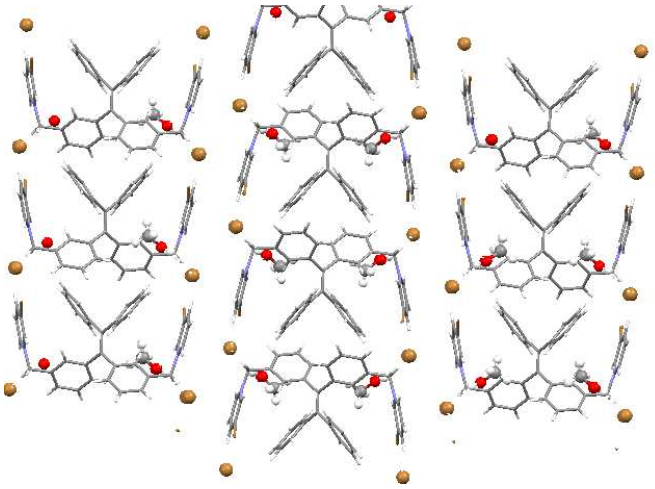

a)

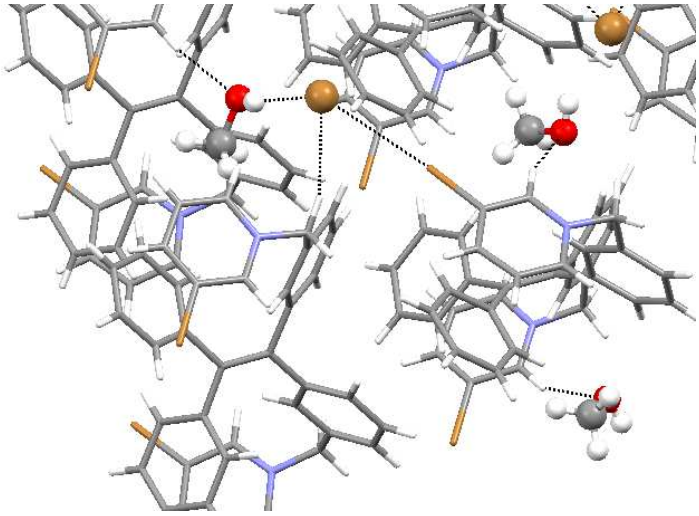

b)

Figure 4.5. (a) 2D arrays of **4.4** with bromide anions interfacing with a porous channel occupied by water solvates (omitted for clarity), view down *b* (b) coordination sphere of anion.

The coordination sphere of the bromide anion features a relatively weak C-Br···Br^- halogen bond (C-Br···Br^- = 3.568 Å, R_{XB} = 0.96; C-Br-Br^- = 169.86^0) in addition to a methanol solvate as a hydrogen bond donor (Figure 4.5b). A pyridinium methylene-CH_2 moiety serves as an additional hydrogen bond donor (d = 2.842 Å). The bromide counterion is bridging in a bifurcated interaction between the 3-bromopyridinium group from one TPE dication and a methylene-CH_2 group on an adjacent dication (C-Br···Br^-

$\cdots$H-C_{py} = 57.54^0) to form an infinite 1D chain where each bromopyridinium moiety is oriented anti to its intramolecular analogue in the solid state

In contrast to the anti- orientation of the 3-bromopyridinium rings in **4.4**, in the PF_6^- salt **4.5** the rings are syn-to one another within the same dication and only one of the bromo pyridinium donors could be considered to be participating in any discernable halogen-bonding (C-Br$\cdots\pi_{arene}$ = 3.310 Å, C-Br-π_{arene} = 167.65^0 Figure 4.6a). The other bromopyridinium arm is engaged in weak interactions with the hexafluorophosphate anion (d = 3.115 Å, R_{XB} = 0.99) while the anion is itself participating in interactions with two methylene –CH_2 moieties, one phenyl ring C-H and one pyridinium C-H. The extended packing of **4.5** shows solvated methanol caught within the binding pocket of the bromopyridinium TPEs, which is also participating in minor interaction with the counterion. There are no indications of additional interactions between adjacent TPE cations, and the halogen bond C-Br$\cdots\pi_{arene}$ synthon is suitable to direct assembly.

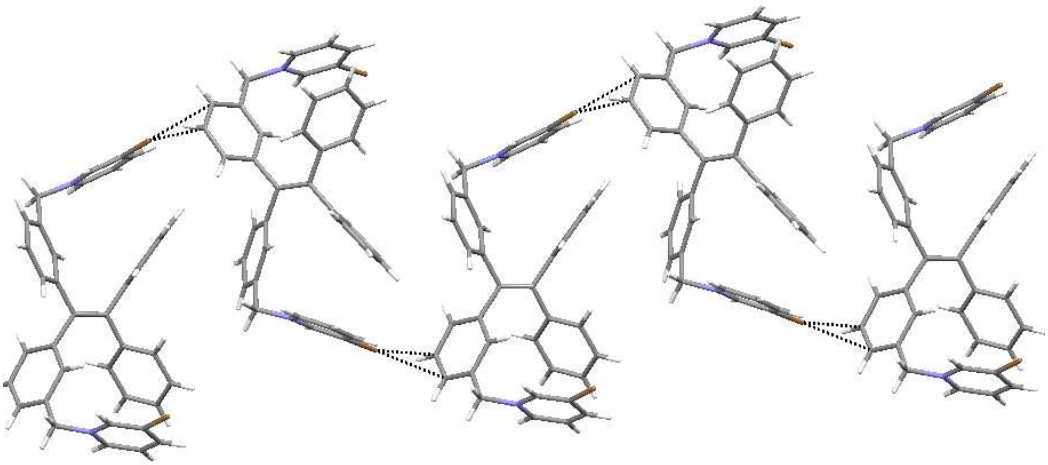

a)

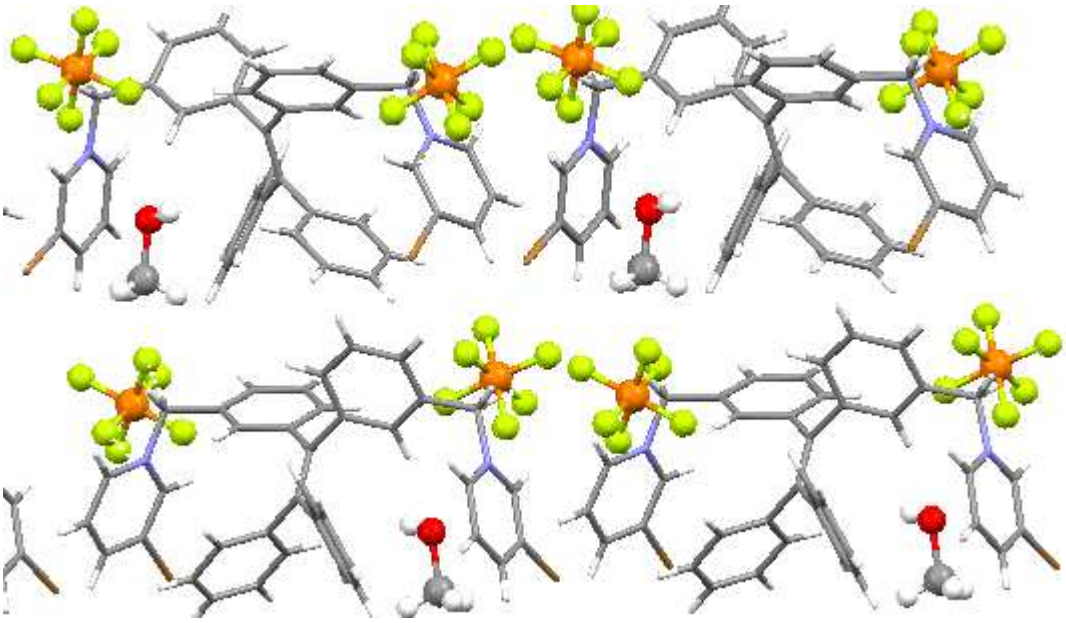

b)

Figure 4.6. a) C-Br···π_{arene} interactioins resulting in zig-zag chains of **4.5** b) extended packing of **4.5** with MeOH solvate, down *a*.

After anion metathesis of **4.4** with $AgNO_3$, the nitrate salt **4.6** was grown from MeOH/acetone (1:1) and was determined to crystallize in a monoclinic cell with space group $P2_1/c$. The nitrate anion and its centrosymmetric equivalent dimerize within a porous channel similar to the packing observed in **4.4** (Figure 4.7a) one methanol and one

water solvate are included. The TPE dications are arranged in arrays of 2D sheets arranged with alternating spatial orientation

The coordination environment around the nitrate anion features contributions from three pyridinium C-H groups, one methylene $–CH_2$ group, one methanol solvate, one water solvate, one phenyl ring C-H and a halogen-bond of modest strength (C-Br···O = 3.059 Å, R_{XB} = 0.93; C-Br-O = 159.64, Figure 4.7b) that compares to the strength of other halogen bonding systems that feature interactions with oxoanions.[133] The trigonal planar nature of the anion allows for coordination of multiple halogen bond and hydrogen bond donors to multiple atoms. The relatively electron-deficient pyridinium C-H and methylene $–CH_2$ groups are particularly well-suited to coordinate to an oxoanion such as nitrate, not only because of the abundance of oxygen acceptors, but also because of the relatively high solvation energy of many oxoanions, making halogen-bonding interactions with such anions relatively rare.[133]

a)

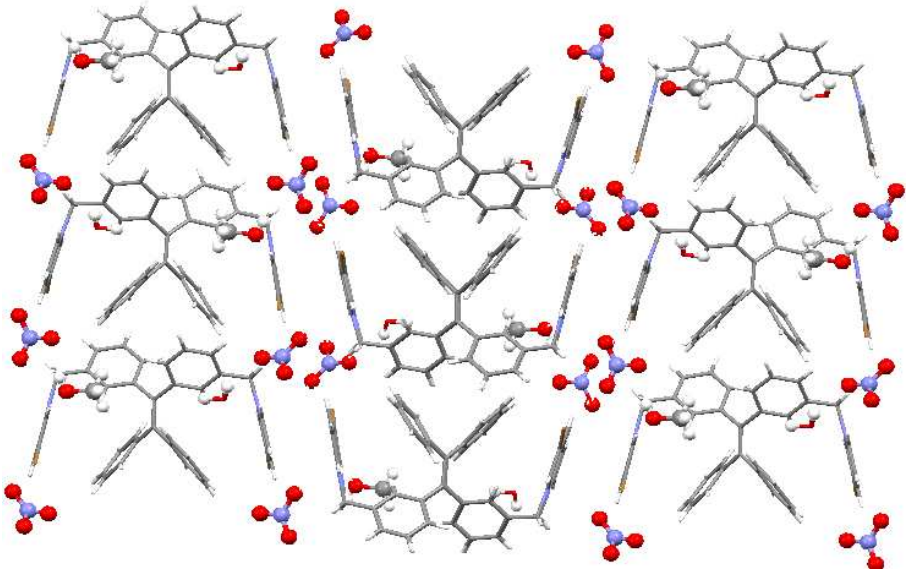

b)

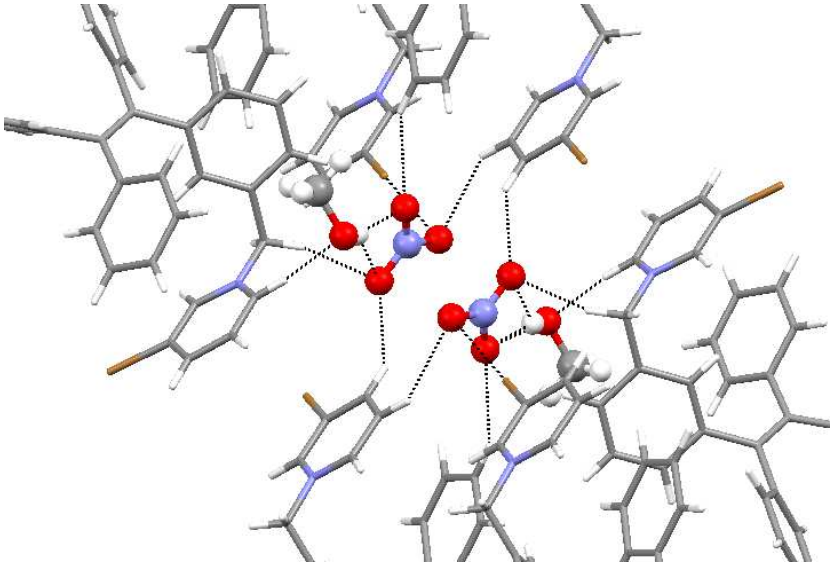

Figure 4.7. (a) 2D arrays of **4.6** with nitrate anions shown occupying porous channels, down *b* (b) coordination sphere of the centrosymmetric nitrate anions (water solvate omitted for clarity).

The combination of coordinating and noncoordinating anions used in these crystallographic studies offer some insight into the role that anions may play in the assembly of TPE-based materials in a combination with charge-enhanced halogen bond donors. In the presence of a coordinating anion, all three structural examples featured the dual hydrogen bonding/halogen bonding motif of py-CH_2···X^-···X'-C (**I** in Figure 4.8). In the case of a relatively strong halogen bond donor (such as in **4.2**) to the anion, the packing becomes sufficient to produce motif **II** as a logical extreme of **I** (with X-X^- -H angle idealized at 60^0; experimentally determined 59.65^0 for **4.2**). For noncoordinating anions such as PF_6^-, motifs **III** and **IV** become primary modes of coordination, with interactions either localized over one aryl carbon (**III**, as in **4.3**) or one aryl-π bond (**IV**, as in **4.5**). These motifs and their variants are well-known and have been discussed in numerous reports.[134,135]

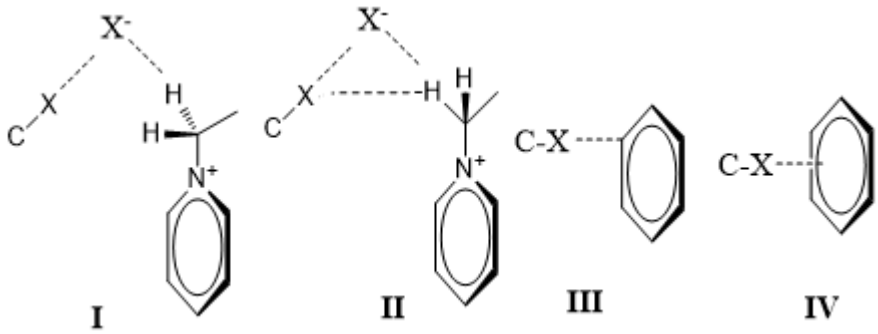

Figure 4.8. Halogen/hydrogen bond synthons observed in compounds **4.2-4.7**.

4.5 Synthesis and studies of TPE-bis-3-iodopyridinium and 2-iodoimidazolium salts as potential solution phase anion sensors

Our studies of anion-mediated assembly of TPE-based materials in the solid state led us to ask whether these compounds or similar compounds could conceivably be used as solution phase anion sensors that would theoretically incorporate halogen bonding as the method of anion recognition. Admittedly, while engineering materials that incorporate halogen bonding motifs has been an effective strategy in the solid state, its utility in solution phase interactions and anion recognition is relatively underexplored, however, notable examples arising from the work of Beer[98] and Resnati,[99] who have

incorporated 2-haloimidazolium sensors onto simple organic groups (bis-napthalene spaced macrocyles for Beer, anthracene groups for Resnati, Figure 4.8) that detect anionic substrates, introduced as tetrabutylammonium salts, through mechanisms of fluorescence emission enhancement and ^{1}H NMR monitoring have been reported.

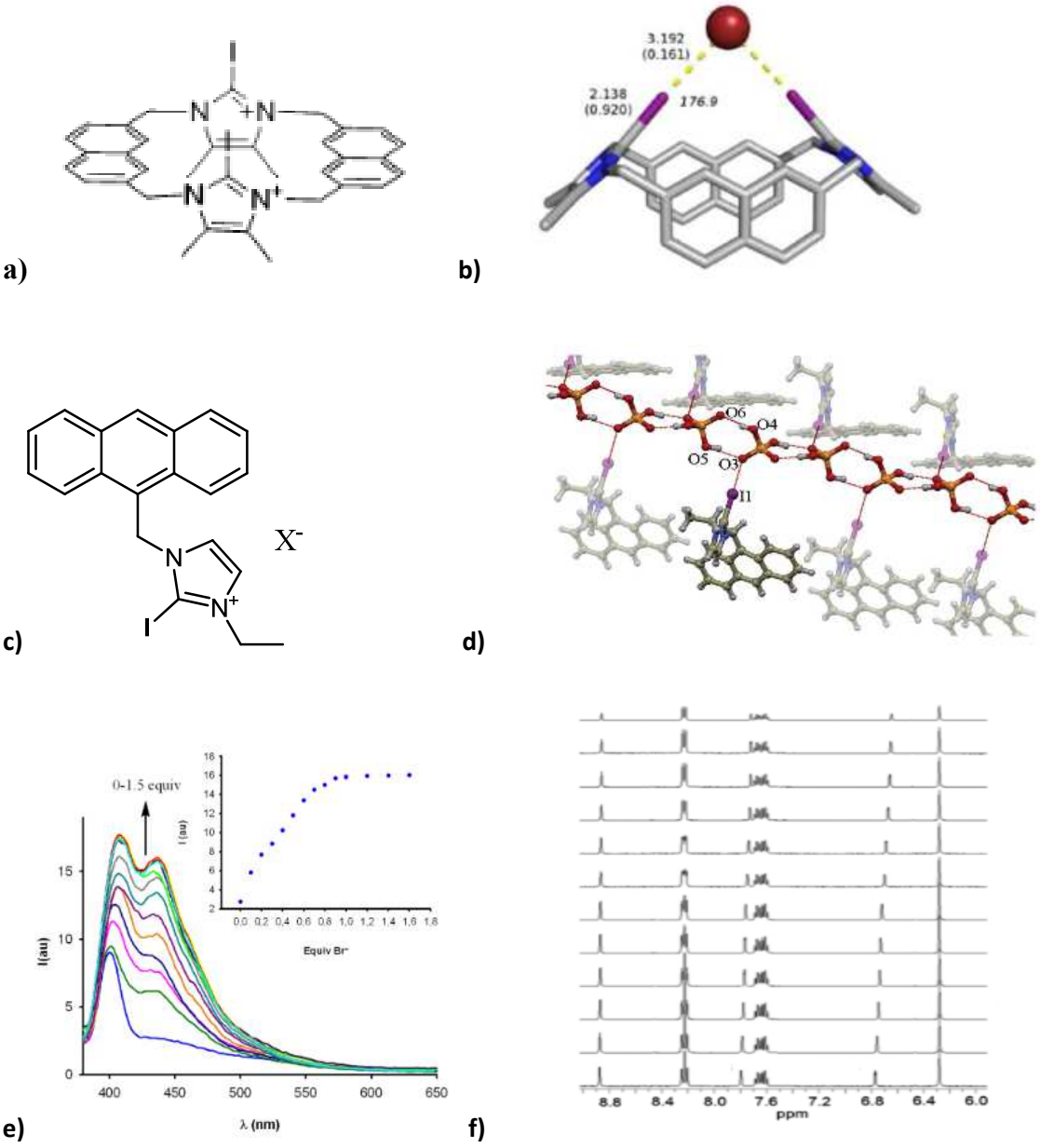

Figure 4.9. (a) Beer's iodoimidazolium-based macrocycles (b) crystal structure of sensor with bromide coordination (c) Resnati's iodoimidazolium sensor incorporating anthracene as fluorescent reporter (d) crystal structure of sensor with hydrogen phosphate coordination. (e) fluorescent response of imidazolium macrocycles in the presence of added bromide (f) ^{1}H NMR spectrum showing titration curve of Resnati's compound with added chloride increasing from bottom to top.

We set out to develop a series of simple TPE-based substrates that would incorporate charge-assisted halogen bonding as an anion recognition strategy and well-established AIE properties of the TPE-derived materials as a reporting mechanism.

To this end, our strategy focused on two classes of compounds; the 3-iodopyridinium-appended TPE derivatives previously discussed, and materials incorporating 2-iodoimidazolium as a recognition unit. Our intent was to investigate the capacity of these materials to participate in solution phase anion recognition relative to unhalogenated analogues, which were used to as controls in subsequent fluorometric studies.

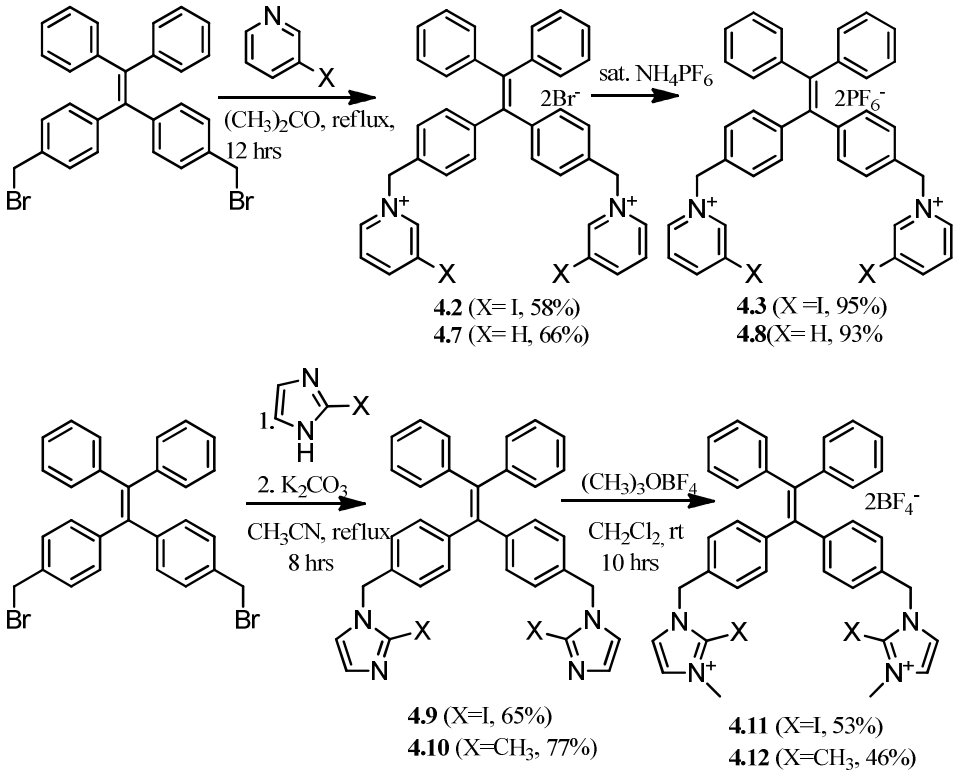

Scheme 4.3. Synthetic routes to pyridinium and imidazolium salts from a common precursor.

The desired pyridinium salts **4.3** and **4.8** were synthesized in a manner described previously in this chapter, with introduction of the 3-iodopyridine or pyridine to produce **4.2** and **4.7** as their bromide salts, which were then subjected to anion metathesis in the next step to produce **4.3** and **4.8** as their hexafluorophosphate salts. Imidazolium products **4.11** and **4.12** were synthesized with the addition of the appropriate 2-substituted imidazole (iodo- or methyl-) and a base under refluxing conditions in acetonitrile to afford the disubstituted neutral precursors **4.9** and **4.10** in good yields. The addition of trimethyloxonium tetrafluoroborate (Meerwein's salt) as a methylating agent under mild conditions in dichloromethane produced **4.11** and **4.12** as tetrafluoroborate salts in modest yields.

THF/0.15% DMSO (v/v) solutions of each of the salts (**4.3**, **4.8** ,**4.11** and **4.12)** were produced and a select group of anions were added to each of these solutions as their tetrabutylammonium salts (pyrophosphate was added as a tributylammonium salt) and their respective fluorescent responses were monitored by fluorescence emission spectroscopy.

The TPE-bispyridinium hexafluorophosphate salts **4.3** and **4.8** unfortunately did not produce any measureable fluorescent response outside of their own background emission when one equivalent of each respective anion was introduced (22.5 μM solution for **4.3**; 20.2 μM solution for **4.8**, in THF/0.15% DMSO v/v)

The bis-(2-iodoimidazolium) salt **4.11** did produce a measureable and variable response in the presence of 1 equiv. of select anions. The fluorescent responses elicited by the anions in descending order of magnitude are observed as $H_2P_2O_7^{2-} > HSO_4^- > CN^- > F^- > Ac^-, Bz^-, Cl^- > Br^-, NO_3^-, ReO_4^-$, and I^-. The same analysis was then performed on **4.12** where a methyl group blocks the 2-position of the imidazolium and hence, if the interactions were a sole consequence of solution-phase halogen bonding interactions with the anion, we would expect to see no significant or discernible changes in the fluorescence emission spectrum of **4.12** with one equivalent of anions added relative to a control sample with no anion added.

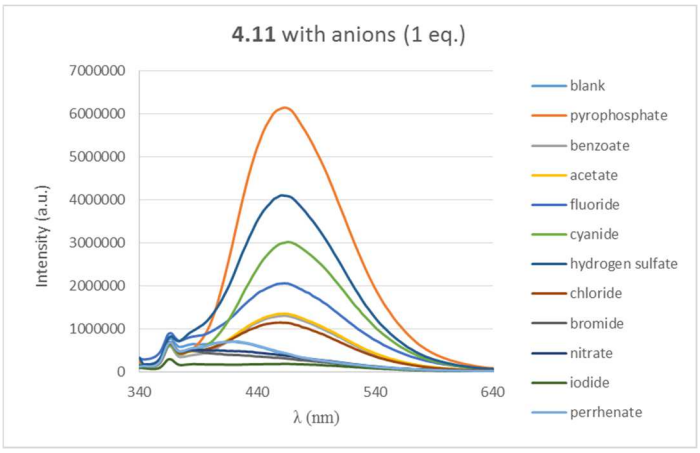

a)

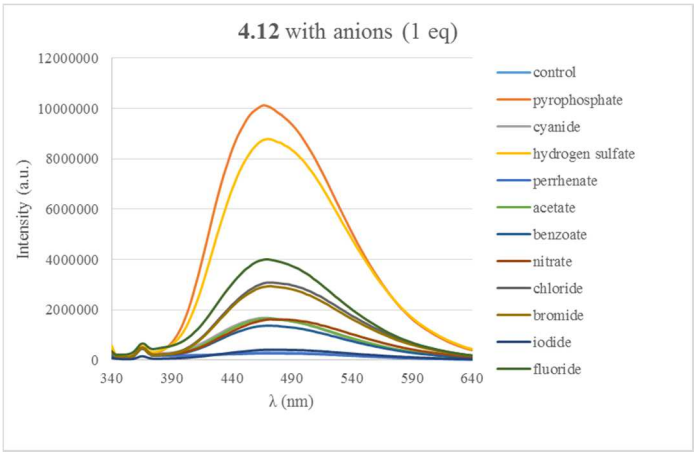

b)

Figure 4.10. (a) Fluorescence emission spectra of bis-imidazolium substrates **4.11** and **4.12** (a) **4.11** (23.2 μM in THF/0.15%DMSO v/v in the absence (control) and presence of one equivalent of anion, added as butylammonium salts (b) **4.12** (15.8 μM in THF/0.15% DMSO v/v in the absence (control) and presence of one equivalent of anion, added as butylammonium salts; λ_{ex} = 330 nm.

Instead what is observed is a similar trend in fluorescence response to the added anions, with $H_2P_2O_7^{2-}$ and HSO_4^- displaying the greatest response and ReO_4^-, I^-, and NO_3^- displaying the lowest response (Figure 4.9). The evidence would suggest that whatever fluorescence response that is generated in solutions of **4.11** and **4.12** is not the result of solution-phase halogen bonding, but rather a simple electrostatic interaction between the positively charged imidazolium rings and the negatively charged anions, with the strong response of $H_2P_2O_7^{2-}$ and HSO_4^- likely a result of their charge and/or possible available modes of interaction. The lack of performance in the pyridinium substrates **4.3** and **4.8**

may be attributed to either the larger ring size effectively delocalizing the positive charge over a larger area relative to the imidazolium substrates or the lack of appropriate donor capability from the iodine substituent. In either case, our attempts to develop TPE-derived anion sensors based upon the recognition mechanism of halogen-bonding interactions were largely unsuccessful, though these results may serve as a suitable starting point for any attempt to refine the method in the near future.

4.6 Summary

Five examples of bis-(3-halo)pyridinium salts of TPE-derived materials were analyzed in the solid state in the presence and absence of coordinating anions. These experiments were initiated to determine what influence, if any, the anion has on the self-assembly of complex materials such as TPE derivatives and also to assess the value of charge-assisted halogen bonding as a tool to effectively link to anionic groups and adjacent TPE molecules in measureable and predictable motifs. Such efforts continue to be of great importance in exploring the utility of halogen bonding and anion coordination chemistry in crystal engineering.

Although our efforts to produce solution-phase anion sensors that coordinate through halogen bond mediated interactions were largely unsuccessful, we maintain our interest in developing TPE-based anion sensors capable of detection through these types of interactions. Our initial unsuccessful attempt is illustrative of exactly how rare solution-phase halogen bonding truly is as an observable and reliable mode of anion recognition, yet we remain hopeful that these barriers may be overcome.

CHAPTER V
SUMMARY AND FUTURE DIRECTIONS

5.1 Summary

The main objective of the research described in the previous chapters was to extend the solution-phase and solid state chemistry of anion recognition and coordination via the study of several novel tetraphenylethylene (TPE) derivatives and N-haloarylpyridinium salts. To this end, the synthesis and application of these new and versatile materials for solution-phase and solid state anion coordination chemistry was described.

Principles of anion sensing in solution were successfully applied toward the synthesis of two new classes of TPE derivatives, each fundamentally distinguished by the implementation of either the urea- or amidopyrrole-moiety as a binding unit. Each unique class of sensors relies upon TPE as a fluorophore reporting unit to elicit the "turn-on" fluorescence effect of aggregation-induced emission (AIE) in the presence of select anions.

Three new examples of tetrasubstituted urea-TPEs were synthesized and characterized; their capacity to detect anions in THF solution (0.15% DMSO v/v) was determined via fluorescence emission spectroscopy and ^{1}H NMR analysis, with aggregation-induced emission (AIE) as the accepted mechanism of detection. The urea-TPEs display the greatest sensitivity toward the most basic anions ($F^- > OAc^- > OBz^- > Cl^- >> Br^- > NO_3^-, N_3^-, I^-$) with a measureable response recorded for each anion, relative to the modest fluorescent response from the TPE sensor in the absence of added anion. The sensors achieve their maximum fluorescence response in the presence of ~ 4 equiv. of added anions, suggesting all four urea moieties on the TPE sensor are engaged in anion binding activity. While the capacity for F^- to deprotonate some urea-based sensors is well-studied, no such deprotonation event is observed for any of the three TPE sensors in these studies.

Attempts to design a more selective TPE-based sensor originated from an initial interest in anionic dicarboxylate substrates, because of their significance in several natural processes. To this end, a new class of three bis-2-amidopyrrole-appended TPE sensors was designed for selective detection of dicarboxylates, with the amidopyrrole-moiety as the expected binding unit, as previous reports have noted. However, it was discovered that the amidopyrrole-TPEs do not display any appreciable sensitivity toward select dicarboxylate substrates, but rather, a noteworthy sensitivity toward pyrophosphate anion with limits of detection < 1 μM at concentrations of amidopyrrole-TPEs ranging from 12.5 to 17.5 μM in solutions of THF/0.15% DMSO (v/v). Deprotonation of the sensors in the presence of added fluoride was observed and was studied via fluorescence emission spectroscopy as well as ^{1}H and ^{19}F NMR titration experiments. The sensors designed are noted as being the first examples of TPE-based pyrophosphate sensors that do not require a Zn^{2+} cofactor (a feature common to several pyrophosphatase enzymes capable of detecting and cleaving pyrophosphate).[136,137]

The principles of anion-directed self-assembly of materials in the solid state were studied and expanded upon with the synthesis of a class of ten N-haloarylpyridinium salts (nine examples showcased the chloride counterion, with one exception containing iodide). The capacity of the bromo- and iodo-substituted pyridinium cations to participate in charge-assisted halogen bonding interactions with the counterion as halogen bond acceptor was assessed through a series of X-ray crystallographic studies. Iodo-substituted pyridinium cations were concluded to be overall better halogen bond donors than their bromo- analogues, an observation in agreement with accepted insights into the mechanism of halogen bonding interactions. In many cases, the halogen-bonding interaction successfully competes with hydrogen-donors in the form of acidic pyridinium C-H groups and adventitious solvent molecules. The presence of an abundance of halogen bond donors relative to chloride anion acceptors presents the opportunity for the formation of extended donor-acceptor-donor networks, which are observed in 2,4-diiodopyridinium substrates with the formation of helical assemblies and macrocyclic dimers. Two additional examples derived from nicotinamide and isonicotinamide bearing the 2,4-diiodophenylpyridinium moiety were synthesized and their capacity to maintain extended halogen-bonded networks in the presence of competing hydrogen bond donors

(the primary amide groups) was observed. These are the first reported examples of charge-assisted halogen bonding with the charged placed on an aromatic ring secondary to the established donor atom.

The last part of this work combined additional studies of solid state halogen-bonding interactions in a series of five TPE-based bis-halopyridinium salts with attempts to synthesize TPE-appended anion receptors capable of detecting anions via charge assisted halogen bonding in the solution phase. Halogen bond donor atoms were limited to either bromine or iodine in TPE-based pyridinium salts with bromide serving as a counterion halogen bond acceptor in two examples; the remaining examples included either hexafluorophosphate (two examples) or nitrate (one example) as a counterion acceptor and were accessed via anion metathesis of bromide precursors. Hexafluorophosphate salts of pyridinium- and 3-iodopyridinium-appended substrates were suspended in THF solution and analyzed in the presence of select anions via fluorescence emission spectroscopy. Unfortunately, there was no significant difference in fluorescence spectra between the 3-iodopyridinium-functionalized TPE and the unhalogenated pyridinium analogue and the AIE effect was not observed. Similarly, the fluorescence profile of TPE's functionalized with 2-iodoimidazolium groups in the presence of different anions was examined. Again, there was no significant difference in the fluorescence of 2-iodoimidazolium salts and their 2-methylimidazolium counterparts, signifying that any AIE fluorescent response elicited by the presence of added anions is likely not the result of halogen-bonding interactions, but rather nonspecific, electrostatic interactions. Investigations into the capability of similar TPE-based systems to participate in anion recognition via halogen bond-mediated interactions are ongoing.

5.2 Future Directions

We have demonstrated that N-haloarylpyridinium salts, particularly iodine-substituted substrates, can reliably form extended networks through halogen-bonding interactions between iodine donors and chloride acceptors and that these synthetic architectures can be accessed with relative ease through well-established chemistry. We seek to extend these studies through the design of increasingly complex, functional

materials, whose physiochemical/optical/electronic properties may in principle be attuned through varied combinations of organohalogen bond donors and anionic acceptors in additional anion-mediated self-assembled architectures in the solid state.

Additionally, we have demonstrated the potential of TPE-based anion sensors to participate in selective and sensitive detection of anions in solution phase studies. While the examples reported in previous chapters were characterized by hydrogen-bonding interactions between the binding unit and the anion to elicit the AIE fluorescent response in solution, future designs may conceivably incorporate additional hydrogen-bonding moieties, halogen bond donors, or both.

5.2.1 Non-linear optical materials incorporating the N-iodophenyl pyridinium motif

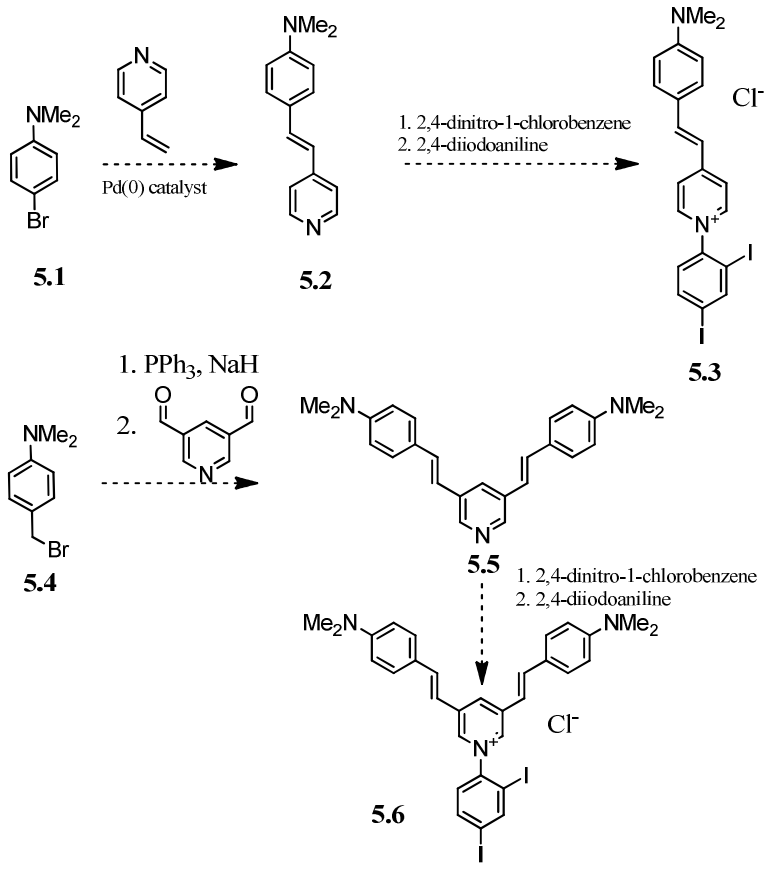

Scheme 5.1. Synthesis of **5.3** and **5.6** for potential studies in non-linear optics.

There is an increasing interest in the design and synthesis of conjugated donor-acceptor organic molecules with non-linear optical (NLO)[138,139] properties due to their increasingly diverse uses in biological imaging,[140] optoelectronics and dye-sensitized solar cells,[141,142] among other applications. Examples of potential 1D (**5.3**) and 2D (**5.6)** pyridinium-based chromophores can be synthesized by a combination of well-established organic/organometallic chemistry and synthetic methods specified in previous chapters of this work where the chromophores can be described as donor-π-acceptor complexes; the electron-donating capability of the aniline is offset by the electron-deficient diiodophenyl pyridinium moiety in a dynamic push-pull interaction characteristic of many NLO chromophores. Resnati and coworkers[143] recently reported the halogen-bond mediated self-assembly of a neutral iodoperfluoroaryl-appended N,N-dimethylaniline into infinite 1D-herringbone chains characterized by iodine-donor/nitrogen-acceptor head-to-tail interactions. NLO properties were discovered to be reliant upon the assembly of these chains and the perpetuation of the halogen bond donor/acceptor interaction. In addition to having the potential to self-assemble through halogen-bond mediated interactions, compounds **5.3** and **5.6**, as organic salts, can be further modified by substituting the counterion to attune the crystal structure/packing and solubility of the complexes, thereby optimizing the NLO capabilities and potential applications for these materials.

5.2.2 N-iodophenylpyridinium salts in additional supramolecular architectures

We have demonstrated the utility of incorporating the N-iodophenylpyridinium moiety into simple substrates with one pyridine ring available, in which the halogen-bond interaction between the iodine donor and halide acceptor is maintained even in the presence of potentially strong competing interactions from other hydrogen bond donors; we wish to expand the relatively simple and versatile synthetic methodology to increasingly complex architectures for further studies of anion-directed assembly in the solid state.

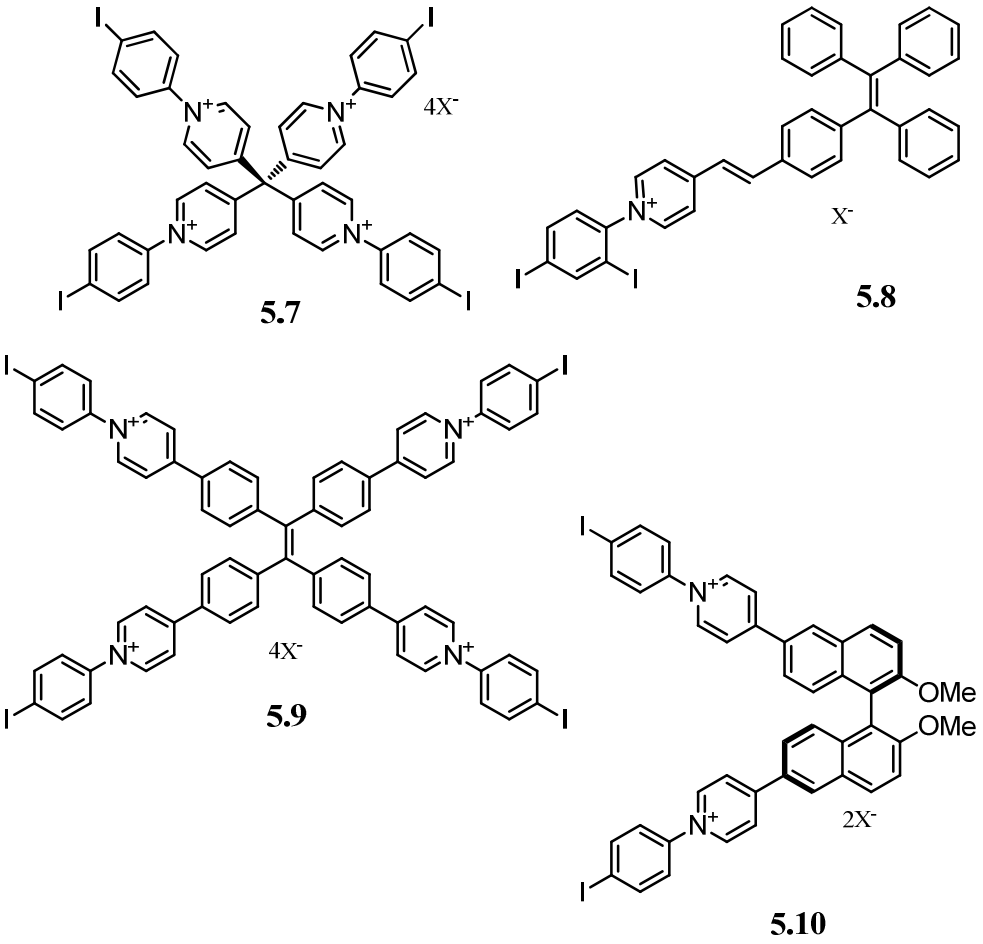

Figure 5.1. Some supramolecular building blocks of interest.

Compound **5.7** features a deviation from the planarity of substrates described in the previous chapter with four pyridine rings available to undergo the Zincke reaction with appropriate iodoaniline substrates resulting in a supramolecular tecton with a tetrahedral geometry. Our continued interest in TPE-based materials extends to the development of novel methods of self-assembly that compounds **5.8** and **5.9** could potentially afford. The enantioselective synthesis of the conformationally locked 1,1'-bi-2-methoxynapthalene derivative **5.10** affords the unique opportunity to engineer crystals with inherent chirality, a topic of growing interest in the field of crystal growth and design.[144,145]

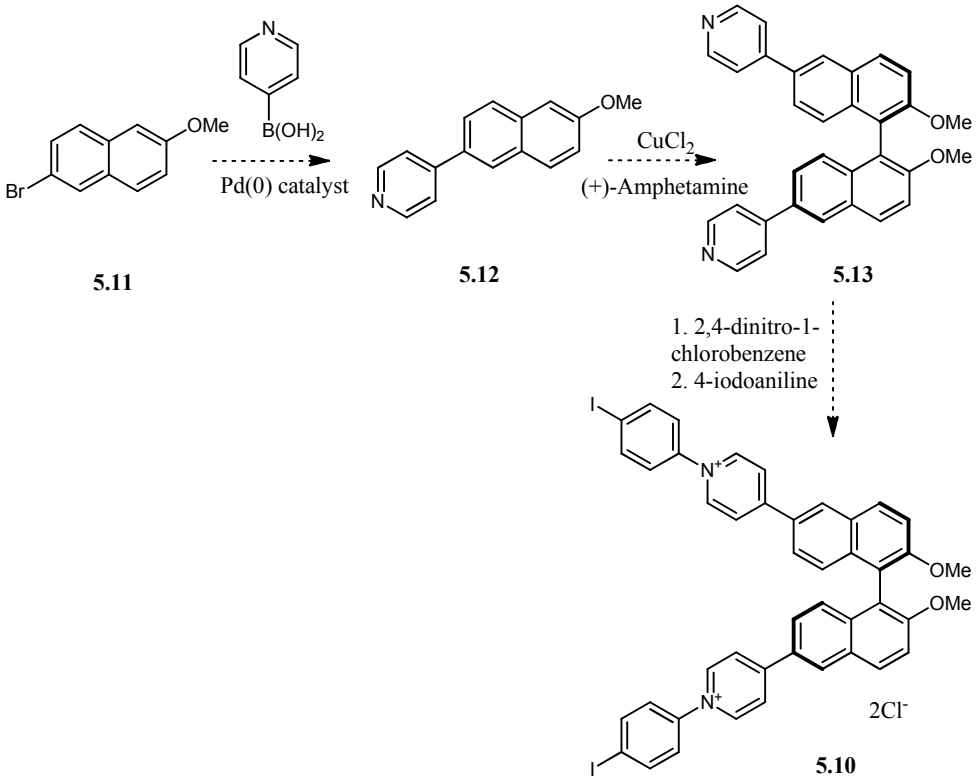

5.11 **5.12** **5.13** **5.10**

Scheme 5.2. Proposed synthetic route to **5.10**.

Neutral pyridine precursors to compounds **5.7,**[146] **5.8**,[82] and **5.9**[87] have been previously synthesized and their conversion to their N-iodopyridinium derivatives should be relatively straightforward. A plausible route to **5.10** is presented in Scheme 5.2 with commercially available starting material **5.11** undergoing Suzuki-coupling to form the pyridine-appended **5.12**. Oxidative coupling by $CuCl_2$ with S-(+)-amphetamine as a ligand should produce the R-enantiomer **5.13** selectively.[147] Two additional steps should produce **5.10**. While the presence of the chloride counterion is included in this proposed scheme to **5.10**, it should be noted that there is always potential to introduce different counterions to **5.7**-**5.9** via conventional methods of anion metathesis for additional studies on the influence of the counterion on the self-assembly and physical properties of these substrates.

5.2.3 Additional potential TPE-based anion receptors

TPE-based anion receptors reported in this work are all based primarily on hydrogen-bonding interactions between select binding units on the receptor and the anions in solution and are relatively simple in design. We wish to expand our studies of TPE-based anion receptors to include materials of increasing structural complexity in our efforts to develop progressively more sensitive and selective detectors.

One possible synthetic strategy that can be envisioned would be to tether two TPE fluorophores together with one binding unit as the linker. A discrete interaction of this binding unit with an anionic substrate may produce a measureable response by other methods of analysis such as ^{1}H NMR, but any fluorescent response from AIE would likely be minimal, as the two TPE fluorophores are constrained by design to one binding unit and an aggregation event would likely require interaction from multiple units. Anions may be excluded from this type of interaction by size, geometry, length, basicity and charge, affording the possibility of highly selective interactions.

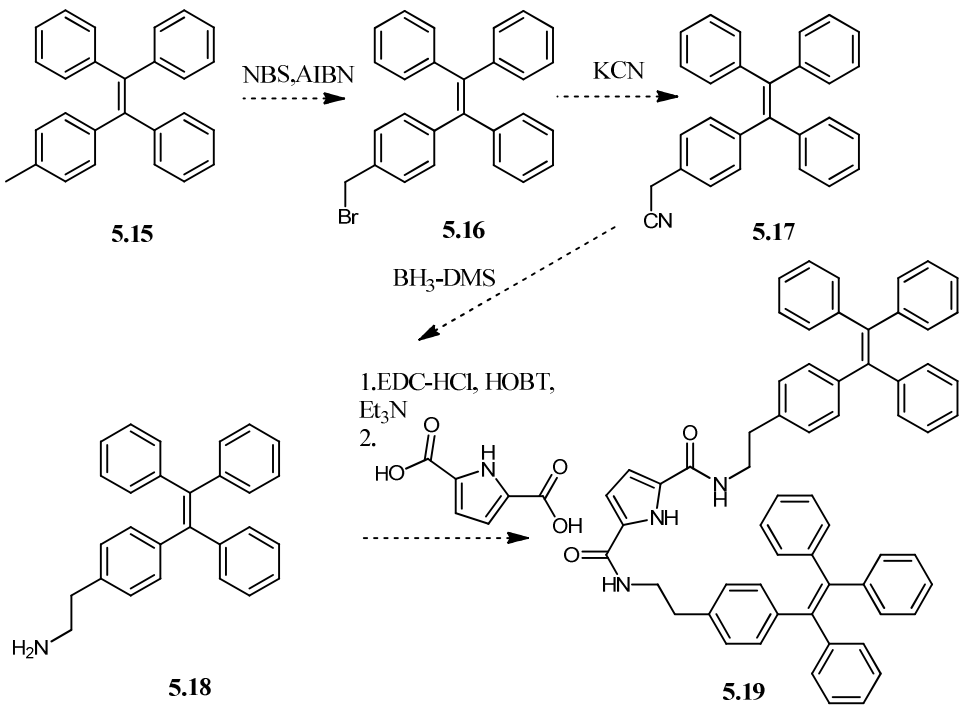

Scheme 5.3. Proposed synthetic route to 2,5 bis(TPE)-amidopyrrole tether **5.19**.

Scheme 5.3 features a plausible synthetic pathway to a 2,5-bis (TPE)-amidopyrrole tether **5.19** that can be accessed through slight modifications to chemistry previously discussed in this work. In this case, the nature of the binding unit may lend itself well to selectivity for anionic substrates such as certain phosphates, pyrophosphates and dicarboxylates, particularly dicarboxylates separated by alkyl chains of varying length. Smaller, spherical halides may be excluded from aggregation events simply based on size, with the bulky TPE fluorophores likely hindering any anion coordination between two units of **5.19**.

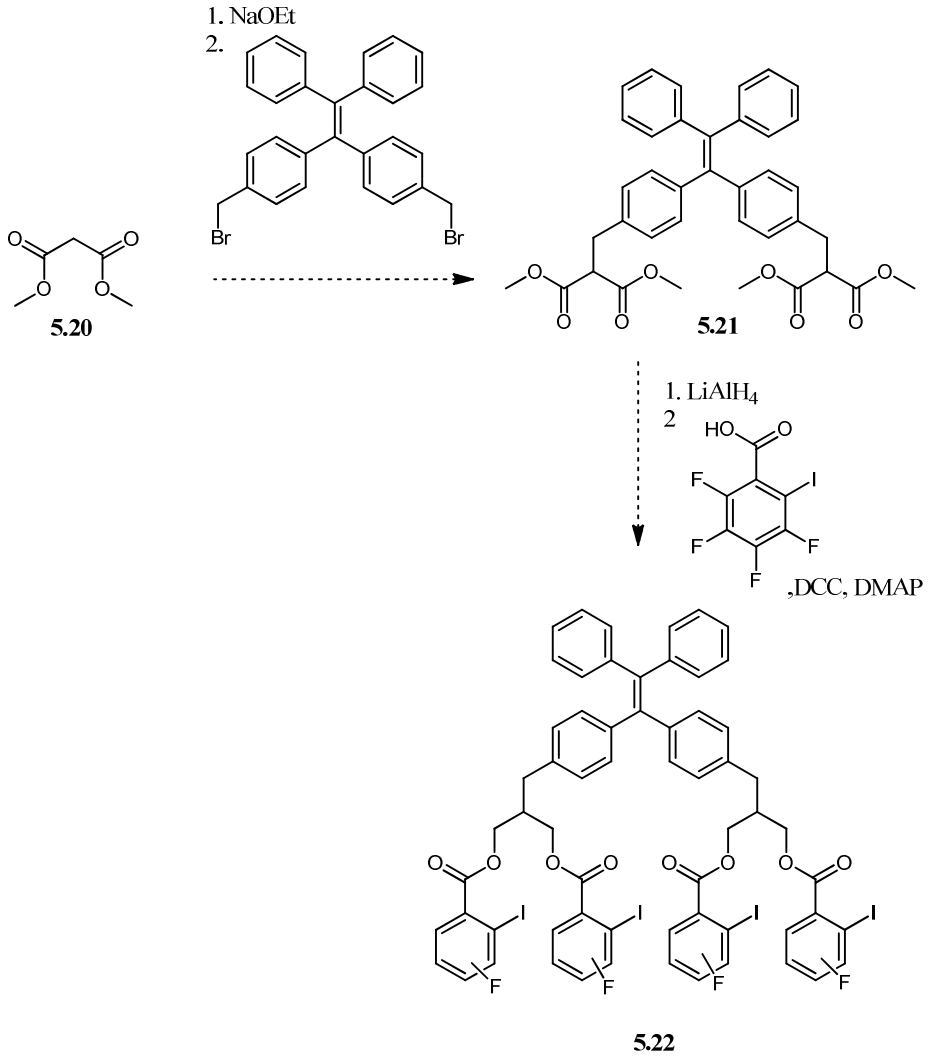

Scheme 5.4. Proposed synthetic route to a possible perfluoroiodoaryl TPE anion receptor **5.22**.

Taylor and coworkers[148] have developed several solution phase anion receptors incorporating iodoperfluoroaryl esters with halogen bonding interactions as the accepted mechanism of interaction and subsequent detection. A conceivable route to TPE-based anion receptor **5.22 (**Scheme 5.4) would begin with addition of a base to dimethylmalonate followed by addition of a bis(4-bromomethyl) tetraphenylethylene along with subsequent reduction by $LiAlH_4$ to a tetraalcohol precursor. Steglich esterification with 2-iodo-3,4,5,6-tetrafluorobenzoic acid should produce the desired receptor **5.22**. Any recognition of anionic substrates would be expected to proceed via

halogen-bonding interactions in solution between an iodine donor and an anionic acceptor.

Using these simple examples and drawing upon a consistent flow of inspiration to synthesize similar materials, we hope to continue to engage in expanding the field of anion coordination chemistry in both the solution phase and solid state in our future research endeavors.

CHAPTER VI

EXPERIMENTAL

6.1 General experimental details

All commercially available starting materials were used as received unless otherwise noted. All reactions were performed under argon atmosphere. Solvents were degassed with argon and purified by passage through activated alumina columns. Proton nuclear magnetic resonance (^{1}H NMR) spectra and carbon nuclear magnetic resonance (^{13}C NMR) spectra were recorded at 300 MHz and 75 MHz, respectively. Chemical shifts are recorded at δ values in parts per million (ppm) relative to tetramethylsilane for ^{1}H NMR and ^{13}C NMR in $CDCl_3$ and residual undeuterated solvent for all other spectra. High resolution mass spectra were obtained using electrospray ionization (ESI). Melting points were recorded using a capillary melting point apparatus and are uncorrected. Single crystal x-ray diffraction data were collected on a Bruker Nonius-Kappa CCD diffractometer. Powder x-ray diffraction data were collected on a Siemens D5000 X-ray diffractometer. UV-vis absorbance spectroscopy was performed on a Varian Cary 100-scan dual beam spectrofluorometer with 1 cm quartz cuvettes. Fluorescence spectroscopy was performed on a Horiba Jobin Yvon Fluoromax 4 spectrofluorometer in a 1 cm quartz cell and commercially available spectroscopy grade solvents were used. Slit width for excitation and emission were 5 nm each and integration time was 0.1s.

SHELXTL was used for processing of X-ray data. Crystallographic data were processed using full matrix least squares refinement of F^2 against all reflections. The weighted R-factor (wR) and goodness of fit S are based on F^2, conventional R-factors (R) are based on F, with F set to zero for negative F^2. The threshold expression of $F^2 > 2\sigma(F^2)$ is used only for calculating R-factors, etc., and is not relevant to the choice of reflections for refinement. R-factors based on F^2 are statistically about twice as large as those based on F, and R-factors based on all data will be even larger.

6.2 Experimental data for Chapter 2

Preparation of **2.5**

Compound **2.4** was prepared according to a previously published procedure. To a 250 mL round bottom flask, 1.10 g (2.78 mmol) of **2.4** was dissolved in 150 mL of acetonitrile. To this solution, 5.88 g (42.6 mmol) of anhydrous K_2CO_3 and 4.0 mL (6.88 g, 63.3 mmol) of bromoacetonitrile were added and the mixture was stirred at reflux for 3 days at which point TLC analysis indicated reaction completion. The reaction mixture was filtered through celite while washing with ethyl acetate. The crude filtrate was adsorbed onto silica and passed through a silica column eluted with 40-50% EtOAc in hexanes. Fractions were collected and solvent was removed by rotary evaporation to yield 0.95g (62%) of light brown solid. Mp 117-121^{0}C. ^{1}H NMR (300 MHz, $CDCl_3$, δ in ppm): 4.73 (s, 2H), 6.75 (d, 2H, J= 9.0 Hz) 6.98 (d, 2H, J= 9.0 Hz). ^{13}C NMR (75 MHz, $CDCl_3$ δ in ppm): 155.0, 138.8, 138.2, 132.7, 115.0, 114.3, 55.5: LRMS (ESI): calculated for $C_{34}H_{24}N_4O_4Na$ $[M+Na]^+$, 575.2; Found: 575.1

Preparation of **2.6**

Compound **2.5** (1.71 g, 3.10 mmol) was dissolved in 100 mL of THF and 18.5 mL (11.9 mmol) of BH_3:DMS (2 M solution in hexanes) was added slowly via syringe while the reaction mixture was stirred at room temperature. The reaction was heated to reflux under argon for 8 hours, during which time the solution thickened and became translucent. The reaction mixture was quenched with methanol and allowed to stir until the solution was homogenous. The mixture was gravity-filtered and the filtrate was rotary evaporated to dryness. The resulting solid was washed with ethyl acetate, acetone and diethyl ether and allowed to dry to yield 1.43 g (80%) of **7** as a light yellow solid. ^{1}H NMR (DMSO-d_6, δ in ppm): 2.88 (t, 2H, J= 5.7 Hz), 3.88 (t, 2H, J= 5.4 Hz), 6.72 (d, 2H, J= 9.0 Hz), 6.87 (d, 2H, J= 9.0 Hz). ^{13}C NMR (75 MHz in DMSO-d_6, δ in ppm) 41.0, 70.0, 113.7, 132.0, 136.2, 138.0, 157.0. HRMS (ESI): calculated for $C_{34}H_{41}N_4O_4$ $[M+H]^+$, 569.3128; Found: 569.3119

General procedure for preparation of tetraureas **2.7-2.9**

Compound **2.6** (0.137 g, 0.241 mmol) and 4 mL of anhydrous DMF were combined in a 20 mL scintillation vial and stirred. To this solution 0.150 mL (0.133 g, 1.34 mmol) of butyl isocyanate was added dropwise over the course of 1 min. The vial was capped and stirred at 40^0C for 4 hours. The reaction mixture was then rotary evaporated to dryness and washed with ethyl acetate. Insoluble material was stirred with acetonitrile for an additional 4 hours, collected by vacuum filtration and dried under vacuum to give 0.184 g (79%) of **2.7** as an off-white solid. Mp: 218-221^{0}C. ^{1}H NMR (300 MHz in DMSO-d_6, δ in ppm): 0.89 (t, 3H, J= 6.9 Hz), 1.34 (m, 4H), 3.01 (q, 2H, J= 6.3 Hz), 3.35 (t, 2H, J= 5.4 Hz), 3.89 (t, 2H, J= 5.1 Hz), 5.96 (t, 1H, J= 5.7 Hz), 6.02 (t, 1H, J= 5.4 Hz), 6.75 (d, 2H, J= 8.7 Hz), 6.86 (d, 2H, J= 8.7 Hz). ^{13}C NMR: (75 MHz, DMSO-d_6, δ in ppm) 13.6, 19.5, 32.0, 38.8, 38.9, 67.0, 113.5, 132.0, 136.4, 138.1, 156.7, 158.1. HRMS (ESI): calculated for $C_{54}H_{77}N_8O_8$ $[M+H]^+$, 965.586.4; Found: 965.5855

The procedure for the preparation of **2.8** was the same as that for **2.7** above with the addition of phenyl isocyanate . Yield 87% Mp: 181-184^{0}C. ^{1}H NMR (300 MHz in DMSO-d_6, δ in ppm) 3.46 (t, 2H, J= 5.1 Hz), 3.95 (t, 2H, J= 5.1 Hz), 6.38 (t, 1H, J= 5.4 Hz) 6.76 (d, 2H, J= 8.7 Hz) 6.88-6.94 (m, 3H), 7.25 (t, 2H, J= 7.5 Hz), 7.41 (d, 2H, J= 7.8 Hz) 8.58 (s, 1H). ^{13}C NMR (75 MHz, DMSO-d_6, δ in ppm), 38.6, 66.8, 113.7, 117.6, 121.1, 128.6, 132.0, 136.4, 137.9, 140.4, 155.2, 156.6. HRMS (ESI): calculated for $C_{62}H_{61}N_8O_8$ $[M+H]^+$, 1045.4612; Found: 1045.4602

The procedure for the preparation of **2.9** was the same as that for **2.8** and **2.7** above with the addition of benzyl isocyanate. Yield 91%. Mp: 202-206^{0}C. ^{1}H NMR (300 MHz in DMSO-d_6, δ in ppm): 3.40 (t, 2H, J= 5.1 Hz), 3.92 (t, 2H, J= 5.1 Hz), 4.26 (d, 2H, J= 6.0 Hz), 6.21 (t, 1H, J= 5.4 Hz), 6.50 (t,1H, J= 6.0 Hz), 6.75 (d, 2H, J= 8.7 Hz), 6.91 (d, 2H, J= 8.7 Hz), 7.24-7.35 (m, 5H). ^{13}C NMR (75 MHz, DMSO-d_6, δ in ppm): 38.9, 42.9, 67.1, 113.7, 126.5, 127.0, 128.2, 132.0, 136.3, 138.0, 141.0, 156.7, 158.0. HRMS (ESI): calculated for $C_{66}H_{69}N_8O_8$ $[M+H]^+$, 1101.5238; Found: 1101.5231

General procedure for preparation of compounds **2.12** and **2.13**

The appropriate unsubstituted precursor (either **2.10**[90] or **2.11**,[91] 1.00 g, 2.7 mmol) was added to a stirring solution of N-bromosuccinimide (1.06 g, 5.94 mmol) in 100 mL CCl_4. Azobisisobutyronitrile (AIBN, 10 mg, 0.10mmol) was added to the reaction mixture, which was then subsequently heated to gentle reflux over 12 hours. The solution was then cooled to room temperature and 100 mL of water was added. The product was extracted with 2 x 50 mL extractions in CH_2Cl_2, extractions were combined, washed with brine, dried over Na_2SO_4, filtered, and the solvent was removed via rotary evaporation. The crude material was deemed suitable for the proceeding steps.

Compound **2.12** obtained as cream-white solid. Yield 83%. Mp: 214-217 ^{0}C. ^{1}H NMR: (300 MHz in $CDCl_3$) 7.11-6.85 (m, 18 H), 4.42 (s, 4 H); ^{13}C NMR: (75 MHz, $CDCl_3$: 144.0, 143.3, 142.0, 139.5, 135.9, 131.4, 130.8, 128.5, 128.0, 126.6, 33.5; LRMS (ESI) calculated for $C_{26}H_{22}Br$ $[M\text{-}Br]^+$ = 438.8; found 438.8 and 440.8

Compound **2.13** obtained as light yellow solid. Yield 88%: Mp: > 220^0 C. ^{1}H NMR: (300 MHz in $CDCl_3$) 7.15-6.9 (m, 18 H), 4.38 (s, 4 H); ^{13}C NMR: (75 MHz, $CDCl_3$) 143.8, 143.5, 142.4, 141.0 140.9, 137.0, 131.2, 130.0, 129.8, 127. 4, 127.2, 126.9, 126.2, 125.3, 34.0; LRMS (ESI) calculated for $C_{26}H_{22}Br$ $[M\text{-}Br_{79}]^+$ = 438.8; found 438.8 and 440.8

Procedure for preparation of compounds **2.14** and **2.15**

Either **2.12** or **2.13** (400 mg, 0.772 mmol) was dissolved in 75 mL of acetonitrile and sodium azide (500 mg, 7.7 mmol) was added and the solution was allowed to reflux for 10 hrs. The solution was cooled to room temperature and the product was extracted with EtOAc (2 x 50mL) after water was added to the mixture. The organic layer was dried with Na_2SO_4 and the solvent was removed via rotary evaporation with the product adsorbed onto silica. The product was purified on a column with 1:8 hexanes/ EtOAc as eluent.

Compound **2.14** obtained as a light yellow semisolid. Yield 80%: ^{1}H NMR: (300 MHz in $CDCl_3$) 7.13-7.02 (m 10H), 6.98 (d, 4H, J = 8.7 Hz). 6.93 (d, 4H, J = 8.7 Hz), 4.54 (s, 4H); ^{13}C NMR: (75 MHz in $CDCl_3$) : 143.8, 143.1, 139.5 134.7, 131.2, 131.0, 128.2, 128.2, 127.7, 126.7, 54.3; LRMS (ESI) calculated for $C_{26}H_{23}N_6$ $[M+H]^+$ = 443.1; found 443.1

Compound **2.15** obtained as a light yellow semisolid. Yield 71%: ^{1}H NMR: (300 MHz in $CDCl_3$) 7.12-7.02 (m, 10 H), 6.97-6.83 (m, 8 H), 4.10 (s, 4 H); ^{13}C NMR: (75 MHz, $CDCl_3$) 143.9, 143.1, 139.5, 134.6, 131.3, 131.1, 131.0, 128.2, 127.8, 127.7, 126.7, 126.5, 54.5; LRMS (ESI) calculated for $C_{26}H_{23}N_6$ $[M+H]^+$ = 443.1; found 443.1

Procedure for preparation of compounds **2.16** and **2.17**

Either compound **2.14** or **2.15** (300 mg, 0.67 mmol) is added to a stirred suspension of lithium aluminum hydride (103 mg, 2.68 mmol) in 30 mL of THF at 0^0 C and allowed to stir on ice for 8 hrs. The mixture is quenched with the sequential addition of 3 mL H_2O, 9 mL of aqueous 15% NaOH, 3 mL of H_2O, and the product is extracted in EtOAc (2 x 20 mL), washed with brine, dried with Na_2SO_4 and removal of the solvent via rotary evaporation. The crude product was deemed suitable by ^{1}H NMR to proceed with the next step.

Compound **2.16** obtained as a yellow solid, yield 66%: Mp: 142-145^0 C: ^{1}H NMR (300 MHz, $CDCl_3$): 7.11-6.92 (m, 18 H), 3.59 (s, 4 H): ^{13}C NMR (75 MHz, $CDCl_3$): 143.6, 142.4, 131.2, 130.2, 129.7, 127.8, 127.6, 127.5, 126.2, 125.1, 46.1; HRMS (ESI) calculated for $C_{28}H_{24}N$ fragment $[M-NH_2]^+$ = 374.1909; found 374.1904

Compound **2.17** obtained as a yellow solid, yield 73%: Mp: 151-154^0 C: ^{1}H NMR (300 MHz, $CDCl_3$): 7.14-6.87 (m, 18 H), 3.63 (s, 4 H): ^{13}C NMR (75 MHz, $CDCl_3$): 143.4, 142.2, 131.2, 130.2, 129.7, 129.5, 128.6, 127.8, 127.6, 127.5, 126.2, 125.1, 46.1; HRMS (ESI) calculated for $C_{28}H_{24}N$ fragment $[M-NH_2]^+$ = 374.1909; found 374.1904

Procedure for preparation of compounds **2.18**, **2.19** and **2.22**

To a stirred solution of 2-pyrrolecarboxylic acid (1.20 mmol) in 30 mL of DMF at 0 ^{0}C was added EDC-HCl (1.00 mmol) and 1-hydroxybenzotriazole (HOBT, 1.00 mmol) and

the mixture was allowed to stir for 10 minutes. At this time the appropriate diamine (**2.16**, **2.17** or **2.21**, 0.500 mmol) was added with 1 mmol of triethylamine and the mixture was allowed to stir overnight for 12 hours at room temperature. The mixture was collected and 250 mL of brine solution was added. The product was extracted into EtOAc (2 x 50 mL). The organic layer was washed with 10% $NaHCO_3$ and dried over Na_2SO_4 with subsequent rotary evaporation of the solvent affording a crude white solid. Trituration of the crude material in hot hexanes, filtering and subsequent drying afforded the desired product.

Compound **2.18** obtained as a cream white solid, yield 78%. Mp: 159-163^0 C. ^{1}H NMR: (300 MHz, d_6-DMSO) (δ): 10.18 (s, 2H), 7.18 (d, 2H), 7.12-6.89 (m, 18H), 6.80 (d, 2H, J = 6.3 Hz) 6.74 (d, 2H, J = 6.3 Hz) 6.21 (t, 2H), 4.26 (s, 4H); ^{13}C NMR (75 MHz, d_6-DMSO): 162.3, 143.4, 142.8, 135.1, 134.8, 133.9, 133.6, 133.4, 132.4, 130.0, 129.5, 127.9, 121.9, 110.3, 109.0, 43.6; HR (ESI) calculated for $C_{38}H_{33}N_4O_2$ $[M+H]^+$ = 577.2604; found 577.2608

Compound **2.19** obtained as a white solid, yield 86%. Mp: 146-148^0 C. ^{1}H NMR: (300 MHz, d_6-DMSO) (δ): 10.06 (s, 2H), 7.16 (d, 2H), 7.12-6.89 (m, 18H), 6.80 (d, 2H, J = 6.3 Hz) 6.74 (d, 2H, J = 6.3 Hz) 6.21 (t, 2H), 4.32 (s, 4H); ^{13}C NMR (75 MHz, d_6-DMSO): 161.8, 143.4, 142.8, 135.1, 134.8, 133.9, 133.6, 133.4, 132.4, 131.6, 131.1, 130.0, 129.5, 127.9, 121.9, 110.3, 109.0, 43.6; HR (ESI) calculated for $C_{38}H_{33}N_4O_2$ $[M+H]^+$ = 577.2604; found 577.2608

Compound **2.22** obtained as a white solid, yield 65%: Mp: 153^0 C (dec). ^{1}H NMR: (300 MHz, d_6-DMSO) (δ): 10.15 (s, 2H), 7.18 (d, 2H), 7.14-6.85 (m, 18H), 6.80 (d, 2H, J = 6.3 Hz) 6.74 (d, 2H, J = 6.3 Hz) 6.21 (t, 2H), 3.05 (t, 4H), 2.81 (t, 4H): ^{13}C NMR (75 MHz, d_6-DMSO): 162.3, 143.4, 142.8, 135.1, 134.8, 133.9, 133.6, 133.4, 132.4, 130.0, 129.5, 127.9, 121.9, 110.3, 109.0, 46.4, 38.1: HR (ESI) calculated for $C_{40}H_{37}N_4O_2$ $[M+H]^+$ = 605.3138; found 605.3116

Preparation of compound **2.20**

Compound **2.12** was dissolved in 50 mL of CH_3CN (400 mg, 0.77 mmol) and potassium cyanide was added (7.72 mmol). The mixture was allowed to stir at reflux for 14 hrs at

which point, the reaction mixture was diluted with water (250 mL) and the crude product extracted with EtOAc (2 x 25 mL), washed with brine and dried over Na_2SO_4, before rotary evaporation removed the solvent and the product was adsorbed onto silica. The product was purified by column chromatography with 9:1 Hexanes: EtOAc as eluent. Product was collected as a dark yellow oil.

Compound **2.20** product obtained as a dark yellow oil, yield 90%; ^{1}H NMR (300 MHz, $CDCl_3$) (δ): 7.26-6.96 (m, 18 H), 3.65 (s, 4H): ^{13}C NMR (75 MHz, $CDCl_3$): 143.3, 142.4, 131.2, 130.5, 129.6, 127.8, 127.6, 127.5, 126.2, 125.1, 117.8, 46.1; LRMS (ESI) calculated for $C_{30}H_{23}N_2$ $[M+ H]^+ = 411.1$; found 411.1

Preparation of Compound **2.21**

To a solution of 50 mL THF at 0^0 C in an ice bath was added 250 mg of compound **2.20** (0.61 mmol) which was dissolved and then 2.4 mL of BH_3-DMS solution was added via syringe under argon to the reaction mixture (4.9 mmol, 2.0 M in THF). The ice bath was removed after 30 minutes and the reaction was allowed to proceed at room temperature for a further 8 hours. The reaction was quenched with 3 mL of EtOH, diluted with 20 mL of water and the product was extracted with EtOAc, dried over Na_2SO_4 and solvent removed under vacuum. Product was triturated with warm hexanes and additional drying.

Compound **2.21** obtained as a light yellow solid, yield 84%. Mp: 160^0 C (dec): ^{1}H NMR (300 MHz, d_4-MeOD) (δ): 7.15-6.83 (m, 18 H), 2.96 (t, 4H), 2.80 (t, 4H): ^{13}C NMR (75 MHz, d_4-MeOD): 143.6, 142.4, 141.1, 131.3, 131.1, 130.2, 129.7, 127.7, 126.3, 125.1, 46.1, 43.4; LRMS (ESI) calculated for $C_{30}H_{31}N_2 = 419.1$: Found 419.1

6.3 Experimental data for Chapter 3

General procedure for the preparation of **3.3**-**3.12**

Zincke salts **3.1**[149] and **3.2**[150] were prepared according to previously published procedures. To a stirring solution of n-butanol (5mL) in a 10mL round bottom flask was added 0.5mmol of the appropriate Zincke salt and 0.75mmol of the appropriate haloaniline. The mixture was stirred at reflux under argon for 3 days when disappearance of the Zincke salt starting material, monitored by LR (ESI) mass spectrometry, indicated reaction completion. The solvent was evaporated under reduced pressure and the crude material

was dissolved in a minimal amount of methanol and added dropwise to a solution of diethyl ether (200mL). The precipitate was filtered and washed sequentially with diethyl ether and ethyl acetate until washings became clear in color and then subsequently dried under vacuum.

The salts are all insoluble in most organic solvents but exhibit good solubility in methanol and n-butanol and are sparingly soluble in acetone and water.

Preparation of Zincke salts **3.13** and **3.15**

Either nicotinamide or isonicotinamide (1.00g, 8.20 mmol) was dissolved in 50 mL of EtOH and 2,4-dinitro-1-chlorobenzene (2.50 g, 12.3 mmol) was added while stirring. The mixture was refluxed for 18 hrs at which point the Zincke salt precipitate was filtered, washed with EtOAc and dried under vacuum.

Preparation of compounds **3.14** and **3.16**

Preparation for compounds **3.14** and **3.16** followed a similar method as was denoted for compounds **3.3**-**3.12**, however concerns with solubility of the salt precursors compelled us to use DMF, rather than n-BuOH with the reaction held at 120^0C over 36 hours with consistent monitoring of the reaction mixture with LR (ESI) mass spectrometry to ascertain the disappearance of the starting material. The solvent was then removed under vacuum and the crude material was rinsed with EtOAc, hexanes and triturated in THF with subsequent drying.

X-ray Crystallography

Single crystals of N-halophenylpyridinium salts **3.3-3.12**, **3.14** and **3.16** were grown by dissolving 5mg of the salt in ~1mL of an acetone:methanol solution (1:1) inside a 20-mL borosilicate glass screw cap scintillation vial. After 1-2 days, crystals suitable for single crystal X-ray diffractometry were obtained.

3.12: The structure contains two sites partially occupied by chloride counterion and water solvate. One site (O3-Cl7) was refined to 0.671(4) occupancy while the other site (O4-Cl6) refined to 0.571(8) occupancy. Atoms in each respective site were modeled with the same anisotropic displacement parameters. Hydrogen bond distances to O1 and O2A were

restrained to 0.85Å. The position of hydrogen atoms bonded to O4 was not successfully modeled but their presence is inferred.

Compound **3.3**

Yield: 77% as light brown powder; Mp: >220^{0}C

^{1}H NMR (d$_4$-MeOD, 300MHz) δ: 9.24 (d, 2H, J =6.9 Hz), 8.79 (t, 1H,), 8.30 (dt, 2H), 8.12 (d, 2H, J=6.9Hz), 7.60 (d, 2H, J=6.9Hz)

^{13}C NMR (d$_4$-MeOD, 75MHz) δ :148.2, 146.0 141.0, 129.6, 127.3, 98.8

HRMS (ESI): 281.9780 calculated for $C_{11}H_9NI$ $[M]^+$: found 281.9785

Compound **3.4**

Yield: 73% as cream-colored powder; Mp: >220^{0}C

^{1}H NMR (d$_4$-MeOD, 300MHz) δ: 9.32 (d, 2H, J =6.9 Hz), 8.86 (t, 1H,), 8.35 (dt, 2H), 7.98 (d, 2H, J=6.9Hz), 7.84 (d, 2H, J=6.9Hz)

^{13}C NMR (d$_4$-MeOD, 75MHz) δ:148.2, 146.1 142.5, 134.8, 129.6, 127.5 127.0

HRMS (ESI): 233.9918 calculated for $C_{11}H_9NBr$ $[M]^+$; found 233.9923

Compound **3.5**

Yield: 85% as light brown powder; Mp: >220^{0}C

^{1}H NMR (d$_4$-MeOD, 300MHz) δ: 9.24 (d, 2H, J =6.0 Hz), 8.80 (t, 1H,), 8.31-8.26 (m, 3H), 8.12 (d, 1H, J=8.1Hz), 7.85 (d, 1H, J=8.1Hz), 7.50 (t, 1H)

^{13}C NMR (d$_4$-MeOD, 75MHz) δ:148.3, 146.1 142.0, 134.5, 133.0, 129.6, 125.2, 95.4

HRMS (ESI): 281.9780 calculated for $C_{11}H_9NI$ $[M]^+$; found 281.9788

Compound **3.6**

Yield: 63% as light yellow powder. Mp: >220^{0}C

^{1}H NMR (d$_4$-MeOD, 300MHz) δ: 9.26 (d, 2H, J =6.9 Hz), 8.86 (t, 1H,), 8.35 (t, 2H), 8.14 (d, 1H, J=2.1Hz), 7.96(d, 1H, J= 8.1Hz), 7.87(dd, 1H), 7.68 (t, 1H)

^{13}C NMR (d$_4$-MeOD, 75MHz) δ:149.7, 147.5 142.5, 137.1, 134.5, 130.9 130.2, 126.1, 125.8

HRMS (ESI): 233.9918 calculated for $C_{11}H_9NBr$ $[M]^+$; found 233.9922

Compound **3.7**

Yield: 38% as dark brown powder; Mp: >220^{0}C

^{1}H NMR (d_4-MeOD, 300MHz) δ: 9.20 (d, 2H, J =6.0 Hz), 8.91 (t, 1H), 8.41 (t, 2H), 8.26 (d, 1H, J= 8.1 Hz), 7.82(m, 2H), 7.53 (t, 1H)

^{13}C NMR (d_4-MeOD, 75MHz) δ:148.0, 146.3, 138.9, 135.5, 134.5, 131.0, 129.7, 128.6, 98.3

HRMS (ESI): 281.9780 calculated for $C_{11}H_9NI$ $[M]^+$; found 281.9783

Compound **3.8**

Yield: 68% as bright yellow powder; mp: >220^{0}C

^{1}H NMR (d_4-MeOD, 300MHz) δ: 9.18 (d, 2H, J =6.9 Hz), 8.86 (t, 1H,), 8.35 (t, 2H), 7.97 (t, 1H), 7.86 (d, 1H, J=8.1 Hz), 7.96(d, 1H, J= 8.1Hz), 7.76-7.64 (m, 2H)

^{13}C NMR (d_4-MeOD, 75MHz) δ:149.3, 147.7, 137.4, 135.5, 134.6, 130.8, 129.7, 128.9, 115.7

HRMS (ESI): 233.9918 calculated for $C_{11}H_9NBr$ $[M]^+$; found 233.9926

Compound **3.9**

Yield: 32% as dark brown powder; mp: >220^{0}C

^{1}H NMR (d_4-MeOD, 300MHz) δ: 9.15 (d, 2H, J =6.1 Hz), 8.91 (t, 1H), 8.58 (d, 1H, J=2.4 Hz), 8.38 (t, 2H), 8.11 (dd, 1H), 7.56 (d, 1H, J= 8.1Hz)

^{13}C NMR (d_4-MeOD, 75MHz) δ:148.1, 146.1, 139.3, 128.4, 127.8, 98.1, 94.8

HRMS (ESI): 407.8746 calculated for $C_{11}H_8NI_2$ $[M]^+$; found 407.8754

Compound **3.10**

Yield: 71% as light yellow powder; mp: >220^{0}C

^{1}H NMR (d_4-MeOD, 300MHz) δ: 9.17 (d, 2H, J = 6.0 Hz), 8.89 (t, 1H), 8.36 (t, 2H), 8.13 (d, 1H, J= 2.1 Hz), 7.92 (dd, 1H), 7.77 (d, 1H, J=8.1 Hz)

^{13}C NMR (d_4-MeOD, 75MHz) δ:149.6, 147.7, 137.8, 134.0, 130.1, 129.7, 127.6, 115.7

HRMS (ESI): 311.9024 calculated for $C_{11}H_8NBr_2$ $[M]^+$; found 311.9034

Compound **3.11**

Yield: 34% as dark brown powder; mp: >220^{0}C

^{1}H NMR (d_4-MeOD, 300MHz) δ: 9.13 (d, 2H, J =6.1 Hz), 8.71 (d, 2H, J= 6.1 Hz), 8.65 (d, 1H, J=2.1 Hz), 8.20 (m, 3H), 7.77 (m, 3H), 7.60 (d, 1H, J=8.1 Hz)

^{13}C NMR (d_4-MeOD, 75MHz) δ: 149.6, 147.3, 144.4, 140.6, 139.5, 134.8, 134.3, 131.2, 129.6, 129.3, 126.1, 98.2, 94.8

HRMS (ESI): 483.9059 calculated for $C_{17}H_{12}NI_2$ $[M]^+$; found 483.9071

Compound **3.12**

Yield: 44% as light yellow powder mp: >220^0 C

^{1}H NMR (d$_4$-MeOD, 300MHz) δ: 9.10 (d, 2H, J =6.9 Hz), 8.65 (d, 2H, J= 6.9Hz), 8.26 (d, 1H, J= 2.1Hz), 8.12 (d, 2H, J= 8.7Hz), 7.95 (dd, 1H), 7.77 (d, 1H, J=8.1 Hz), 7.69-7.71 (m, 3H)

^{13}C NMR (d$_4$-MeOD, 75MHz) δ:147.3, 142.5, 137.8, 134.8, 134.2, 134.1, 133.0, 131.2, 130.3, 129.7, 127.5, 126.1, 120.7

HRMS (ESI): 387.9332 calculated for $C_{17}H_{12}NBr_2$ $[M]^+$; found 387.9339

Compound **3.13** obtained as white solid, yield 68%; Mp: > 220^0 C; ^{1}H NMR (d$_6$-DMSO, 300 MHz) δ (ppm): 10.04 (s, 1 H), 9.60 (d, 1 H, J = 6.0 Hz), 9.43 (d, 1H, J = 6.0 Hz), 9.15 (d, 1 H, J = 2.4 Hz), 9.11 (m, 1 H), 9.00 (dd, 1H J= 6.0 Hz; 2.4 Hz), 8.58 (d, 1 H, 6.3 Hz): ^{13}C NMR (75 MHz in d^6-DMSO): 162.3, 149.1, 147.5, 146.6, 146.4 138.5, 133.4, 131.2, 130.8, 126.0, 121.6, 115.6; LRMS (ESI): 289.1 calculated for $C_{12}H_9N_4O_5$ $[M]^+$; found 289.1

Compound **3.14** obtained as yellow solid, yield 43%; Mp: 190^0 C (dec); ^{1}H NMR (d$_6$-DMSO, 300 MHz) δ (ppm): 10.04 (s, 1 H), 9.60 (d, 1 H, J = 6.0 Hz), 9.43 (d, 1H, J = 6.0 Hz), 9.15 (d, 1 H, J = 2.4 Hz), 9.11 (m, 1 H), 9.00 (dd, 1H J= 6.0 Hz; 2.4 Hz), 8.58 (d, 1 H, 6.3 Hz): ^{13}C NMR (75 MHz in d^6-DMSO): 162.3, 149.1, 147.5, 146.6, 146.4 138.5, 133.4, 131.2, 130.8, 126.0, 121.6, 115.6; LRMS (ESI): 451.1 calculated for $C_{12}H_9N_2OI_2$ $[M]^+$; found 451.1

Compound **3.15** obtained as a white solid, yield 75%; Mp: > 220^0 C; ^{1}H NMR (d$_6$-DMSO, 300 MHz) δ (ppm): 9.68 (d, 2 H, J = 6.6 Hz), 9.15 (d, 1 H, J = 2.4 Hz), 8.86 (d, 2 H, 6.6 Hz), 8.52 (m, 1 H), 8.49 (s, 1 H): ^{13}C NMR (75 MHz in d^6-DMSO): 163.2, 150.4, 149.4, 147.4,131.2, 126.0, 121.6, 115.6, 114.1; LRMS (ESI): 289.1 calculated for $C_{12}H_9N_3O_5$ $[M]^+$; found 289.1

Compound **3.16** obtained as yellow solid, yield 36%; Mp: > 220^0 C; ^{1}H NMR (d$_6$-DMSO, 300 MHz) δ (ppm): 9.70 (d, 2 H, J = 6.6 Hz), 8.90 (d, 2 H, 6.6 Hz), 8.70 (d, 1 H, J = 2.4 Hz),8.42 (m, 1 H), 8.39 (s, 1 H): ^{13}C NMR (75 MHz in d^6-DMSO): 163.2, 150.4, 149.4, 147.4,131.2, 126.0, 121.6, 115.6, 114.1; LRMS (ESI): 451.1 calculated for $C_{12}H_9N_2OI_2$ $[M]^+$; found 451.1

6.4 Experimental Data for Chapter 4

Preparation of compounds **4.2**, **4.4** and **4.7**

Compounds **4.2**, **4.4** and **4.7** can be easily obtained by added by adding 1.2 mmol of the appropriate halopyridine (or simply pyridine) to 0.48 mmol of the appropriately substituted bis-bromomethyl precursor stirring in acetone, which is subsequently set to gentle reflux over 12 hours. In that time, the desired bromide salts will precipitate out of solution and after filtration can be subsequently dried and used for further syntheses.

Compound **4.2** Obtained as a white solid, yield 58%; Mp: > 220^0 C; ^{1}H NMR (300 MHz, d_6-DMSO) (δ): 9.46 (s, 2H), 9.04 (d, 2H, J = 4.2 Hz), 8.94 (d, 2H, J = 6.0 Hz), 7.89 (t, 2H), 7.28-6.93 (m, 18 H), 5.64 (s, 4 H); ^{13}C NMR (75 MHz, d^6-DMSO): 157.3, 150.4, 149.8, 141.4, 141.2, 140.4 137.3, 134.8 133.6, 130.5, 128.9, 128.6, 128.5, 127.9, 100.6, 61.0

Compound **4.4** Obtained as a white solid, yield 46%. Mp: > 220^0 C; ^{1}H NMR (300 MHz, d_6-DMSO) (δ): 9.52 (s, 2H), 9.11 (d, 2H, J = 4.2 Hz), 8.92 (d, 2H, J = 6.0 Hz), 7.82 (t, 2H, J = 6.0 Hz), 7.21-6.90 (m, 18 H), 5.59 (s, 4 H); ^{13}C NMR (75 MHz, d^6-DMSO): 157.5, 150.6, 149.6, 141.4, 141.0, 140.4, 138.1, 137.6, 137.0, 134.5 133.6, 130.8, 128.9, 128.6, 128.3, 127.9, 119.6, 61.8

Compound **4.7** Obtained as a white solid, yield 58%; Mp: > 220^0 C; ^{1}H NMR (300 MHz, d_6-DMSO) (δ): 9.46 (s, 4H), 9.04 (t, 4H), 8.94 (t, 2H), 7.89 (t, 2H, J = 6.0 Hz), 7.28-6.93 (m, 18 H), 5.64 (s, 4 H); ^{13}C NMR (75 MHz, d^6-DMSO): 157.5, 150.6, 149.6, 141.4, 141.0, 140.4 137.0, 134.5 133.6, 130.8, 128.9, 128.6, 128.3, 127.9, 100.6, 61.0

Preparation of compounds **4.3**, **4.5** and **4.8**

The hexafluorophosphate derivatives **4.3**, **4.5** and **4.8** can be prepared by stirring the corresponding bromide salt in a saturated aqueous solution of NH_4PF_6 for six hours. The reaction mixture can then be diluted with water and the product can be extracted with EtOAc from the aqueous layer with subsequent drying over Na_2SO_4 and evacuation of the solvent to obtain the salts in good yields.

Compound **4.3** yield 95% Mp: > 220^0 C; ^{1}H NMR (300 MHz, d_6-DMSO) (δ): 9.52 (s, 2H), 9.04 (d, 2H, J = 4.2 Hz), 8.88 (d, 2H, J = 6.0 Hz), 7.80 (t, 2H, J = 6.0 Hz), 7.22-6.91 (m, 18 H), 5.64 (s, 4 H); ^{13}C NMR (75 MHz, d^6-DMSO): 157.5, 150.6, 149.6, 141.4, 141.0, 140.4 137.0, 134.5 133.6, 130.8, 128.9, 128.6, 128.3, 127.9, 100.6, 61.0 ^{19}F NMR (TBAF standard) (δ) :-65 (PF_6^-)

Compound **4.5** Mp: > 220^0 C; ^{1}H NMR (300 MHz, d^6-DMSO) (δ): 9.46 (s, 2H), 9.04 (d, 2H, J = 4.2 Hz), 8.94 (d, 2H, J = 6.0 Hz), 7.89 (t, 2H, J = 6.0 Hz), 7.28-6.93 (m, 18 H), 5.64 (s, 4 H); ^{13}C NMR (75 MHz, d^6-DMSO): 157.5, 150.6, 149.6, 141.4, 141.0, 140.4, 138.1, 137.5., 137.0, 134.5 133.6, 130.8, 128.9, 128.6, 128.3, 127.9, 119.8, 59.8 ^{19}F NMR (TBAF standard) (δ) :-65 (PF_6^-)

Compound **4.8** obtained as a white solid, yield 93%. Mp: > 220^0 C; ^{1}H NMR (300 MHz, d_6-DMSO) (δ): 9.55 (s, 2H), 9.12 (d, 2H, J = 4.2 Hz), 8.88 (d, 2H, J = 6.0 Hz), 7.89 (t, 2H, J = 6.0 Hz), 7.28-6.93 (m, 18 H), 5.64 (s, 4 H); ^{13}C NMR (75 MHz, d^6-DMSO): 157.5, 150.6, 149.6, 141.4, 141.0, 140.4, 137.6, 137.0, 134.5 133.6, 130.8, 128.9, 128.6, 128.3, 127.9, 61.0: ^{19}F NMR (TBAF standard) (δ) :-65 (PF_6^-)

Compound **4.6** can be obtained by placing 0.120 mmol of the bromide precursor **4.4** in 10 mL of a 1:1 MeOH/H_2O solution with 0.240 mmol of $AgNO_3$. Stirring continues for 12 hours at room temperature at which time, the precipitated AgBr is removed by filtration and the solution is concentrated under vacuum to remove methanol. As this occurs the desired nitrate salt will precipitate out as a result of its insolubility in a water solution. The water can be filtered off and the product dried and subjected to analysis.

Compound **4.6** Mp: > 220^0 C; ^{1}H NMR (300 MHz, d_6-DMSO) (δ): 9.48 (s, 2H), 9.02 (d, 2H, J = 4.2 Hz), 8.14 (d, 2H, J = 6.0 Hz), 7.89 (t, 2H, J = 6.0 Hz), 7.24-6.92 (m, 18 H), 5.64 (s, 4 H); ^{13}C NMR (75 MHz, d^6-DMSO): 157.5, 150.6, 149.4, 141.4, 140.8, 140.4, 137.3, 137.0, 136.8, 134.5 133.6, 130.8, 128.9, 128.6, 128.5, 127.9, 119.8, 61.0: (IR, thin film, MeOH): 1300-1500 cm^{-1} (broad)

Preparation of compounds **4.9** and **4.10**

To a stirring solution of 75 mL acetonitrile and 2.10 mmol of the appropriate imidazole 8.50 mmol of K_2CO_3 was added and the mixture was allowed to stir for 5 minutes under

argon, when 1.00 mmol of bis-4,4'bromomethyl TPE was added. The mixture was then allowed to reflux for 8 hours. The solution was then cooled down to room temperature, diluted with 100 mL of H_2O and extracted with 2 x 50 mL of EtOAc, the organic layer was washed with brine and dried over Na_2SO_4. The solvent was dried under rotary evaporation, while the product was adsorbed onto silica and subsequently eluted on a column with a gradient of 25-40% EtOAc in hexanes.

Compound **4.9** isolated as a light brown solid, yield 65%. Mp: 170-173^0 C: ^{1}H NMR (300 MHz, in $CDCl_3$) (δ): 7.81 (d, 2H, J = 6.6 Hz) 7.72 (d, 2 H, J = 6.6 Hz), 7.20-6.89 (m, 18 H), 4.96 (s, 4H): ^{13}C NMR (75 MHz, in $CDCl_3$): 143.4, 143.0, 133.4, 132.4, 131.6, 131.0, 130.0, 128.9, 128.8, 128.2, 127.6, 126.6, 90.3, 52.7

Compound **4.10** isolated as a light brown solid, yield 77%. Mp: 148-151^0 C: ^{1}H NMR (300 MHz, in $CDCl_3$) (δ): 7.62-7.58 (m, 4H), 7.29- 6.88 (m, 18H), 4.96 (s, 4H), 2.28 (s, 6H): ^{13}C NMR (75 MHz, in $CDCl_3$) 144.7, 143.0, 134.2, 131.6, 131.0, 128.8, 128.2, 127.7, 126.9, 126.6, 126.1, 125.9, 119.9, 49.4, 14.2

Preparation of compounds **4.11** and **4.12**

Either **4.9** or **4.10** (1.0 mmol) is dissolved in 30 mL of CH_2Cl_2 at 0^{0}C when 3.0 mmol of Me_3OBF_4 is added to the reaction mixture. This mixture is allowed to react for 10 hours. At this time, the CH_2Cl_2 is gently removed under vacuum and the crude product is washed with ether and dried under hi-vacuum conditions the crude product was deemed sufficiently pure to proceed with fluorimetric analysis.

Compound **4.11** isolated as dark brown solid, yield 53%: Mp: 184^0 C (dec): ^{1}H NMR (300 MHz, d_6 -DMSO) (δ): 8.00 (d, 2H, J = 6.0 Hz), 7.89 (d, 2H, J = 6.0 Hz), 7.29-7.00 (m, 18H), 5.36 (s, 4H), 3.94 (s, 6H): ^{13}C NMR (75 MHz, d^6-DMSO): 142.3, 141.1.3, 132.5, 131.3, 130.8, 128.1, 127.3, 126.8, 122.2, 122.0, 121.6, 121.0, 103.4, 52.3, 35.4

Compound **4.12** isolated as a light brown solid, yield 46% Mp: > 220^0 C : ^{1}H NMR (300 MHz, d_6-DMSO) (δ): 7.64-7.61 (m, 4H), 7.16-7.01 (m, 18 H), 5.34 (s, 4H), 3.79 (s, 6 H), 2.59 (s, 6 H): ^{13}C NMR (75 MHz, d^6-DMSO): 142.7, 141.3, 132.7, 131.2, 130.5, 127.9, 127.5, 127.3, 126.8, 122.6, 122.2, 121.1, 113.9, 51.4, 35.1, 34.8

APPENDIX

CRYSTALLOGRAPHIC DATA TABLES

Table A1 Crystallographic Data for **3.3-3.7**

	3.3	***3.4***	***3.5***	***3.6***	***3.7***
CCDC number	1052260	1052261	1052262	1052263	1052264
Crystal system	monoclinic	monoclinic	tetragonal	triclinic	monoclinic
Space group	$P2_1/c$	$P2_1/n$	$P4_12_12$	P-1	$P2_1/c$
a/Å	8.9791(5)	17.0693(12)	8.3557(6)	7.4154(4)	13.6280(14)
b/Å	7.4795(4)	7.4556(5)	8.3557(6)	11.0476(6)	6.9633(7)
c/Å	19.7533(11)	19.5710(13)	34.1012(3)	13.9173(8)	13.4276(13)
$\alpha/^0$	90.0000	90.0000	90.0000	102.3083(14)	90.0000
$\beta/^0$	96.2197(12)	102.9486(17)	90.0000	95.2744(13)	102.5700(12)
$\gamma/^0$	90.0000	90.0000	90.0000	90.0762(12)	90.0000
$V/Å^3$	1318.8(2)	2427.3(5)	2380.9	1108.97	1243.69(15)
Z	4	8	8	4	4
D_{calc}	1.781	1.629	1.822	1.674	2.184
μ (mm^{-1})	2.617	3.586	2.887	3.918	5.021
T/K	190(2)	190(2)	190(2)	190(2)	190(2)
No. of reflections	17377	38104	41165	13789	16298
No. of unique reflections	2507	5214	3373	5120	2294
No. of reflections with $I > 2\sigma$ (I)	2357	4029	3207	4425	2014
No. of params.	161	304	136	265	127
R_1 [$I > 2\sigma$ (I)]	0.0257	0.0293	0.0178	0.0254	0.0372
wR_2	0.0955	0.1028	0.0464	0.0923	0.1273

Table A2 Crystallographic data for **3.8-3.12**

	3.8	***3.9***	***3.10***	***3.11***	***3.12***
CCDC number	1052265	1052266	1052267	1052268	1052269
Cystal system	monoclinic	monoclinic	monoclinic	monoclinic	triclinic
Space group	$P2_1/n$	C2/c	$P2_1/c$	C2/c	P-1
a/Å	8.4925(11)	31.759(2)	10.4651(5)	9.2519(4)	9.9620(6)
b/Å	9.9455(13)	9.0729(7)	8.5805(3)	19.9679(10)	11.8679(13)
c/Å	13.5872(19)	19.9453(14)	16.0117(7)	19.1621(9)	16.181(2)
$\alpha/^0$	90.0000	90.0000	90.0000	90.0000	107.803(6)
$\beta/^0$	90.684(3)	90.4430(13)	107.987(2)	99.712(2)	98.300(6)
$\gamma/^0$	90.0000	90.0000	90.0000	90.0000	105.069(6)
$V/Å^3$	1147.5(5)	5747.1(12)	1367.52(15)	3489.3(4)	1705.9(4)
Z	4	16	4	8	4
D_{calc}	1.670	2.175	1.872	2.008	1.719
μ (mm^{-1})	3.786	4.544	6.112	3.755	4.908
T/K	190(2)	190(2)	190(2)	190(2)	190(2)
No. of reflections	15431	35759	22401	19769	19097
No. of unique reflections	2105	6940	3280	3343	6202
No. of reflections with $I > 2\sigma(I)$	1422	5855	2767	2923	2698
No. of params	144	307	155	192	417
R_1 [$I > 2\sigma(I)$]	0.0434	0.0255	0.0311	0.0366	0.0653
wR_2	0.1210	0.0811	0.1028	0.1241	0.1674

Table A3 Crystallographic data for **3.14, 3.16**

	3.14	***3.16***
CCDC number	Pending	pending
Crystal system	monoclinic	Orthorhombic
Space group	$P2_1/c$	Pbcn
a/Å	18.9626(19)	13.4753(13)
b/Å	19.2914(19)	14.2298(14)
c/Å	8.8229(9)	15.3212(15)
$\alpha/^0$	90.0000	90.0000
$\beta/^0$	90.0000	90.0000
$\gamma/^0$	90.0000	90.0000
V/Å^3	3227.6(6)	2937.9(5)
Z	8	8
D_{calc}	2.002	2.200
μ (mm^{-1})	4.053	4.453
T/K	190(2)	190(2)
No. of reflections	11258	66234
No. of unique reflections	2971	3017
No. of reflections with $I > 2\sigma$ (I)	2194	2466
No. of params.	164	163
R_1 [I > 2σ (I)]	0.0977	0.0321
wR_2	0.1740	0.0718

Table A4 Crystallographic data for **4.2-4.6**.

	4.2	***4.3***	***4.4***	***4.5***	***4.6***
CCDC number	Pending	Pending	Pending	Pending	pending
Cystal system	orthorhombic	monoclinic	orthorhombic	monoclinic	triclinic
Space group	Iba2	C2/c	Pccn	$P2_1$	P-1
a/Å	12.4259(12)	31.738(2)	29.559(3)	9.0652(9)	8.0910(14)
b/Å	12.4259(12)	14.9748(15)	8.1432(8)	16.9502(17)	29.144(5)
c/Å	15.5655(16)	9.3174(9)	16.3648(16)	13.3578(13)	16.386(3)
$\alpha/^0$	90.0000	90.0000	90.0000	90.0000	90.0000
$\beta/^0$	90.0000	92.251(5)	90.0000	92.538(5)	91.319(5)
$\gamma/^0$	90.0000	90.0000	90.0000	90.0000	90.0000
V/Å^3	3931.5(6)	4424.9(7)	3939.1(7)	2050.5(4)	3862.9(12)
Z	4	8	4	2	4
D_{calc}	1.595	3.442	1.569	1.581	1.370
μ (mm^{-1})	3.661	4.544	4.132	2.142	2.146
T/K	190(2)	190(2)	190(2)	190(2)	190(2)
No. of reflections	23942	22618	37909	33092	59798
No. of unique reflections	3586	4213	3622	7286	7051
No. of reflections with $I > 2\sigma(I)$	2452	3495	2798	5024	4435
No. of params	166	254	229	525	488
R_1 [$I > 2\sigma(I)$]	0.0863	0.0721	0.0365	0.0606	0.0844
wR_2	0.1223	0.0857	0.0589	0.1019	0.1331

BIBLIOGRAPHY

1. Beer, P. D.; Gale, P. A. *Angew. Chem., Int. Ed.* **2001**, *40*, 486
2. Bianchi, A.; Bowman-James, K.; Garcia-España, E. *Supramolecular Chemistry of Anions*, John Wiley & Sons, **1997**, 81
3. Bianchi, A.; Bowman-James, K.; Garcia-España, E. *Supramolecular Chemistry of Anions*, John Wiley & Sons, **1997**, 6
4. Park, C. H.; Simmons, H. E. *J. Am. Chem. Soc.* **1968**, *90*, 2431
5. Simmons, H. E.; Park, C. H.; Uyeda, R. T.; Habibi, M. F.; *Trans. New York Acad Sci.* **1970**, *32*, 521
6. Lehn, J.-M.; Sonveaux, E.; Willard, A. K. *J. Am. Chem. Soc.* **1978**, *100*, 4914
7. Heyer, D.; Lehn, J.-M. *Tetrahedron Lett.* **1986**, *7*, 5969
8. Hosseini, M. W.; Lehn, J.-M. *J. Am. Chem. Soc.* **1982**, *104*, 3525
9. Busschaert, N.; Caltagirone, C.; van Rossum, W.; Gale, P. A. *Chem Rev.* **2015**, *115*, 8038
10. Bazzicalupi, C.; Biagini, S.; Bencini, A.; Faggi, E.; Giorgi, C.; Matera, L.; Valtancoli, B. *Chem. Commun.* **2006**, 4087
11. Malojčić, G.; Piantanida, L.; Marinić, M.; Žinić, M.; Marjanović, M.; Kralj, M.; Pavelić, K.; Schneider, H. J. *Org. Biomol. Chem.* **2005**, *3*, 4373
12. Descalzo, A. B.; Marcos, M. D.; Martínez-Mañez, R.; Soto, J.; Beltran, D.; Amoros, P. *J. Mater. Chem.* **2005**, *15*, 2721
13. Jubian, V.; Dixon, R. P.; Hamilton, *J. Am. Chem. Soc.* **1992**, *114*, 1120
14. Miao, R.; Zheng, Q. Y.; Chen, C. F.; Huang, Z. T. *Tetrahedron Lett.* **2005**, *46*, 2155
15. Singh, A. S.; Sun, S.-S. *J. Org. Chem.* **2012**, *77*, 1880
16. Haketa Y.; Sakamoto, S.; Chigusa, K.; Nakanishi, T.; Maeda, H. *J. Org. Chem.* **2011**, *76,* 5177
17. Katayev, E. A.; Boev, N. V.; Khrustalev, V. N.; Ustynyuk, Y. A.; Tananaev, I. G.; Sessler, J. L. *J. Org. Chem.* **2007**, *72*, 2886
18. Chmielewski, M. J.; Charon, M. Jurczak, J. *Org. Lett.* **2004**, *6*, 3501

19. Brown, A.; Mullen, K. M.; Ryu, J.; Chmielewski, M. J.; Santos, S. M.; Felix, V.; Thompson, A. L.; Warren, J. E.; Pascu, S. I.; Beer, P. D. *J. Am. Chem. Soc.* **2009**, *131*, 4937
20. Martínez-Aguirre , M. A.; Yatsimirsk, A. K. *J. Org. Chem.* **2015**, *80*, 4985
21. Jamkratoke, M.; Ruangpornvisuti, V.; Tumcharern, G.; Tuntulani, T. Tomapatanaget, B. *J. Org. Chem.* **2009**, *74*, 3919
22. Badugu, R.; Lakowicz, J. R.; Geddes, C. D. *Sens. Actuators, B.* **2005**, *104*, 103
23. Hoque, M, N.; Basu, A.; Das, G. *Cryst. Growth & Des.* **2014**, *14*, 6
24. Turner, D. R.; Paterson, M. J.; Steed, J. W. *J. Org. Chem.* **2006**, *71*, 1598
25. Boyle, E. M.; Comby, S.; Molloy, J. K.; Gunnlaugsson, T. *J. Org. Chem.* **2013**, *78*, 8312
26. Duke, R. M.; McCabe, T.; Schmitt, W.; Gunnlaugsson, T. *J. Org. Chem.* **2012**, *77*, 3115
27. Gunnlaugsson, T.; Kruger, P. E.; Jensen, P.; Pfeffer, F. M.; Hussey, G. M. *Tetrahedron Lett.* **2003**, *44*, 8909
28. Boiocchi, M.; Del Boca, L.; Gómez, D. E.; Fabbrizzi, L.; Licchelli, M.; Monzani, E. *J. Am. Chem. Soc.* **2004**, *126*, 16507
29. Lou, X.; Qiang, L.; Qin, J.; Li, Z. *ACS Appl. Mater. Interfaces,* **2009**, *1*, 2529
30. Yang, Y.-K.; Tae, J. *Org. Lett.* **2006**, *8*, 5721
31. Chen, C. L.; Chen, Y. H.; Chen, C. Y.; Sun, S. S. *Org. Lett.* **2006**, *8*, 5053
32. Dong, M.; Peng, Y.; Dong, Y. M.; Tang, N.; Wang, Y. W. *Org. Lett.* **2012**, *14*, 130
33. Steed, J. W. *Chem. Soc. Rev.* **2010**, *39*, 3686
34. Valero, J.; Escuder, B.; Miravet, J. F.; de Mendoza, J. *Chem*.- Eur. J. **2012**, *18*, 13038
35. Piepenbrock, M. O. M.; Lloyd, G. O.; Clarke, N.; Steed, J. W. *Chem. Commun.* **2008**, 2644
36. Devadasu, V. R.; Bhardwaj, V.; Kumar, M. N. V. R. *Chem. Rev.* **2013**, *113*, 1686
37. Lepry, W. C.; Nazhat, S. N. *Chem. Mater.* **2015**, *27*, 4821
38. Ozdemir, E. *Energy Fuels,* **2009**, *23*, 5725
39. Collins, A. M.; Maslin, C.; Davies, R. J. *Org. Process. Res. Dev.* **1998**, *2*, 400

40. Sheldon, R. A. *Org. Process. Res. Dev.* **2011**, *15*, 213
41. Zhang, Z.; Schreiner, P. R. *Chem. Soc. Rev.* **2009**, *38*, 1187
42. Beckendorf, S.; Asmus, S.; Mancheño, O. G. *ChemCatChem* **2012**, *4*, 926
43. Taylor, M. S.; Jacobsen, E. N. *J. Am. Chem. Soc.* **2004**, *126*, 10558
44. Sigman, M. S.; Jacobsen, E. N. *J. Am. Chem. Soc.* **1998**, *120*, 4901
45. Zhao, Y.; Beuchat, C.; Domoto, Y.; Gajewy, J.; Wilson, A.; Mareda, J.; Sakai, N.; Matile, S. *Angew. Chem. Int. Ed.* **2013**, *52*, 9940
46. Matile, S.; Vargas Jentzsch, A.; Montenegro, J.; Fin. A. *Chem. Soc. Rev.* **2011**, *40*, 2453
47. Welsh, M. J.; Smith, A. E. *Cell*, **1993**, *73*, 1251
48. Lloyd, S. E.; Pearce, S. H. S.; Fisher, S. E.; Steinmeyer, K.; Schwappach, B.; Scheinman, S. J.; Harding, B.; Bolino, A.; Devoto, M.; Goodyer, P.; Rigden, S. P. A.; Wrong, O.; Jentsch, T. J.; Craig, I. W.; Thakker, R. V. *Nature,* **1996**, *379, 445*
49. Moseley, R. H.; Höglund, P.; Wu, G. D.; Silberg, D. G.; Haila, S.; De La Chapelle, A.; Holmberg, C.; Kere, J. *J. Physiol. Gastrointest. Liver Physiol.* **1999**, *276*, G185
50. Pajewski, R.; Ferdani, R.; Pajewska, J.; Li, R.; Gokel, G. W. *J. Am. Chem. Soc.* **2005**, *127*, 18281
51. Gorteau, V.; Bollot, G.; Mareda, J.; Matile, S. *Org. Biomol. Chem.* **2007**, *5,* 3000
52. Perez-Velasco, A.; Gorteau, V.; Matile, S. *Angew. Chem. Int. Ed.* **2008**, *47*, 921
53. Guo, X.; Facchetti, A.; Marks, T. J. *Chem. Rev.* **2014**, *114*, 8943
54. Vasimalla, S.; Senanayak, S. P.; Sharma, M.; Narayan, K. S.; Iyer, P. K. *Chem. Mater.* **2014**, *26*, 4030
55. Xie, W. J.; Gao, Y. Q. *J. Phys. Chem. Lett.* **2013**, *4*, 4247
56. Sakai, N.; Brennan, K. C.; Weiss, L. A.; Matile, S. *J. Am. Chem. Soc.* **1997**, *119*, 8726
57. Vargas Jentzsch, A.; Matile, S. *J. Am. Chem. Soc.* **2013**, *135*, 5302
58. Elie, C.-R.; Noujeim, N.; Pardin, C.; Schmitzer, A. R. *Chem. Commun.* **2011**, *47*, 1788
59. Elie, C.-R.; Hebert, A.; Charbonneau, M.; Haiun, A.; Schmitzer, A. R. *Org. Biomol. Chem.* **2013**, *11*, 923

60. Guo, W.; Tian, Y.; Jiang, L. *Acc. Chem. Res.* **2013**, *46*, 2834
61. Izzo, I.; Licen, S.; Maulucci, N.; Autore, G.; Marzocco, S.; Tecilla, P.; De Riccardis, F. *Chem. Commun.* **2008**, 2986
62. Boccalon, M.; Iengo, E.; Tecilla, P. *J. Am. Chem. Soc.* **2012**, *134*, 20310
63. Madhavan, N.; Robert, E. C.; Gin, M. S. *Angew. Chem. Int. Ed.* **2005**, *44*, 7584
64. Chang, K.-J.; Kang, B.-N.; Lee, M.-H.; Jeong, K.-S. *J. Am. Chem. Soc.* **2005**, *127*, 12214
65. Petitjean, A.; Cuccia, L. A.; Schmutz, M.; Lehn, J.-M. *J. Org. Chem.* **2008**, *73*, 2481
66. Arunkumar, E.; Ajayaghosh, A.; Daub, J. *J. Am. Chem. Soc.* **2005**, *127*, 3156
67. Wang, Y.; Bie, F.; Jiang, H. *Org. Lett.* **2010**, *12*, 3630
68. Zhang, D.-W.; Zhao, X.; Li, Z.-T. *Acc. Chem. Res.* **2014**, *47*, 1961
69. White, N. G.; Costa, P. J.; Carvalho, S.; Félix, V.; Beer, P. D. *Chem.-Eur. J.* **2014**, *19*, 17751
70. Langton, M. J.; Beer, P. D. *Chem. Commun.* **2014***, 50*, 8124
71.
    a) Spence, G. T.; Beer, P. D. *Acc. Chem. Res.* **2013**, *46*, 571
    b) Spence, G. T.; Pitak, M. B.; Beer, P. D. *Dalton Trans.* **2011**, *40*, 12052
72. Evans, N. H.; Beer, P. D. *Angewandte Chemie Int. Ed.* **2014**, *53*, 11716
73. Zhang, D.; Chatelet, B.; Serrano, E.; Perraud, O.; Dutasta, J.-P.; Robert, V.; Martinez, A. *ChemPhysChem.* **2015**, *16*, 2931
74. Gilday, L. C.; Robinson, S. W.; Barendt, T. A.; Langton, M. J.; Mullaney, B. R.; Beer, P. D. *Chem. Rev.* **2015**, *115,* 7118
75. Wang, H; Lin, J.; Huang, W.; Wei, W. *Sensors & Actuators B*, **2010**, *150*, 798
76. Mei, J.; Leung, N. L. C.; Kwok, R. T. K.; Lam, J. W. Y.; Tang, B.-Z. *Chem. Rev.* **2015**, *115*, 11718
77. Hong, Y.; Lam, J. W. Y.; Tang, B.-Z. *Chem. Soc. Rev.* **2011**, *40*, 5361
78. Shustova, N. B.; Ong, T.-C.; Cozzolino, A. F.; Michaelis, V. K.; Griffin, R. G.; Dinca, M. *J. Am. Chem. Soc.* **2012**, *134*, 15061
79. Gui, S.; Huang, Y.; Hu, F.; Jin, Y.; Zhang, G.; Yan, L.; Zhang, D.; Zhao, R. *Anal. Chem.* **2015**, *87*, 1470

80. Mei, J.; Wang, Y.; Tong, J.; Wang, J.; Qin, A.; Sun, J.-Z.; Tang, B.-Z. *Chem.- A. Eur. J.* **2013**, *19*, 613
81. Feng, H.-T.; Wang, J.-H. ; Zheng, Y.-S. *ACS Appl. Mater. Interfaces*, **2014***, 6*, 20067
82. Chen, X.; Shen, X.-Y.; Guan, E.; Liu, Y.; Qin, A.; Sun, J.; Tang, B.-Z. *Chem. Commun.* **2013**, 1503
83. Kato, T.; Kawaguchi, A.; Nagata, K.; Hatanaka, K. *Biochem and Biophys. Res. Comm.* **2010**, *394*, 200
84. Khandare, D. G.; Joshi, H.; Banerjee, M.; Majik, M. S.; Chatterjee, A. *RSC Adv.* **2014**, *4*, 47076
85. Kapadia, P. P; Ditzler, L. R; Baltrusaitis, J.; Swenson, D. C; Tivanski A. V.; Pigge, F. C. *J. Am. Chem. Soc.* **2011**, *133*, 8490
86. Kapadia, P. P.; Swenson, D. C.; Pigge, F. C. *Cryst. Growth & Des.* **2012**, *12*, 698
87. Pigge, F. C.; Kapadia, P. P.; Swenson, D. C. *CrystEngComm*. **2013**, *15*, 4386
88. Gotor, R.; Costero, A. M.; Gavina, P.; Gil, S.; Parra, M. *Eur. J. Org. Chem,* **2013**, *2015*, 1515
89. Noguchi, T.; Shiraki, T.; Dawn, A.; Tsuchiya, Y; Lien, L.-T.-N.; Yamamoto, T.; Shinkai, S. *Chem. Commun.* **2012**, 8090
90. Hindermann, D. K.; Robin, M. B.; Kuebler, N. A, *Journal of Magnetic Resonance*. **1969**, *1*, 479
91. Banerjee, M.; Emond, S. J.; Lindeman, S. V.; Rathore, R. *J. Org. Chem.* **2007**, *72*, 8054
92. Mills, N. S.; Tirla, C.; Benish, M. A.; Rakowitz, A. J.; Bebell, L. M.; Hurd, C. M. M.; Bria, A. L. M. *J. Org. Chem.***2005**, *70*, 10709
93. Jimenez, B.; Calle, E.; Caballero, C. *Sensors,* **2009**, *9*, 1534
94. Wang, J.-H.; Xiong, J.-B.; Zhang, X.; Song, S.; Zhu, Z.-H.; Zheng, Y.-S. *RSC Adv.* **2015**, *5*, 60096
95. Park, C.; Hong, J.-I. *Tetrahedon Lett.* **2010**, *51*, 1960
96. Kassl, C. J.; Pigge, F. C. *Tetrahedron Lett.* **2014**, *55*, 4810
97. Zhao, J; Yang, D.; Zhao, Y.; Yang, X.-J.; Wang, Y.-Y.; Wu. B. *Angew. Chem. Int. Ed.* **2014**, *53,*6632

98. Zapata, F.; Caballero, A.; White, N. G.; Claridge, T. D. W.; Costa, P. J.; Felix, V.; Beer, P. D. *J. Am. Chem. Soc.* **2012**, *134*, 11533

99. Cametti, M.; Raatikainen, K.; Metrangolo, P.; Pilati, T.; Terraneo, G.; Resnati, G. *Org. Biomol. Chem.* **2012**, *10*, 1329

100.Metrangolo, P.; Resnati, G. *Chem. – A. Eur. J.* **2001**, *7*, 2511

101. Rissanen, K. *CrystEngComm.* **2008**, *10*, 1107

102. Metrangolo, P.; Meyer, F.; Pilati, T.; Resnati, G.; Terraneo, G. *Angew. Chem. Int. Ed.* **2008**, *47*, 6114

103. Guthrie, F. *J. Chem. Soc.* **1863***, 16,* 239

104. Mulliken, R. S. *J. Am. Chem. Soc.* **1950**, *72*, 600

105. Hassel, O.; Hvoslef, J.; Vihovde, E. Hadler; Sörensen, Nils Andreas, *Acta. Chem. Scand.* **1954**, *8*, 873

106. Politzer, P.; Lane, P; Concha, M. C.; Ma, Y.; Murray, J. S. *J. Mol. Modeling*, **2007**, *13*, 305

107. Politzer, P.; Lane, P; Concha, M. C.; Ma, Y.; Murray, J. S. *J. Mol. Modeling*, **2007**, *13*, 643

108. Metrangolo, P.; Resnati, G.; Pilati, T.; Biella, S. *Structure and Bonding (Berlin, **2008**)*, *126* (Halogen Bonding), 105-136

109. Goroff, N. S.; Curtis, S. M.; Webb, J. A.; Fowler, F. W.; Lauher, J. W. *Org. Lett.* **2005**, *7*, 1891

110. Chudzinski, M. G.; McClary, C. A.; Taylor, M. S. *J. Am. Chem. Soc.* **2011**, *133,* 10559

111. Cabot, R.; Hunter, C. A. *Chem. Commun.* **2009**, *2005*

112. Lieffrig, J.; Jeannin, O.; Frackowiak, A.; Olejniczak, I.; Swietlik, R.; Dahaoui, S.; Aubert, E.; Espinosa, E.; Auban-Senzier, P.; Fourmigue, M. *Chem.- a. Eur. J.* **2013**, *19,* 14804

113. Clark, T.; Hennemann, M.; Murray, J. S.; Politzer, P. *J. Mol. Modeling,* **2007**, *13*, 291

114. Chudzinski M. G; McClary C. A; Taylor, M. S. *J. Am. Chem. Soc.* **2011**, *133*, 10559

115. Stephens, S. L.; Mizukami, W.; Tew, D. P.; Walker, N. R.; Legon, A. C. *Journal of Molecular Spectroscopy,* **2012**, *280*, 47

116. Gonzalez, L.; Gimeno, N.; Tejedor, R. M.; Polo, V.; Ros, M. B.; Uriel, S.; Serrano, J. L. *Chem. Mater.* **2013**, *25*, 4503

117. Aakeroy, C. B.; Wijethunga, T. K.; Desper, J.; Djakovic, M. *Cryst. Growth & Des.* **2015**, *15*, 3853

118. Caronna, T.; Liantonio, R.; Logothetis, T. A.; Metrangolo, P.; Pilati, T.; Resnati, G. *J. Chem. Soc.* **2004**, *126*, 4500

119. Aakeroy, C. B.; Chopade, P. D.; Desper, J. *Cryst. Growth & Des.* **2011**, *11*, 5333

120. Jungbauer, S. H.; Huber, S. M. *J. Am. Chem. Soc.* **2015**, *137*, 12110

121. Kniep, F.; Walter, S. M.; Herdtweck, E.; Huber, S. *Chem.- a Eur. J.* **2012**, *18*, 1306

122. Takeda, Y.; Hisakuni, D.; Lin, C.-H.; Minakata, S. *Org. Lett.* **2015**, *17,* 318

123. Kuhn, N.; Abu-Rayyan, A.; Eichele, K.; Piludu, C.; Steimann, M. *Z. Anorg. Allg. Chem.* **2004**, *630*, 495

124. Gray, L.; Jones, P. G. *Z. Naturforsch.* **2002**, *57*, 61-72

125. Genisson, Y.; Marazano, C.; Mehmandoust, M.; Gnecco, D.; Das, B. C. *Synlett.* **1992**, *5*, 431

126. Vanderwal, C. *J. Org. Chem.* **2011**, *76*, 9555

127. Lamb, J. D.; Christenson, J. J.; Izatt, S. R.; Bedke, K.; Astin, M. S.; Izatt, R. M. *J. Am. Chem. Soc.* **1980**, *102*, 3399

128. Kassl, C. J.; Swenson, D. C.; Pigge, F. C. *Cryst. Growth & Des.* **2015**, *15*, 4571

129. Rybalova, T.; Krivopalov, V.; Gatilov, Y.; Nikulicheva, O.; Shkurko, O. *J. Structural. Chem.* **2007**, *48*, 318

130. Pigge, F. C.; Vangala, V. R.; Swenson, D. C.; Rath, N. P. *Cryst Growth & Des.* **2010**, *10*, 224

131. Pigge, F. C.; Vangala, V. R.; Kapadia, P. P. Swenson, D. C.; Rath, N. P. *Chem. Commun*. **2008**, 4726

132. Zhuo, H.; Li, Q.; Li, W.; Cheng, J. *Phys. Chem. Chem. Phys.* **2014**, *16*, 159

133. White, N. G.; Caballero, A.; Beer, P. D. *CrystEngComm*, **2014**, *16*, 3722

134. Mukherjee, A. *Cryst. Growth & Des.* **2015**, *15*, 3076

135. Mukherjee, A.; Tothadi, S.; Desiraju, G. R. *Acc. Chem. Res.* **2014**, *47*, 2514

136. Corder, C. N.; Lowry, O. H. *Biochem. et Biophysica Acta, Enzymology,* **1969**, *191*, 579

137. Yamaguchi, M.; Yamaguchi, R. *Biochem. Pharmacol.* **1986**, *35*, 773

138. Lin, W.; Evans, O. R.; Xiong, R.-G.; Wang, Z. *J. Am. Chem. Soc.* **1998**, *120*, 13272

139. Croitor, L.; Coropceanu, E. B.; Masunov, A. E.; Rivera-Jacquez, H. J.; Siminel, A. V.; Fonari, M. S. *J. Phys. Chem. C.* **2014**, *118*, 9217

140. Zipfel, W. R.; Williams, R. M.; Webb, W. W. *Nat. Biotech.* **2003**, *21*, 1369

141. Nithya, R.; Senthilkumar, K. *Phys. Chem. Chem. Phys.* **2014**, *16*, 21496

142. Beverina, L.; Salice, P. *Euro. J. Org. Chem.* **2010**, *7*, 1207

143. Cariati, E.; Cavallo, G.; Forni, A.; Leem, G.; Metrangolo, P.; Meyer, F.; Pilati, T.; Resnati, G.; Righetto, S.; Terraneo, G.; Tordoin, E. *Cryst. Growth & Des.* **2011**, *11*, 5642

144. Robbie, K.; Broer, D. J.; Brett, M. J. *Nature,* **1999**, *399*, 764

145. Goldberg, I. *CrystEngComm.* **2008***, 10*, 637

146. Matsumoto, K.; Kannami, M.; Inokuchi, D.; Kurata, H.; Kawase, T.; Oda, M. *Org. Lett.* **2007**, *9*, 2903

147. Brussee, J.; Jansen, A. C. A. *Tetrahedron Lett.* **1983**, *24*, 3261

148. Sarwar, M. G.; Dragisic, B.; Dimitrijevic, E.; Taylor, M. S. *Chem.- a Eur. J.* **2013**, *19*, 2050

149. Yang, B.; Zhang, J.; Zhao, D.; Wang, Y.; Jia, H. *Chem. Lett.* **2013**, *42*, 930

150. Steinhardt, S. E.; Silverston, J. S.; Vanderwal, C. D. *J. Am. Chem. Soc.* **2008**, *130*, 7560